The Impact of Target Volume Density Overrides on Stereotactic Body Radiation Therapy of Lung Cancer

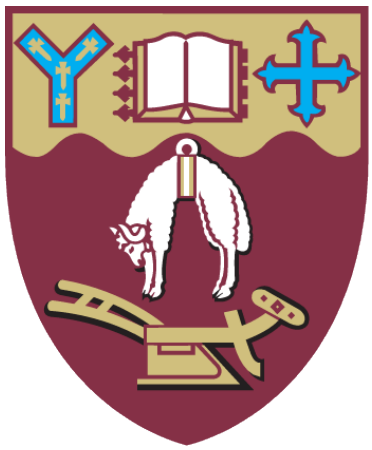

Grace Elizabeth Alice Healy

Department of Physics and Astronomy
University of Canterbury
Febuary 2017

This thesis is submitted to fulfil the requirements for the degree of
Master of Science in Medical Physics

Contents

Acknowledgements

I would like to acknowledge the immense support of my clinical supervisor Dr Andrew Cousins, principle physicist at Christchurch Hospital, and my senior supervisor Dr Steven Marsh. Dr Andrew Cousins provided a depth of knowledge and expertise that without I would have been disadvantaged greatly. Dr Steven Marsh provided a great deal of support and feedback, especially in the final few months of the project.

Additionally, I would like to thank the Medical Physics staff at Christchurch Hospital for their continued support and willingness to act as soundboards throughout this project. Paul Tolson from the Bioengineering workshop provided invaluable support developing the 3D-printed and cork inserts used in this study.

Finally, I would like to thank my family and friends for their support over the past two years. It would have been easy to lose focus in a project while also working, however they provided the motivation and stress relief to maintain the long nights and weekends of work. I cannot thank you all enough.

Abstract

Introduction: Stereotactic body radiation therapy (SBRT) is a method for treating of lung cancer currently used at Christchurch Hospital. The combined effects of lung tumour motion and the limitations of treatment planning systems calculating dose in lung regions creates uncertainty in the dose delivered to the tumour and surrounding normal tissues. In turn, this uncertainty has the possibility to negatively affect the clinical outcomes of the patient. This study overrides the treatment volumes to different densities between water and lung, and looked at the effect on plan quality and accuracy.

Method & Materials: Modified cork cylindrical inserts, each with a spherical tumour of either 15mm, 22mm, or 30mm diameter, and the QUASAR phantom were used to simulate the motion of a lung tumour. A four-dimensional computed tomography (4DCT) scan was taken for each insert on a Siemens Somatom RT Pro CT scanner. A treatment plan was generated on Monaco 5.1 treatment planning software, based on clinical protocols. Two standard plans (free breathing (FB), average intensity projection (AIP)) were compared to eight density overridden plans that focused on different target volumes (internal target volume (ITV), planning target volume (PTV), and a hybrid plan (HPTV)). The target volumes were set to a variety of densities between lung-equivalence and water-equivalence. The Dose Volume Histogram (DVH) statistics were used to compare the target coverage, conformity, and heterogeneity of the plans. The plans were delivered on an Elekta Synergy linac, and verified using ionisation chamber and radiographic film measurements.

Results: Minimal differences were seen in the 30mm tumour in terms of target coverage, plan conformity, and improved dosimetric accuracy. For the smaller tumours, a PTV override showed improved target coverage as well as plan conformity compared to the baseline plans. Minimal differences were seen with the ITV overrides. In terms of dosimetric accuracy, the ITV plans showed the highest gamma pass rate agreement between treatment planning system (TPS) and measured dose ($p<0.05$). However the low density PTV and HPTV plans also showed a significantly improved gamma pass rates ($p<0.05$)

Discussion & Conclusion: This study suggests that low density PTV overrides improves the plan quality and accuracy for small tumours only. Although an ITV override generates the

most significant increase in accuracy, the low density PTV plans have the additional benefit of plan quality improvement. Although this study and others agree that density overrides improve the treatment of SBRT, the optimal density override and the conditions under which it should be applied depend on the department.

List of Figures

List of Tables

Acronyms/Abbreviations

3D	Three dimensional
3DCRT	Three-dimensional conformal radiotherapy
4DCT	Four dimensional computed tomography
AAA	Analytical anisotropic algorithm
AIP	Average intensity projection
AXB	Acuros XB algorithm
CAX	Central axis
CCC	Collapsed cone convolution
CDHB	Canterbury district health board
CI	Conformity index
CPE	Charged particle equilibrium
CRT	Conventionally fractionated radiotherapy
CT	Computed tomography
CTV	Clinical tumour volume
DCAT	Dynamic conformal arc therapy
DNA	Deoxyribose nucleic acid
DTA	Distance-to-agreement
DVH	Dose volume histogram
ED	Electron density
FB	Free breathing
GTV	Gross tumour volume
Gy	Gray (J/kg)
HI	Homogeneity index
HPTV	Hybrid planning target volume
HU	Hounsfield unit
IAEA	International Atomic Energy Agency
ICRU	International commission on radiation units and measurements
IMRT	Intensity modulated radiotherapy
ITV	Internal target volume
KERMA	Kinetic energy released per unit mass
LED	Lateral electronic disequilibrium
Linac	Linear accelerator
MC	Monte Carlo
MIP	Maximum intensity projection
MLC	Multileaf collimator
MRI	Magnetic resonance imaging
MU	Monitor units
MV	Megavoltage
NSCLC	Non-small cell lung cancer
NTCP	Normal tissue complication probability
OAR	Organ at risk
OD	Optical density
PET	Positron emission tomography
PMMA	Poly-methyl methacrylate
PRV	Planning organ-at-risk volume
PTV	Planning target volume
QA	Quality assurance

QUASAR	QUASAR^{TM} Programmable Respiratory Motion Phantom
RPM	Real-time Positioning Management
RTOG	Radiation Therapy Oncology Group
SBRT	Stereotatic body radiation therapy
SCLC	Small cell lung cancer
TCP	Tumour control probability
TCPE	Transient charged particle equilibrium
TERMA	Total energy released per unit mass
TPS	Treatment planning system
TROG	Trans-Tasman radiation oncology group
TRS	Technical report series
TV	Target volume
VMAT	Volumetric arc therapy
XVMC	X-ray voxel-based Monte Carlo algorithm

1 Introduction

1.1 Radiotherapy

1.1.1 Treating Lung Cancer with Radiation

Cancer is the leading cause of death both worldwide and in New Zealand, contributing to 30% of all deaths [9]. The term 'carcinogenesis' describes the development of cancer at the cellular level, and involves the uncontrolled development of mutated cells. Currently there are three main treatment modalities for cancer: surgery, chemotherapy and radiation therapy (radiotherapy). These treatment options can be used independently or in conjunction with each other for curative or palliative purposes.

Lung cancer is the malignant transformation of lung tissue and applies to tumours of the lobes, bronchi, and bronchioles of the lung. Lung cancers are grouped into two main categories; non-small cell lung cancer (NSCLC) which makes up about 80% of all lung cancers, and small cell lung cancer (SCLC) which contributes the other 20% [10]. NSCLC refers to three main cancer types; adenocarcinoma, squamous cell carcinoma, and large cell carcinoma. NSCLC is typically slower growing and has a lower tendency for distant metastasis, compared to SCLC. As of 2012, lung cancer was the 5th most commonly registered cancer in New Zealand, contributing to 10% of all newly registered cancers [11]. However, lung cancer is the most common cause of cancer death for both men and women, contributing to 18% of all cancer deaths in New Zealand[11].

The lung cancer category that is most commonly treated with radiotherapy is early-stage NSCLC. The stages of NSCLC that are relevant to curative radiotherapy include stages T1N0 and T2aN0. For these stages, the tumour extent should be either less than 3cm (T1) or greater than 3 cm but less than or equal to 5cm in greatest dimension (T2a), surrounded by lung, and show no evidence of further invasion [12]. The primary treatment modality for early-stage NSCLC is surgery, which is associated with a 3-5 year survival and local control rate of 60-80% for stage 1, and a 3-5 year survival and local control rate of 30-50% for stage 2 [13]. However, for some patients

surgery is not an option. This may be due to a host of medical problems such as pulmonary disease, heart disease, diabetes, or vascular disease that render them 'medically inoperable', or if the patient declines surgical treatment. Conventional radiotherapy is less effective than surgery at achieving local control and an acceptable survival rate (15-45% for stage 1, and 10-30% for stage 2)[13], so it is necessary to improve these for patients that are unable to receive surgery.

1.1.2 The Linear Accelerator

Over the past century, there have been major improvements in the delivery of radiation for therapeutic purposes. Initially, radiation therapy was only used for superficial disease; however with the development of the Cobalt-60 teletherapy unit it was possible to produce higher energy and hence more penetrating beams [6]. In current practice, Cobalt-60 units have limited application and have largely been replaced with Mega-Voltage (MV) Linear Accelerators (linacs) for the production of high-energy photon and electron beams. The linac used in Christchurch Hospital, and for this study, is an Elekta Synergy linac as seen in Figure 1.1.

In the linac, electrons are injected into a long evacuated cylindrical tube, called an accelerating waveguide, where they are synchronise with a radio-frequency electromagnetic field. This causes the electron to be accelerated by the potential difference to a velocity close to the speed of light.

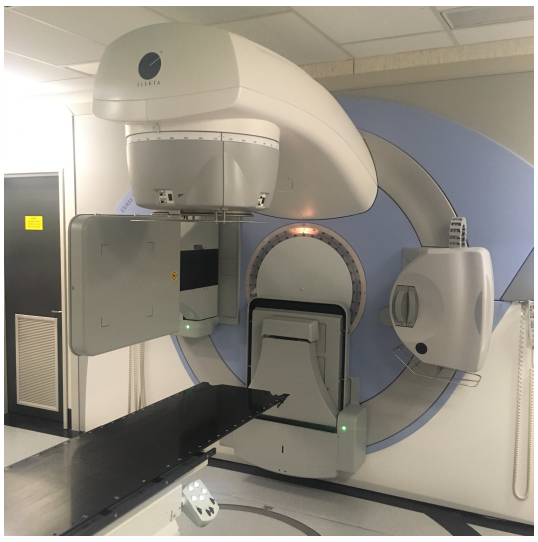

Figure 1.1: Elekta Synergy linac installed at Christchurch Hospital.

These electron beams can be converted into photons by focusing them onto a high atomic number target. As linacs are able to produce photon energies in the range of 6-18MV, deep tumours are able to be reached due to the penetrating power of the X-rays.

Modern linacs come equipped with collimation systems to shape the radiation beams to the tumour volume. The linac treatment heads contain large lead jaws that define the maximum radiation field size that is achievable, to limit the amount of out-of-field dose the patient receives. Additionally, multileaf collimators (MLCs) are used to finely shape the beam to the tumour. The MLC consists of a large number of tungsten blocks that can be driven in and out of the radiation field independently. The amount of radiation delivered by the linac is determined by an ionisation chamber in the head of the machine. This chamber measures the amount of charge that passes through it, and correlates the charge to a dose value (cGy) through the use of the Monitor Unit (MU). One MU is the amount of charge in the ion chamber that corresponds to 1cGy measured under reference conditions outside the linac.

1.1.3 The Radiotherapy Process

Once radiotherapy is the agreed upon course of treatment for a patient, a clearly defined process is followed from the initial planning Computed Tomography (CT) scan to the treatment delivery on the linac. Quality assurance (QA) is performed at each step of the process so that accuracy is maintained. A visualisation of the radiotherapy process can be seen in Figure 1.2.

Initially, a planning scan is performed on a CT scanner. This scan is then used for tumour delineation and for treatment planning. It is therefore important that the image quality be sufficient good so as to accurately determine the position of the tumour and surrounding organs. However, the image quality for radiotherapy scans does not need to be as high as that found in diagnostic scans as the presence of the tumour is already known. The image quality needs to be assessed against the dose received by the patient for the scan; an improvement to the image quality does not always coincide with improvements to patient outcomes, so the additional dose is unnecessary. The use of imaging is discussed further in Section 1.5. During the CT scanning process, the patient may require immobilisation devices, so that they do not move during treatment and so each fraction of treatment is reliably reproducible.

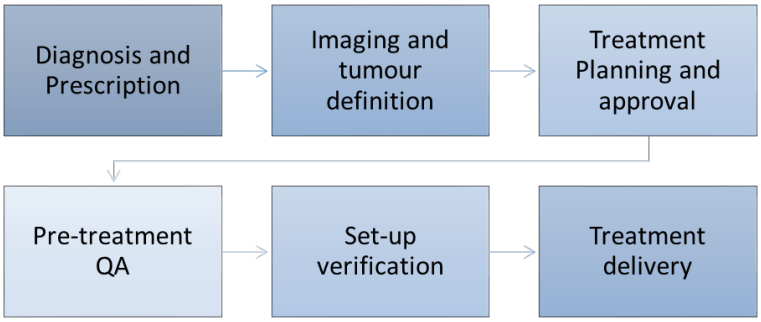

Figure 1.2: A basic schematic diagram of the Radiotherapy patient process, from diagnostic to treatment delivery.

The CT scan data is then imported into the Treatment Planning System (TPS), a software system where the radiation beams are defined and dose is computed, so that the plan can be generated for the patient-specific anatomy data. Three-dimensional conformal radiation therapy (3DCRT) involves delivering multiple beams from different angles with radiation fields that are shaped to the tumour volume, where the doses from the multiple beams are preferentially weighted to create an optimised dose distribution[5]. Multiple beams are required as each individual beam delivers a spectrum of radiation to the patient, resulting in entrance and exit dose. If the skin dose is too high, this can result in toxic effects to the patient. Multiple beams that coincide at the centre of the tumour ensure the entrance and exit dose is spread out, while delivering a high therapeutic dose to the tumour.

Treatments were originally planned on two dimensional orthogonal images, with the target volumes localised using bony anatomy as the reference frames. Prior to the widepread use of computers for dose calculations, the radiation fields were mostly simple squares or rectangles so that the calculations could be completed manually [5]. The introduction of computerised TPS and CT allowed for better tumour delineation and has led to the development of more conformal treatments. The treatment planning process is discussed further in Section 1.6.

Once a treatment plan has been accepted by the radiation oncologist, the delivery of the plan needs to be assessed so that it is sufficiently accurate prior to delivery. Extensive plan-specific QA is performed to ensure the dosimetric accuracy and this can be achieved with point dose measurements

or with dose distribution measurements. Plans that involve smaller fields and high doses are more difficult for the TPS to model accurately, so require the highest degree of QA. The QA process is discussed further in Section 1.7.

Once the QA program determines if the plan is sufficiently accurate, the patient treatment process can begin on the linac. This involves using a combination of external set-up lasers, the immobilisation devices from imaging, and pre-treatment imaging to ensure the set-up of the patient is as accurate as it can be. Following this, the treatment plan is delivered, with the set-up process maintained for each treatment delivery.

1.2 Radiobiology

Radiobiology provides the conceptual basis of radiotherapy by identifying the processes and mechanisms that normal tissues and tumours go through when exposed to radiation. Radiation can be separated into two distinct categories; ionising and non-ionising radiation, of which ionising radiation is relevant to radiotherapy. Ionising radiation causes cell damage either directly, through the production of ionising particles which cause either direct DNA double strand breaks, or indirectly through the production of free radicals which undergo chemical reactions with the DNA, as seen in Figure 1.3.

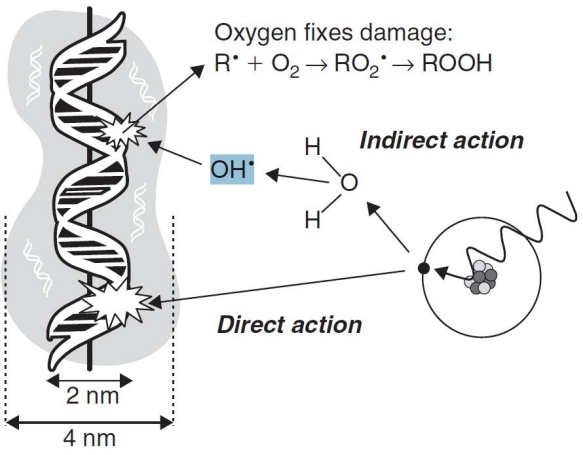

Figure 1.3: The two radiation action pathways for cell damage; direct and indirect. Adapted from [1]

In direct cell damage, the atoms in the DNA structure may be ionised or excited by the interactions with the radiation. If the excitation is sufficiently high, this may cause the removal of electrons, causing the DNA bonds to break, resulting in either a double or single-strand break. As the energy of the ionising radiation increases, it is more likely to create double strand breaks as the wavelength more closely matches the separation between DNA strands. In indirect cell damage, the water molecules inside the cell are ionised, creating simple free radicals such as H or OH. While these cannot travel far enough to damage the DNA, hydrogen peroxide may be formed which can lead to cell death through nutrient deficiency [2]. If a cell is unable to repair the damage caused by ionising radiation, it will either become inactive and incapable of proliferation, or the cell will undergo programmed cell death (apoptosis).

To remove the complications associated with single, high-dose radiation therapy, such as fibrosis, necrosis, organ dysfunction and the induction of secondary cancer, treatment is delivered in small fractions of the total desired dose, known as fractionated radiotherapy. Fractionation allows normal tissues that receive sub-lethal damage to repair and repopulate between treatments, while also causing lethal damage to tumour cells. Although this also applies to tumour cells, the repair process is faster in normal tissues than in tumour cells.

1.2.1 The Therapeutic Ratio

Curative radiotherapy aims to deliver sufficient radiation to the tumour site in order to destroy the tumour cells, while not irradiating the normal tissue to a dose level that will lead to serious complications. As the radiation dose increases, the effect of the radiation on the tumour cells and the normal tissue cells increases. For tumour cells, low doses of radiation are ineffective as the cells will be able to repair a small number of strand breaks, but delivering a large radiation dose can theoretically cause any tumour to be (locally) controlled [2]. The damage caused by radiation in the various normal tissues of the body varies in both type and severity. For tissues such as the lungs, intestine, and bone marrow, radiation damage may lead to death or decreased quality of life for the patient. Damage to other tissues such as the skin, limbs, and gonads, although not life-threatening, can lead to significant complications such as erythema, lymphatic drainage issues, infertility, and the induction of secondary cancers.

The probability of local tumour control increases with dose following a sigmoid relationship defined through Poisson statistics, known as the tumour control probability (TCP). The probability of normal tissues complications also increases with dose with a similar sigmoid relationship, known as the normal tissue complication probability (NTCP)[12]. In the case of NTCP, the lower part of the curve is the only region of interest as serious complications are deemed clinically unacceptable. In the clinic, the radiation oncologist decides on a maximum complications level that is acceptable (tolerance level), which in turn determines the level of tumour control that will be theoretically achieved.

The steepness of the TCP curve is clinically important and depends on several factors; the underlying Poisson relationship, variations in the probability of control among similar tumours due to differences in size, radiosensitivity, repopulation, and cell oxygenation, and patient-to-patient variation in the radiation dose delivered [2].

The principle is illustrated by plotting the two sigmoid curves for the TCP and the NTCP, as seen in Figure 1.4. The therapeutic ratio generally refers to the ratio of the TCP and NTCP percentages for a defined dose, and so a large therapeutic ratio corresponds to a likely more successful treatment. By plotting the therapeutic ratios for given TCP and NTCP curves, the optimal dose can be found as this corresponds to when the therapeutic ratio is largest[2].

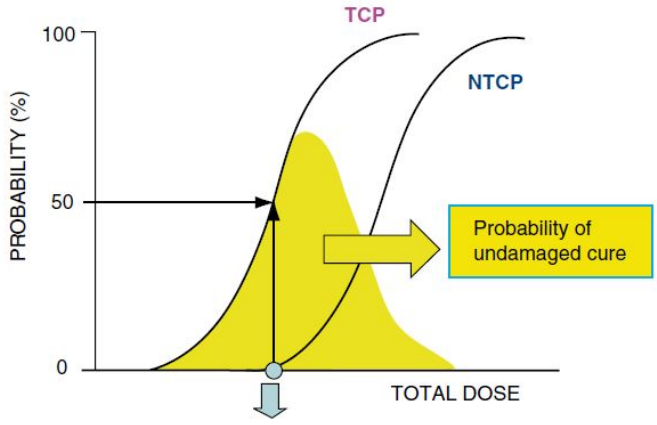

Figure 1.4: Dose response curves for a theoretical tumour control probability (TCP) and normal tissue complication probability (NTCP). Adapted from [2].

1.2.2 Treatment Volumes in Radiotherapy

The International commission on radiation units and measurements (ICRU) Reports No. 50[14], 62[15], and 83[3] describe several structure volumes related to both tumour and normal tissues that are defined for use in the treatment planning process and as a basis for the comparison of treatment outcomes. The following volumes are the principal volumes relevant to this project: gross tumour volume (GTV), clinical target volume (CTV), internal target volume (ITV), planning target volume (PTV), treated volume (TV), organs at risk (OAR), and the planning organ-at-risk volume (PRV). A visualisation of some of these volumes can be seen in Figure 1.5

The GTV, CTV, and OAR correspond to volumes that have an anatomical or physiological basis. The GTV is the gross palpable or visible extent of the malignant growth. The CTV is the volume that contains the GTV and any microscopic malignant disease that may not be visible on the imaging scan. The OAR is the tissue volume that should avoid irradiation as much as possible to minimise the risk of significant morbidity. As a result, the treatment plan and absorbed dose prescription will be affected by having to avoid the OARs.

The ITV, PTV, and PRV are radiotherapy concepts to ensure that the dose received by the CTV and OAR is achieved, taking into account the physical limitation of the treatment delivery system. The ITV consists of the CTV plus an internal margin. This internal margin takes into account the variations in the size and position of the CTV due to organ motions such as breathing and bladder filling. The PTV is a geometric concept, and takes into account the net effect of all possible geometrical variations in patient set-up. The PTV is created when a margin is

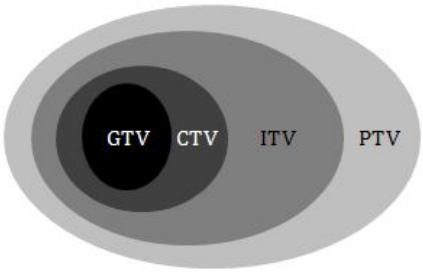

Figure 1.5: Geometric representation of the GTV, CTV, ITV and PTV concepts defined in ICRU 83[3]

added to the CTV to take into account tumour position uncertainties and variations. The use of patient-immobilisation devices, quality-assurance programs, image-guidance systems, and other uncertainty-reduction techniques can significantly reduce the size of the required margins.

The delineation of the GTV and CTV should be independent of the irradiation techniques, and is based only on oncological evidence. The volume delineation is not dependent on whether photons, electrons, protons, or any other type of radiation is being used. In order to compare or retrospectively analyse treatment plans for more than one radiation modality, it is important to not let the modality define the treatment volume delineation. Unlike the GTV and CTV, the ITV and PTV are dependent on the technique and are part of the treatment prescription.

Even though the GTV, CTV, and OAR are anatomical concepts, outlines on an imaging modality scan form representative volumes that are used in the planning process, a snapshot of the anatomy at a given time. As the patient's position will affect the location and shape of the internal anatomy, all volumes should be contoured as a representation of the patient's anatomy under treatment conditions. Movement or anatomical changes in the patient can be visualised using a four-dimensional representative imaging scan: a respiration-correlated CT scan for a lung cancer patient, where the fourth dimension is time, allows visualisation of time-dependent changes in the shape and position of the lung tumour so that its full extent can be covered for treatment.

1.3 Radiation Physics Principles

In radiotherapy, the amount of dose that is deposited in the patient is determined by the interactions of the incident photons through the various tissues. These interactions are governed by a set of physical processes that depend on the energy of the radiation beam.

Initially, the photon interactions are determined by the linear attenuation coefficient (μ, cm^{-1}) between the photon and the tissue. The linear attenuation coefficient is the probability of a interaction occurring per unit distance, and is dependant on the incident photon energy (E, MeV), the tissue density ($\rho, g/cm^2$), and the tissue effective atomic number (Z_{eff})[16].

Energy fluence ($\Psi, MeV/cm^2$) is determined by the photons that reach a defined point within the patient. At that point, the total energy released per unit mass (TERMA) is a product of the

mass attenuation coefficient (μ/ρ) and the energy fluence [16, 17].

$$TERMA = \frac{\mu}{\rho}\Psi \tag{1.1}$$

However, not all of this energy is absorbed by the medium, and the absorbed dose is dependant on the kinetic energy released per unit mass (KERMA) to charged particles only. The deposition of energy in the patient is therefore a two step process; firstly the incident photons release kinetic energy to charged particles (KERMA), and secondly the charged particles release this energy through ionisation interactions along the charge particle tracks (Dose) [16, 17].

1.3.1 Particle Interactions with Matter

Three photon-tissue interactions dominate the KERMA process: the photoelectric effect, the Compton effect, and pair production. For the energy range seen in radiotherapy (0.1-18MeV), the Compton effect dominates for water-equivalent tissues (Z=8), contributing to >80% of all interactions [16], as seen in Figure 1.6a. The proportion of Compton scattering is also dependent on the electron density (ED) of the medium, where ED relates to the ratio of the number of electrons in an atom of volume V.

The Compton effect represents the interaction between a photon and an orbital electron, and is

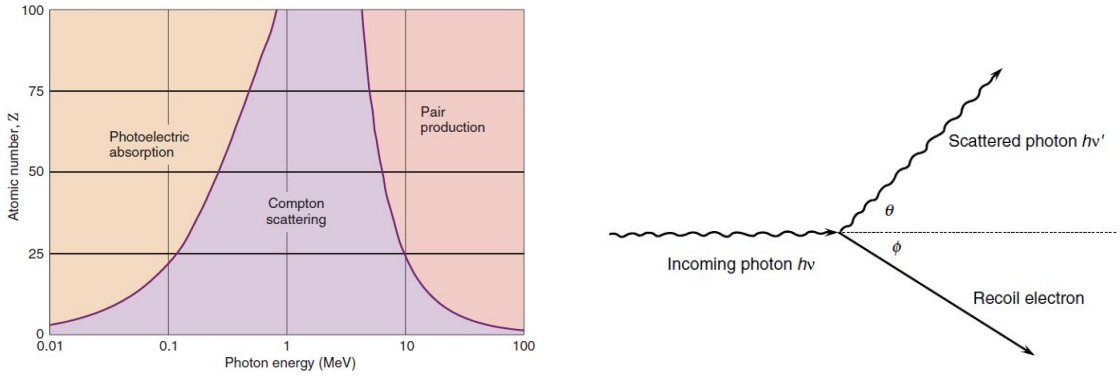

(a) (b)

Figure 1.6: (a) The most probable interaction versus photon energy (MeV) for tissues of different atomic numbers (Z). Compton scatter is most common in the megavoltage radiotherapy energy range (6-18MeV). Adapted from [4]. (b) A basic visualisation of the Compton effect. An incoming photon interacts with an orbital electron, producing a scattered photon and a recoil electron. Adapted from [5].

visualised in Figure 1.6b. In this case, the energy (hv) of the incident photon energy is greater than the energy binding the orbital electron to the atom [6]. The incident photon imparts a portion of its energy to the recoil electron, allowing it to exit the atom, while the photon is scattered with energy hv' through a scattering angle θ.

The Compton electrons ultimately deposit energy in the tissue through multiple Coulomb collisions over the particle track. This process converts the kinetic energy of the electrons to ionisations and excitations in the tissue. The mass collisional stopping power (S_{col}/ρ) describes the rate at which the energy is lost by the electron per unit path length and per unit density of the medium.

The range (R) of charged particles is determined by integrating the mass collisional stopping power over the possible electron energies. Although the charged particles lose energy in bursts with each interaction, a continuous slowing-dose approximation (CSDA) is used to define the range (R_{CSDA}).

1.3.2 Particle Equilibrium

A charged particle equilibrium (CPE) exists when the charged particles entering and leaving a small theoretical volume are in equilibrium. When CPE is achieved, the dose absorbed in a volume is equal to KERMA. In practice, achieving CPE is impossible, due to beam divergence, scattering, and photon attenuation [16]. As a result, transient charged particle equilibrium (TCPE) is defined,

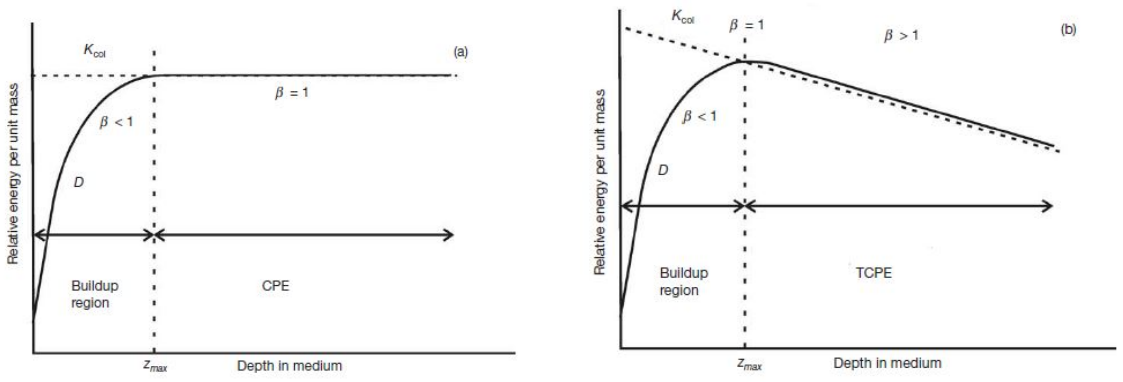

(a) CPE (b) TCPE

Figure 1.7: KERMA and absorbed dose as a function of depth in a medium irradiated by a high energy photon beam for the cases of CPE and TCPE. Adapted from [6]

where the dose is in an approximately constant relationship to KERMA as photon attenuation is assumed to be constant.

The differences between CPE and TCPE are outlined in Figure 1.7. In both cases, CPE is not maintained at shallow depths as KERMA is greater than the dose absorbed, resulting in a build up of dose. This is due to the fact that the secondary electrons are directed in the forward direction, and deposit dose away from the point of interaction. As the depth approaches the range of the secondary electrons (z_{max}), TCPE can be achieved in both the longitudinal and lateral directions.

1.3.3 Lateral Electronic Disequilibrium (LED)

In reality, under TCPE conditions the secondary electrons generated from high-energy photons travel farther in low-density lung tissue than in water-density tissue due to the fact that there are fewer opportunities for energy release. This is known as lateral electronic disequilibrium (LED), and occurs when the lateral range of the electrons that are depositing dose in a medium become greater than the range of the volume [17]. As a result, more electrons scatter beyond the intended volume and are not replaced, so the dose along the central axis decreases and more dose is deposited out of field[17]. This is visualised in Figure 1.8.

The lateral spread of dose has an effect on the shape of the beam. Modelling this effect results in an increase in the field width and a decrease in dose at the edge of the field [18]. This effect has also been shown to increase with smaller fields, higher beam energy, and lower lung densities

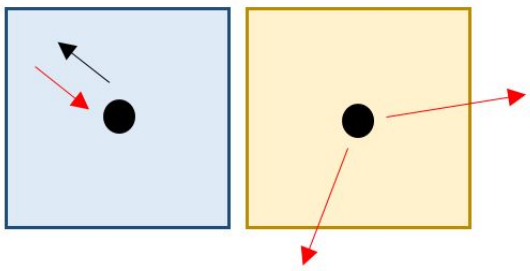

Figure 1.8: A visualisation of the concept of LED. In the water medium, the range of the scattered electrons is less than the size of the field, so outwardly scattered electrons (red) are replaced by inwardly scattered electrons (black). In the lung medium, the range of the outwardly scattered electrons is greater than the field size, so they are not replaced.

[19]. The concept of LED is of particular interest to this study, as it limits the accuracy of dose calculation in the target volumes.

1.3.4 Primary and Scattered Dose

Although both primary and secondary particles contribute to the dose received by the patient, it is more common to separate the total dose into 'primary' and 'scattered' components. Primary dose refers to the the photons that are incident on the surface of the patient. This can arrive directly from the radiation source, or from interactions with the treatment head [16]. These interactions produce secondary electrons as well as scattered photons. The primary contribution to dose measured at depth in a material will depend on the distance from the source, the amount of head scatter, and the attenuation of the beam. Attenuation is determined by the degree of absorption and scatter, both of which depend on the beam energy and depth of material [16].

The 'scattered' proportion of dose is deposited by photons that have previously interacted with the medium. This includes Compton-scatter photons. After each interaction, the recoil angle of the photon changes randomly and the energy spreads away from the initial interaction point. As the majority of the dose is projected in a forwards direction, with scatter contributing less at greater distances from the central axis, the lateral profile of the beam can be simplified to a Gaussian distribution, as seen in Figure 1.9 without the flattening filter.

In the linac, a flattening filter is used to create a uniform dose across the central region of the

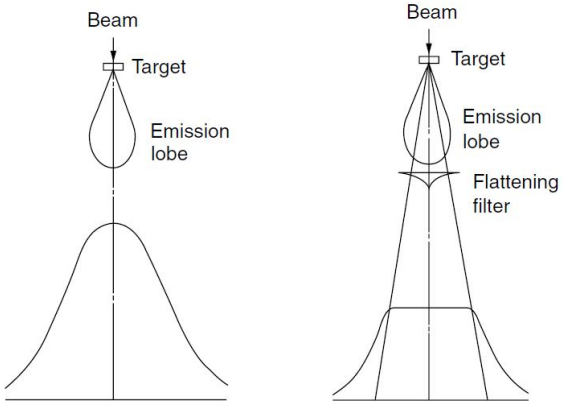

Figure 1.9: An idealised linac beam profile, without and with the flattening filter. Adapted from [5].

beam profile, which is achieved by attenuating the Gaussian shape of the profile as seen in Figure 1.9. The uniform central region is desired as dose calculations were based on look up tables, which could be simplified for uniform beams. Although dose calculation is now performed by computerised planning system, the majority of linacs still contain the flattening filter.

The beam profile consists of three key areas; the central region, the penumbra, and the umbra [6]. The central region consists of the area within 1-1.5cm from the field edge. The penumbra region falls off rapidly and is defined by the field edge and the degree of LED, and relates to the distance between the 80% and 20% dose regions. At greater depths, the degree of scattering is greater, and so the penumbra of the beam increases. The umbra region is the far out of field low dose region, outside the 20% dose region. Although the majority of dose is delivered in the central region of the field, the penumbra region contributes a non-negligible dose to the patient, so requires accurate modelling.

1.4 Stereotactic Body Radiation Therapy

Stereotactic Body Radiation Therapy (SBRT), also referred to as Stereotactic Ablative Radiation Therapy, is a method of delivering high doses of radiation to small tumour volumes in a smaller number of fractions compared to conventional radiation therapy [20, 21]. The main characteristics of SBRT include;

- a total prescribed dose in the order of 10-50Gy or higher to a small planning target,
- a small (3-5) number of fractions, compared to conventional treatment schedules (20-30),
- accurate positional delivery of the dose to the target,
- and a highly conformal dose distribution to the target shape with a steep dose gradient outside of the target volume [22].

Through the use of SBRT, the patient is able to receive a dose equivalent to the biological effect of delivering 100Gy with conventional radiation therapy[20]. Not only does this method increase local control of the tumour, SBRT also has the added benefit of shortening the overall treatment schedule, making it a desirable treatment from a patient's perspective.

However, SBRT is not a suitable treatment option for all radiotherapy patients. An increase in local control of the tumour is only achieved through a labour and resource-intensive patient selection, simulation, planning, and treatment delivery process. Studies comparing the effects of SBRT on lesions located in the centre and periphery of the lung have shown an increase in high-grade toxicities for centrally located lesions [23]. While the peripherally located lesions showed acceptably low toxicities, for centrally located lesions the toxic effect on the central airway, esophageal, pulmonary, chest wall and skin resulted in radiation pneumonitis, vascular injury, airway stricture, and necrosis, to name a few [23]. This resulted in limiting the cases in which SBRT would be recommended, as the associated risks were deemed too high.

In order to maintain acceptably low toxicity, several steps are taken to limit the dose received by the OARs surrounding the tumour site [22]. This includes more accurate immobilisation to ensure the patient is in the same position during every treatment, allowing smaller margins to be used around the target; the use of intensity modulated radiation therapy to shape the dose away from the OARs; more advanced treatment planning; and extensive imaging techniques, including the use of four-dimensional computed tomography (4DCT) for accurate delineation of the tumour and imaging both prior to and during treatment to ensure accurate patient positioning [24].

1.4.1 Historical Development of SBRT

The founding principles of SBRT were initially developed in 1951 by Swedish Neurosurgeon Lars Leksell, as a technique for the treatment of intracranial disease known as stereotactic radiosurgery [5]. Initially, this technique involved delivering a high dose of radiation (100s of Gy) in a single session with 200kVp orthovoltage X-rays, providing a once-off treatment more similar to surgery[6].

A three dimensional stereotactic system was developed for locating targets within the brain using an external frame attached to the skull of the patient[22]. With the increased accuracy in dose delivery provided by the stereotactic frame, it was possible to increase the amount of dose delivered to the tumour without increasing the dose received by the organs at risk around the target, due to the rapid dose fall off outside the PTV.

Based on the clinical experiences of stereotactic radiosurgery, the principles were transferred to extra-cranial sites in the 1990s, at Karolinska Hospital in Sweden, in particular lung and liver sites.

This technique involved the use of megavoltage X-rays and became known as SBRT.

1.4.2 Radiobiological Basis for SBRT

A fraction size of approximately 2Gy is considered the 'gold standard' for conventional fractionation for most radiotherapy treatments sites [25]. The 2Gy fraction has formed the basis for the majority of long term clinical studies, and as a result is deemed as a standard fraction size. With the technological advancements of the past few decades, in terms of three and four-dimensional imaging, computerised planning, and the introduction of intensity modulated radiation therapy, it is now possible to achieve highly conformal radiation therapy [25].

In accordance with TCP and NTCP principles, this allows for an increased amount of sparing in the adjacent normal tissue, making it possible to increase the dose delivered to the target. In addition to the technological advancements, the radiobiological modelling of TCP and NTCP have been redeveloped to include the dependence of cell killing on total dose, fraction size, and dose rate, as well as the 'volume effect' for late complications in normal tissues[25]. This described the different behaviour for different tissues, where either damaging a sub-unit of the organ disables it's entire function, e.g. spinal cord, or the organ can still function when a large number of sub-units are damaged, e.g. lung.

1.4.3 SBRT for Lung Cancer

In moving from intracranial stereotactic radiosurgery to extracranial sites such as the lung, there is a departure from the assumption that the PTV is immobile inside the stereotactic frame [22]. This introduces the potential for dose-delivery errors as it is possible for the soft tissue to be mobile. To overcome this, extensive pre-treatment imaging and immobilisation management is required.

One of the issues associated with treating lung cancer with radiotherapy is the motion of the tumour caused by the patient breathing. In SBRT, this issue becomes an even greater challenge with the addition of the smaller expansion of the PTV around the ITV, with a sharp dose gradient beyond this target volume [22].

The SBRT Lung program at Christchurch Hospital is based on the criteria introduced by the Trans-Tasman Radiation Oncology Group (TROG) trial 09.02, known as the CHISEL trial. The full

title of this trial was *"A Randomised Phase III Trial of Highly Conformal Hypofractionated Image Guided ("Stereotactic") Radiotherapy vs Conventionally Fractionated Radiotherapy for Inoperable Early Stage I Non-Small Cell Lung Cancer (NSCLC)"*. The primary objective of this trial was to test whether hypofractionated radiotherapy (SBRT) results in better local control in patients with inoperable T1, and T2a NSCLC compared with the standard care of 3DCRT. The patient selection criterion excludes the following patients:

1. Those with tumours larger than 5cm.
2. Tumours close to critical structures such as the chest wall, heart, and mediastinum.
3. Prior chemotherapy or radiotherapy to the area being treated.

1.5 Tumour Imaging for Radiation Therapy

In order for a course of Radiation therapy to limit the damage to the normal tissue, the exact location of the target needs to be determined. With highly conformal techniques, such as SBRT as well as intensity modulated radiotherapy (IMRT), accurate knowledge of the tumour object in three dimensions is critical to creating an accurate three-dimensional dose distribution [26].

Pre-treatment imaging in Radiation therapy serves two main purposes. First, the clinician must define the shape, size, and location of the tumour volume, as well as any surrounding objects at risk. Following this, the images are used to calculated the dose to be delivered to the target volumes[5].

CT is the most commonly used modality for pre-treatment imaging, due to the high levels of geometric accuracy, wide availability, and speed of acquisition [6]. CT scanners exhibit good contrast resolution for both soft tissues for target delineation and bony anatomy for aligning the patient during treatment or visualising bone invasion.

A 3D set of imaging data is produced by the CT scanner, which is imported into a commercial TPS. Other treatment modalities can be used for target volume and OAR definition, in particular magnetic resonance imaging (MRI) with it's improved low contrast resolution compared to CT. However, CT images are particularly advantageous for calculating dose. This is due to the fact that CT images create an indirect representation of the EDs for the different tissue types in the CT image set [6].

As previously mentioned, the megavoltage radiation interacts with the different tissue types predominately via Compton Scattering. As the tissue changes, the radiation attenuation within the tissue also changes [6]. By applying a correction factor to go from the kilo-voltage CT image data to the megavoltage radiotherapy beam, the CT image ED data set can be used for calculating the dose to the region [6].

The pixel information in a CT image is defined using Hounsfield Units (HU), an arbitrary scalar with a value of -1000 for air and 0 for water. The relationship between HU and ED is specific to the scanner and the energy, and is defined using a CT to ED lookup table in the TPS. The use of ED information is especially important for inhomogeneous regions, such as the lungs with lung, bone, and soft tissue all present, as the different attenuation properties of the tissues have a large effect on dose calculation [6].

A standard CT scan is primarily defined by two parameters, the beam energy (kV) and the beam current (mA). mAs relates to the number of X-rays that are produced at a given time, where as kV describes the penetrative power of the beam. These two parameters are changed depending on the area being imaged. kV changes the CT to ED table, so usually only one kV value is used for all adult patients. A lower kV can be used for paediatric patients as there is less tissue to penetrate. The mAs parameter is primarily varied, increasing for dense regions where more X-rays are required to form an image of clinical use. However, increasing the mAs increases the dose to the patient. As this increased dose may not be of clinical benefit, the mAs is kept sufficiently low so that good image quality is achieved but the patient is not unnecessarily overdosed.

1.5.1 Lung tumour imaging and localisation

The delineation of the target in lung cancer imaging is especially difficult due to the additional issue of patient breathing motion. In addition to a CT scan, a positron emission tomography (PET) scan can be used as more information about the functional extent of the tumour can be determined with PET. However, while a PET scan is useful for Lung SBRT, it cannot be used for contouring. Rather, it can only confirm the extent of the ITV determined from the CT scan, as PET does not have the required spatial resolution for contouring. Also, PET image acquisition is slow and so all phases of lung motion are shown on the final image.

With three-dimensional planning, a dose distribution that closely conforms to the target volume is achieved, however this also increases the potential for a partial or full miss of the target. It is possible to include the temporal changes in the imaging, treatment planning, and delivery processes to minimise the effect of the uncertainty in the tumour position on the patients outcome [27].

The most common technique for managing the temporal tumour variation is four-dimensional imaging, including respiration-correlated 4DCT scanning [28]. This technique is now routine for treatment planning in lung cancer treatment. A 4DCT scan is in essence a time resolved CT scan, comprising of a series of CT data sets of the patient anatomy in several phases of the breathing cycle. It is usually acquired using a scan with fast rotation period and slow couch movement. From this it is possible to acquire enough information for all phases of the breathing cycle for all parts of the anatomy, providing both spatial and temporal information on the tumour volume as well as surrounding structures[28, 27].

The data from the 4DCT is retrospectively sorted following the completion of the scan, following the correlation of the 4DCT scan with the patient breathing trace that is recorded concurrently [28]. Typically, ten 3D data sets are correlated to the respiration pattern (bins), such that structures can be identified in each individual phase of the breathing cycle. Delineating the GTV therefore requires contouring on each of the phases of the 4DCT scan. In practice, this is time consuming, so a composite of the the 4DCT scan is used to represent the full extent of tumour motion, known as the Maximum Intensity Projection (MIP) [28]. A MIP image displays each voxel as the highest intensity value across all phases of the breathing cycle. A lung tumour is therefore displayed as a

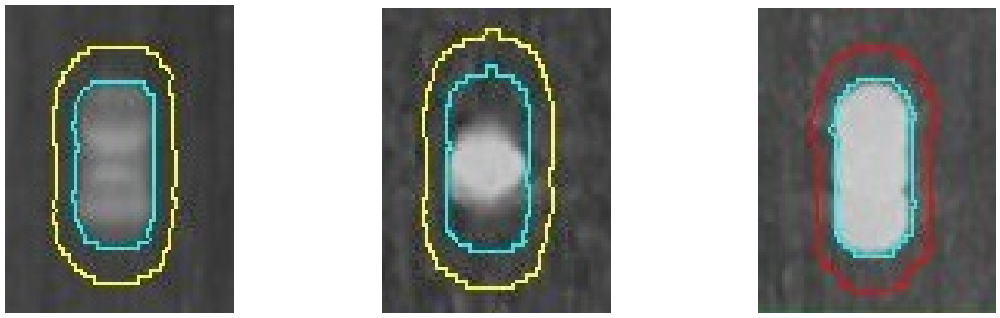

(a) (b) (c)

Figure 1.10: Various clinical representations of 4DCT image data. (a) the Average Intensity Projection (AIP), (b) the Free Breathing (FB) representative phase, (c) the Maximum Intensity Projection (MIP).

solid object where each location of the tumour during the breathing cycle is taken into account, simplifying the generation of the ITV [28].

While this allows for accurate definition of the tumour volume for contouring purposes, an issue arises when applying the 4DCT data set to dose calculation algorithms [27]. In practice, a 'static' treatment plan is generated for a 4DCT data set. A static dose distribution is calculated based on the EDs for a single point in the breathing phase, the free breathing (FB) phase, or an average projection of the tumour position, the average intensity projection (AIP). These different projections can be seen in Figure 1.10. Treatment planning on a scan that does not represent the tumour position adequately will result in systematic errors being applied to the plan, where the calculated dose does not represent the dose delivered during treatment [27].

1.5.2 Issues with 4DCT

4DCT data are used to localise and quantify the extent of the tumour and surrounding normal tissue, so are used extensively in the treatment planning process, in particular when deciding to treat the patient with motion management techniques. As a result, ensuring the 4DCT is accurate is paramount to achieve effective control of the tumour.

In practice, imaging moving objects commonly results in a variety of motion artifacts, separate to the artifacts already seen in CT imaging. Motion artifacts most commonly take the form of discontinuities in voxel intensity in the scan direction, and depend largely on the relationship between the scanning parameters and the breathing motion [27]. If the tumour is moving faster than the CT scanning speed, the tumour can appear elongated. If the scanning speed is much faster than the tumour speed, the tumour shape and position will be reconstructed based on an arbitrary part of the breathing phase, resulting in a distorted position or shape. [29] Even with optimal scanning parameters, artifacts can still occur due to irregular breathing traces, for example coughing or patient motion during the scanning process [30].

In addition to the issues associated with motion artifacts, 4DCT also results in a higher dose being delivered to the patient as 10 times the amount of data is acquired. This poses issues with re-scanning the patient, making artifact reduction even more critical. Errors caused by a poor 4DCT pass through to all facets of the treatment process, with every fraction being delivered incorrectly.

Due to this, careful acquisition and analysis of the 4D scan is required.

1.6 Treatment Planning

The aim of a treatment planning algorithm is to accurately calculate the dose to different regions of the patient anatomy to determine if a plan has the necessary therapeutic effect. For a course of radiotherapy to be successful, it is therefore important that the dose calculation algorithm is highly accurate[31]. ICRU Report 50 recommends that for the best clinical outcomes, the dose to the PTV should be within +7 or -5% of the prescribed dose [14]. To achieve this, accuracy in every stage of the treatment process is required to deliver an acceptable dose.

1.6.1 History of Dose Calculation in Radiation Therapy

Prior to the extensive use of computers, dose was calculated manually based on patient port film images and isodose curves. In the 1970s, a digital computer system was developed for treatment planning, known as the Bentley-Milan model[32]. This model involved beam data specific to the linac being sorted in a tabular form, comprising of central axis depth-dose data and off-axis ratio data[5].

The use of computer-based TPSs was first described in ICRU Report 42, which outlined the development of photon and electron dose calculation algorithms [33]. Several models for beam calculation are described in ICRU 42, including Tabular or Matrix formats and Beam Generating functions. However, these models were limited to calculating 2D dose distributions for square and rectangular fields and do not separate primary and scattered radiation. The advances to patient imaging, in particular CT, introduced the need for 3D dose calculations, and the need to account for inhomogeneities within the patient[34].

1.6.2 Dose Calculation Algorithms

As mentioned previously, separating the components of the radiation beam into primary and scattered radiation results in a more accurate dose calculation method. Primary radiation is defined as the component of the radiation that is incident on the surface of the target, and includes photons

coming from the target as well as any scattered photons from the collimation system. Scattered radiation, or secondary radiation, is created through interactions that the primary radiation has with the medium. Currently, dose calculation algorithms can be grouped into three distinct groups; correction-based, model-based, and principle-based algorithms [35]. Model-based and principle-based algorithms are of the greatest relevance to most modern TPSs.

Model-based algorithms originated by defining simple beams in water based on empirical methods for dose calculation. Initially, these involved two mathematical equations for central axis depth-dose values and off-axis ratios, with dose determined by multiplying the two parts. The limitation of this was that the dose was accurate under reference conditions, but required many correction factors when applying them to situations involving patients. These correction factors become inadequate as the situation becomes more complex and greater accuracy is needed for more conformal treatments.

The superposition method can be seen as an extension of the simple empirical method. The superposition method involves considering both primary and secondary particles, where the dose at a point $P(x, y, z)$ can be considered the sum of both energy contributions for volume elements $dV(x', y', z')$. The initial energy can be defined as the sum of the energy fluence of the primary photons, $p(x', y', z')$, and the scatter energy per unit photon fluence that reaches point P, $s(x, x', y, y', z, z')$, over a scattering volume V[5]. This can be seen in Equation 1.2, and visualised in Figure 1.11.

$$D_P(x, y, z) = \iiint_V p(x', y', z')s(x, x', y, y', z, z')dV \tag{1.2}$$

In addition to the analytical model-based algorithms, Monte Carlo (MC) simulations can be used to predict radiation transport. This involves calculating the dose based on the individual interactions for million of photons originating in the treatment head and interacting with the medium, based on the statistical likelihood of a particular interaction happening [34]. In terms of accuracy, this results in the most realistic model of dose transport for both homogeneous and inhomogeneous media, however the amount of time and computer processing power required for this is high[5].

Although MC algorithms are routinely used clinically for particular situations where addi-

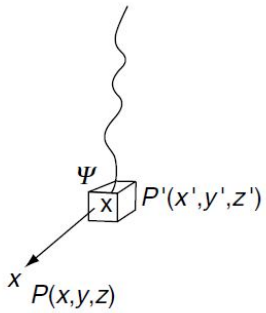

Figure 1.11: A visualisation of the dose at P, calculated from the integration of the energy released from a volume dV' centred on P'. Adapted from [5]

tional accuracy is required, modern TPSs most commonly implement a point kernel convolution/superposition algorithm [5]. This is seen as an acceptable compromise between the limitations of superposition methods and the accuracy achieved with the resource intensive MC calculations. For point kernel convolution/superposition algorithms, physical processes are simplified using a convolution equation that convolves the total energy released per unit mass of primary photons with a point kernel that describes the contribution from scattering photons and electrons [35]. If the algorithm takes into account the change in the radiological path length for different types of media, the method is called convolution/superposition [35].

For a homogeneous medium, the dose to a point can be described as the 3D integration over the entire volume, determined using Equation 1.3 [5]. In this case, μ/ρ is the mass attenuation coefficient for the medium, $\Psi(x', y', z')$ is the energy fluence at point P', $K(x - x', y - y', z - z')$ is the energy deposition kernel, also referred to as the point spread function, and $dV = dx, dy, dz$ is the elementary computation voxel for point P.

$$D(x, y, z) = \iiint \frac{\mu}{\rho} \Psi(x', y', z') K(x - x', y - y', z - z') dV' \tag{1.3}$$

Although the superposition/convolution algorithms can achieve similar results to MC for simple clinical situations, but with improved speed of computation, there are inherent limitations. The most important of these, and the most relevant to this research, is the poor accuracy of the algorithms with respect to inhomogeneous media and build-up regions. This is of particular importance in the lung with high energy photon beams, where the incident radiation needs to be deposited in

a high density tumour volume, taking into account the dosimetric impact of the surrounding lung and bone.

1.6.3 Dose Calculation in Inhomogeneous Media

Several studies have examined the impact of different dose calculation algorithms on the dose delivered to inhomogeneous media, in particular lung [31, 36, 37]. It is recommended that collapsed cone convolution (CCC) algorithms, a variation on the convolution-superposition algorithm, be used when MC is not readily available. CCC algorithms model energy transport along fixed axes, scaling the energy deposited in the different voxels according to the physical properties of the materials along the axis [31].

Although CCC algorithms can model the lack of backscatter outside of the patient contour, as well as the dose distributions inside homogeneous regions of lung and soft tissue, the model is unable to accurately calculate dose at the interfaces between lung and tumour[31]. This is due to the fact that the TCPE at the tumour-lung interface does not hold, and the CCC algorithms cannot accurately model this [37]. These uncertainties have been shown to increase with smaller treatment volumes, where the the ratio of tumour-lung interface to tumour volume increases with decreasing target volume [36, 37].

In addition to this, during treatment as the GTV moves through the ITV that was defined with the 4DCT scan, the dose to the tumour will change relative to the original treatment plan. As the GTV moves to part of the ITV that is under-dosed on the treatment plan, the GTV will receive a larger dose than expected due to preferential dose build-up in higher density areas[38, 36]. Both of these factors compound to increase the uncertainty in the treatment planning process for lung tumours.

1.7 Quality Assurance in Radiotherapy

Although QA is performed on all aspects of the Radiotherapy process, including linac, treatment-planning, and imaging, for SBRT additional patient-specific QA needs to be performed. This is to ensure the accurate and safe treatment of the patient. The goal of dose validation is to verify that

the dose distribution determined by the TPS matches what would be delivered to the patient [6]. This is achieved by performing a variety of physical end-to-end measurements, which can either measure the dose at a specific point or the full dose distribution. This study involves performing both point dose and dose distribution measurements.

Measurements of point dose can be performed with ionisation chamber or diodes, whereas dose distribution measurements can be performed with radiochromatic film or dedicated QA phantom detectors that resemble the shape of the patient, with multiple small detectors positioned to create an array. The type of test and its specificity results in different pass criteria being applied. For dose distribution measurements, gamma analysis is performed to quantify how well the measured dose plane agrees with the TPS dose plane. The gamma analysis criteria used for this study is explained in full in Appendix A. For point dose measurements, a measured charge in an ionisation chamber is converted to a dose value which is compared to the expected dose from the TPS at the same point. The conversion from charge to dose used for this study is explained in full in Appendix B.

1.8 Literature Review

A literature review was conducted to look at the current state of knowledge regarding the use of density overrides for 4DCT-based treatment planning and the alignment of this with stereotactic ablative radiotherapy for lung patients.

From this literature search, three papers specifically investigated either ITV or PTV density overrides for Lung SBRT planning [39, 40, 41] while others investigated the issues surrounding lung SBRT planning, including temporal and density variations in PTV/ITVs, and other predictive dosimetric factors that affect conformity in Lung SBRT [42, 43, 44, 45, 46, 38].

Several studies also looked at the dosimetric effect of different TPSs in SBRT for lung cancer, including comparisons between algorithms such as Acuros XB (AXB), Analytical anisotropic algorithm (AAA), X-ray voxel-based Monte Carlo algorithms (XVMC), and their implementation in systems such as SmartArc (Pinnacle) and RapidArc (Eclipse) planning [47, 48, 49].

Fu et al. (2013) devised a method for overriding the density of the PTV to reduce the planned MU while still delivering sufficient dose to the tumour for SBRT lung planning [39]. Twelve patients had their plan MU recalculated with the PTV density assigned to $0.8 g/cm^3$ using Pinnacle treatment planning software, with no algorithm being specified. Three patients had four CTV structures copied and placed at the PTV border, with the CTV density set to $1.0 g/cm^3$ and the PTV-CTV volume density set to $0.2 g/cm^3$. These plans were then recalculated with the MU from the density override plan.

For nine of the twelve patients, the MU was reduced by an average of 3% while for the other three patients who had CTV sizes of less than $1.2 cm^3$, the reduction in MU was on average 10%. Density redistribution was applied to these plans with an average CTV coverage of 95%. This study was able to show a significant reduction in MU for small CTV volumes whilst still delivering a tumouricidal dose to the intended area. The limitation of this study is that it only looked at the MU reduction for a PTV density nominally set to $0.8 g/cm^3$, which may not necessarily be clinically relevant.

Also, this study only looked at the reduction of MU and Dose Volume Histograms (DVHs) from the generated plans, rather than any other statistical analysis between the density overridden plans

and the original densities of the CTV/PTV. The analysis that is used is based off the TPS results only, and it would need to be verified with in-phantom measurements that the treatment planning algorithm is calculating the dose in the overridden density correctly.

Wiant et al. (2013) compared the use of free-breathing CT scans, time average scans, and ITV density overridden scans for lung SBRT to evaluate how accurate each method is at predicting dose deposition in lung tissue [40]. A QUASAR Respiratory Motion (QUASAR) Phantom was used to model the target motion while a free breathing (FB) and 4D-CT scan were acquired. The ITV was defined on the 4D-CT with the PTV set as a 5mm expansion. Four image sets were created from this data: The time average, free breathing, free breathing with the ITV set to tissue density, and free breathing with the PTV set to tissue density.

Plans on the TPS, which in this case was an Eclipse TPS with no specified algorithm, of 10Gy to 96% of the PTV were planned and delivered, with measurement coming from Gafchromic EBT3 film placed inside the phantom target of the QUASAR Phantom. This was then analysed with a gamma metric of 1mm/1%. The gamma pass rates were 77.9%, 83.6%, 89.1%, and 92.7%, for time averaged, free breathing, ITV, and PTV plans respectively. Profiles were also taken in the direction of travel, which showed doses 5-10% higher than the prescribed dose for the FB and time averaged plans, approximately 2% for the ITV plan, and good agreement for the PTV. This gives a simplified overview of the possibilities of overriding density, which opens up many avenues for further research.

The study only looks at the 2D sinusoidal motion of a QUASAR Phantom that does not correspond directly to patient breathing motion. Further statistical analysis could also be done between the plans, as well as looking at creating a density gradient between the ITV and PTV so as to more realistically portray the density in the target volume. Also, this only uses one TPS, so the result is only valid for the Eclipse TPS software, rather than being valid across algorithms.

A further study by Wiant et al. (2014) took a specific look at volumetric modulated arc therapy (VMAT) plans, an extension of the previous study [41]. Five VMAT plans were created on free breathing (FB) scans, time average scans (TA) , free breathing with the ITV set to tissue density (IFB), and free breathing with the PTV set to tissue density (PFB), and a hybrid override with the ITV set to tumour density and PTV-ITV set to an intermediate density between lung and tumour

(HP), and looked at the result on a selection of patient cases as well as for a 4D Motion Phantom.

Although these previous studies have looked at simple cases for validating density overrides of the ITV and PTV, this has currently not been extended to any other dose calculating algorithms and a range of tumours sizes. Table 1.1 shows the variation between different studies in terms of equipment and density overrides investigated. in It is known that LED has a larger effect on small fields in the lung, so a single density override may not apply to all cases as the contribution of the uncertainties may be greater. Also overriding the density of the PTV to a variety of low densities between lung and water has not been investigated. This study will look into these areas to quantify the effect of density overrides to see if there there is a trend based upon the relative sizes of the ITV and PTV.

Study	Linac	TPS Software	Density Override
Fu (2013) [39]	Not specified	Pinnacle	PTV
Wiant (2013) [40]	Varian TrueBeam	Eclipse	ITV, PTV
Wiant (2014) [41]	Varian TrueBeam	Eclipse	ITV, PTV, and Hybrid

Table 1.1: Overview of the parameters and equipment used for the previously published density override studies

2

Method & Materials

To assess the impact of various density overrides on SBRT lung plans, a phantom study was conducted on the Christchurch Hospital Elekta Synery Linac and Monaco 5.1 TPS. A phantom was used to mimic an adult patient, including lung and tissue density materials and breathing motion. An end-to-end test using the phantom was performed, including 4DCT data acquisition, tumour definition, treatment planning, and pre-treatment QA. This followed the standard procedure for the patient process in Radiotherapy as discussion in section 1.1.3. The following section covers the experimental set-up, equipment used, and the measurement process. Two different areas of measurement were considered; the improvement to the plan in terms of target coverage and conformity on the TPS, and the dosimetric accuracy of the plans when delivered, measured using two independent systems.

2.1 Phantom Study

2.1.1 QUASAR Phantom

A QUASAR^{TM} Programmable Respiratory Motion Phantom (Modus Medical Devices Inc., London, Ontario, Canada) and modified inserts were used to simulate the motion of a lung tumour inside a SBRT patient. The QUASAR phantom mimics the temporal variation of a lung tumour by moving cylindrical inserts in a superior/inferior direction (head to feet) within a thorax-shaped poly-methyl methacrylate (PMMA) block. The dimensions of this phantom are 20cm anterior/posterior, 30cm left/right, and 8cm superior/inferior. To indicate the position of the centre phantom for easy alignment with the CT and treatment room lasers, positioning lines are located on the sides and top surface of the PMMA block. The PMMA block has three 8cm diameter cylindrical cavities that run superior/inferior, as seen in Figure 2.1. These cavities can be used to house different types of inserts for holding chambers and film, and also for assessing the image quality of 4DCT systems. There is an additional 2cm diameter cavity below the central cavity used to represent the spinal

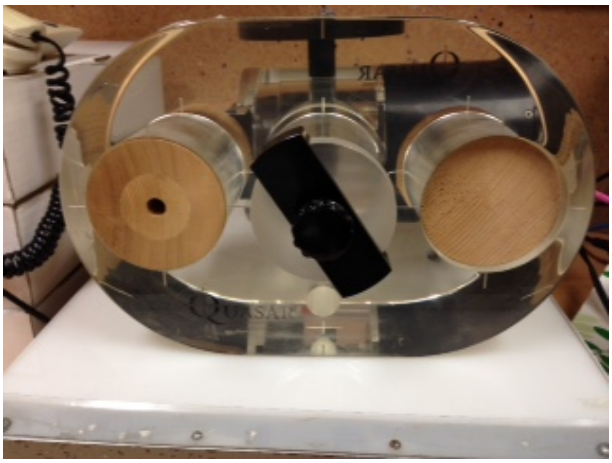

Figure 2.1: The QUASAR^{TM} Programmable Respiratory Motion Phantom used at Christchurch Hospital, with a cedar ion chamber insert on the left and a cedar filler insert on the right.

column; however this was not used for this research.

The dimensions of the phantom are similar to the shape and size of an adult patient, while still remaining easy to position and set-up, with a sufficient amount of build-up for dosimetric purposes. It also has the ability to vary both the speed and amplitude of the connected inserts through the use of a DC motor and adjustable amplitude scale, while keeping the rest of the phantom stationary. In this way, a tumour object embedded in a cylindrical insert appears to move like a lung tumour, while the rest of the phantom remains stationary like a patient. The QUASAR phantom comes with a MATLAB program and graphical user interface so that sinusoidal, regular, and irregular breathing patterns can be created.

2.1.2 Lung Inserts

The simple design of the QUASAR Phantom cavities allow for a large variety of inserts to be developed to meet a range of purposes. For this research, it was necessary to design a QUASAR insert that met the following criteria:

1. It must be made from a lung equivalent material,
2. It must have a centrally located sphere made from tumour equivalent material,
3. It must be able to hold either a piece of film or an ionisation chamber for dosimetric purposes.

The specificity of the lung insert design meant that it would need to be manufactured in-house, so a range of materials were investigated as options for the low density material. Initially, cedar wood was considered as Modus Medical Devices already used it as their lung equivalent material, however there were issues with procurement and cost. As a solution to this, the feasibility of 3D-printing the low density material was investigated to utilise the in-house 3D Printing Program at Christchurch Hospital.

3D Printing Lung Inserts

In order to ensure the lung insert was made from a lung equivalent material, a reference lung material had to be determined so as to act as a baseline. The lung material described in ICRU-44 was chosen as the reference as this is the most common lung reference in radiotherapy [7]. Several physical and radiological properties were available for this material, a list of which can be found in Table 2.1.

For a material to be deemed an acceptable lung substitute, it needs to have comparable values to those seen in Table 2.1. The suitability of a 3D printed lung material was initially tested to meet these properties.

Initially, a test insert was printed incorporating a reticulated lattice structure of water-density plastic and air cells. The air cells had an approximate dimension of 2mm with an outer shell 0.14mm thick, and a density of $0.27 g/cm^3$. The cedar inserts used by Modus Medical Devices had a physical density of $0.4 g/cm^3$, so this density of 3D printed material was an improvement compared to cedar, and as a result an acceptable physical density for this study [50].

The 3D printed lung insert was then scanned on the Christchurch Oncology CT Scanner to compare the HU to those described in ICRU-44. A large region of interest, as seen in Figure 2.2, in the centre of the 3D printed material gave a mean HU of -749.22. The mean HU was consistent

Property	ICRU-44
Physical Density (g/cm^3)	0.26
Electronic Density (e^{-1}/g)	3.35×10^{23}
Effective Atomic Number	3.43
CT Number (HU)	-950 to -750

Table 2.1: Relevant physical and radiological properties for idealised lung material, as per ICRU–44 [7]

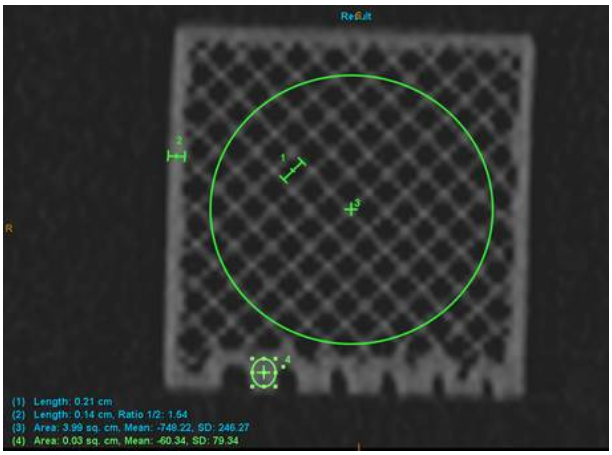

Figure 2.2: GE Lightspeed CT Scan of the 3D printed low density material, with acquisition settings of 120kV and 13mAs.

with the 3D printed material being slightly more dense than ICRU-44, however the HU variations due to the lattice structure of the air cells was far larger than the range seen in ICRU-44. Although the lattice structure was clearly visible in the CT scan, as seen in Figure 2.2, the dosimetric effect of this needed to be quantified.

The change in attenuation of the 3D material at different angles of incidence was measured by printing 2 cylinders with the lattice printed in perpendicular directions. The cylinders were then placed on top of a 2mm piece of solid water with a small volume ionisation chamber placed below the field. The cylinders where then irradiated with 200MU three times to determine the average electrometer reading, and rotated to positions at 0°, 90°, 180°, and 270°. This allowed the effect of the differences in attenuation to be determined as the photon beam passes through differing amounts of plastic and air. There were minimal differences in attenuation for both lattice

Cylinder rotation position	Mean Charge Collected (nC)	
	Horizontal lattice direction	Vertical Lattice direction
0°	6.402	6.473
90°	6.403	6.476
180°	6.401	6.470
270°	6.400	6.468
Maximum % difference	0.05%	0.13%

Table 2.2: The variation in mean charge collected (nC) with changing cylinder rotation, for both the vertical and horizontal lattice direction cylinders.

directions, with the maximum percentage difference found to be 0.13%, seen in Table 2.2. This result however only reflects the dose to a point. As a high level of resolution was required for analysis, film was required for the rest of the project. Given the positive initial dosimetric results, a 3D printed lung insert for the QUASAR phantom was developed and tested with film.

Cork-based Lung Inserts

A study by Chang et. al. 2012 compared the use of several lung substitute materials to reference lung material as listed in ICRU-44 [51]. From that study, composition cork was found to be an acceptable lung substitute based on physical and dosimetric properties. The decision was made to investigate the feasibility of the use of cork as a lung substitute material.

A composition cork block was purchased with the dimensions of 227mm by 100mm by 152mm, giving a volume of $3450.4cm^3$. The weight of the cork block was measured as 1025g, creating a physical density of $0.297g/cm^3$. The mean CT number and standard deviation of the cork block was obtained from CT acquisitions with set-up conditions of 120kV and 130mAs, where a region of interest was selected on the central slice of the cork CT scan. Comparisons of the lung insert cork material to the results from the study by Chang et. al. 2012 can be found in Table 2.3.

The physical and radiological properties for cedar lung inserts are also included to act as an appropriate tolerance level for the cork. While the cork obtained in Christchurch was denser than the ICRU-44 material and the reference composition cork, it is more comparable than the cedar. The HUs for the Christchurch cork are also closer to the range demonstrated by the ICRU-44 material, more so than the cedar. From this comparison, there is a justification to the use of the cork block for the lung equivalent material for the remainder of this research.

	Physical Density (g/cm^3)	Mean CT Number (HU)	Standard Deviation ($\pm HU$)
ICRU-44 [7]	0.260	-850	100
Reference Cork [51]	0.270	-743	11
Christchurch Cork	0.297	-711	54
QUASAR cedar [52]	0.400	-670	32

Table 2.3: The relevant physical and dosimetric properties of potential lung materials considered for this study.

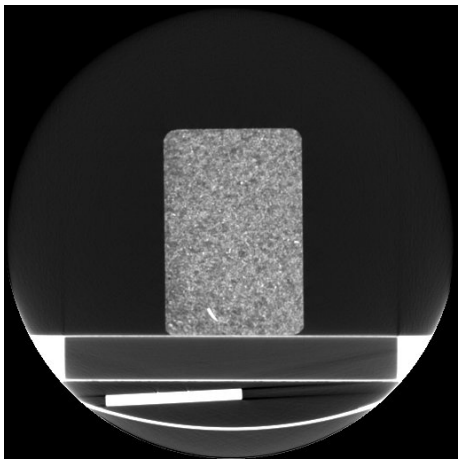

Figure 2.3: CT scan of the Christchurch Hospital Cork block.

QUASAR-compatible inserts used in this project were designed and manufactured in-house by the Bioengineering Workshop group at Christchurch Hospital. These custom built lung inserts had dimensions of an 8cm diameter and 17.5cm length, in keeping with other QUASAR phantom inserts. The PMMA tumour lesions had a density of $1.18 g/cm^3$and were spherical in shape. So that a range of lung tumour sizes could be investigated, three lung inserts were manufactured with PMMA sphere diameters of 15mm, 22mm, and 30mm, corresponding to a range applicable to the lung tumour sizes treated clinically. Once the inserts were manufactured, the variation in density between cork blocks was measured with a Siemens CT Scanner with set-up conditions of 120kV and 130mAs. A representative CT scan for one of the cork blocks can be seen in Figure 2.3. A region of interest was generated in each of the inserts, and there was found to be minimal difference between each insert in terms of minimum HU, maximum HU, mean HU, and standard deviation. The mean HU and ED for a given insert were found to lie within the standard deviation of the other two inserts, as seen in Table 2.4.

	Min (HU/ED)	Max (HU/ED)	Mean (HU/ED)	SD (HU/ED)
15mm	-780/0.205	-644/0.343	-722/0.270	23/0.025
22mm	-776/0.209	-654/0.335	-715/0.278	20/0.021
30mm	-780/0.205	-626/0.359	-713/0.280	22/0.023

Table 2.4: Variations in the HU and ED between the three cork inserts.

2.1.3 Breathing Patterns

A recent study by Callahan et al (2012) from the Department of Radiation Oncology, Peter MacCallum Cancer Centre, showed that after observing 100 different patient breathing traces from 4D-PET/CT scans, four general categories were identified. This includes breathing traces where;

1. Inspiration was equal to Expiration (Sinusoidal),
2. Inspiration was equal to Expiration, with a pause after Expiration,
3. Inspiration was greater than Expiration,
4. Expiration was greater than the Inspiration.

From these 4 general breathing motion categories, the sinusoidal pattern was selected as the waveform to be used for the duration of the study due to its simplicity and reproducibility. The sinusoidal waveform was created using the Wave Editor tool in the QUASAR Programmable Respiratory Motion Software. The maximum amplitude corresponds to the peak inspiration and the inferior position of the tumour lesion, whereas the minimum amplitude corresponds to the peak expiration and the superior position of the tumour lesion so that it is consistent with what would be seen in a patient.

From previous patient breathing traces, the average breathing period was 4 seconds, from a selection that ranged from 3-9 seconds, as seen in Table 2.5. This average breathing period was used for the computer generated breathing pattern, corresponding to a patient breathing rate of 12 breaths per minute. While the breathing trace categories are based on evidence for 4DPET-CT scans, they are applicable for testing the 4DCT imaging where the tumour object reaches the

Patient	Minimum Period (s)	Maximum Period (s)	Average (s)	Patient Breathing Rate (bpm)
1	3.52	16.31	6.26	10
2	3.48	6.08	3.94	15
3	2.36	33.12	8.97	7
4	3.08	6.08	4.45	13

Table 2.5: A representative sample of clinical patient breathing pattern data for Lung SBRT patients at Christchurch Hospital.

extreme of the amplitude every time. Realistically, this is not the case as patient breathing traces show that full inspiration and expiration are not reached every breathing period.

Breathing Pattern Amplitudes

For the computer-generated breathing patterns, four amplitudes were initially studied that reflected the possible range of amplitudes found in previous patient studies. From the patient data set, amplitudes of 5mm to 15mm corresponded to the realistic range of motion that lung tumours can exhibit during treatment, whereas an amplitude of 20mm corresponded to a possible worst case scenario. The average amplitude of the four SBRT lung patients in the superior/inferior direction was taken from the patient's 4DCT scan by comparing the position of the tumour in the coronal plane through each of the 0% to 90% 4DCT images. The average patient motion amplitude was found to be 7mm, with a maximum recorded amplitude of 15.1mm. A large breathing motion corresponded to a large uncertainty on the 4DCT scan, allowing for the effect of density overrides to be examined more clearly. As a result, the largest patient-relevant amplitude of 15mm was chosen as the amplitude for the sinusoidal waveform.

2.2 4DCT of the QUASAR Phantom

2.2.1 CT Imaging Equipment

A Siemens SOMATOM Definition AS 64 Open RT Pro CT scanner (Siemens Healthcare Limited) was used to acquire the 4DCT and supplementary CT image sets of the QUASAR Phantom. The CT scanner had an 80 cm bore and a 65 cm field of view, with a tube voltage range of 70-140 kVp and a current range of 10-440 mA. For this study, a 120kV, 110mAs scan was used as this is the clinical chest protocol in our department. 120kV is the standard X-ray energy for out department, and a relatively low 110mAs allows for high spatial resolution of the low density lung material while keeping the dose as low as possible for the required image quality.

The Siemens CT scanner uses the Respiratory Gating and Triggering option to acquire 4DCT scans, binning the CT slices acquired into 10 phases for image reconstruction (0-10%, 10-20%, etc), with 0% relating to peak inspiration and 50% relating to peak expiration. With the Respiratory

Gating tool, the respiratory data was synchronised to the acquired CT data so that the images were retrospectively reconstructed based on the corresponding breathing amplitude. The Respiration Triggering tool was used to select a point in the respiratory cycle at which sequence images would be acquired.

For respiratory gating, the sequential CT scanning mode was used, where multiple tube rotations are performed at the same table position. The table was then translated to the next position and scanning was resumed. The duration of the scan in each position was the length of the breathing scan plus one full rotation of the X-ray tube. The number of scan positions was determined by the length of the volume to be covered.

The set-up and positioning of the QUASAR phantom on the Siemens CT scanner can be seen in Figures 2.4a and 2.4b. The position of the RPM infrared camera at the end of the couch can also be seen.

2.2.2 Motion Tracking for 4DCT

While the patient is being scanned using the sequential acquisition protocol, the respiratory waveform file is simultaneously being recorded with an external respiratory gating system, in this case the Varian Real-time Position Management^{TM} (RPM) system. The RPM system uses an infrared

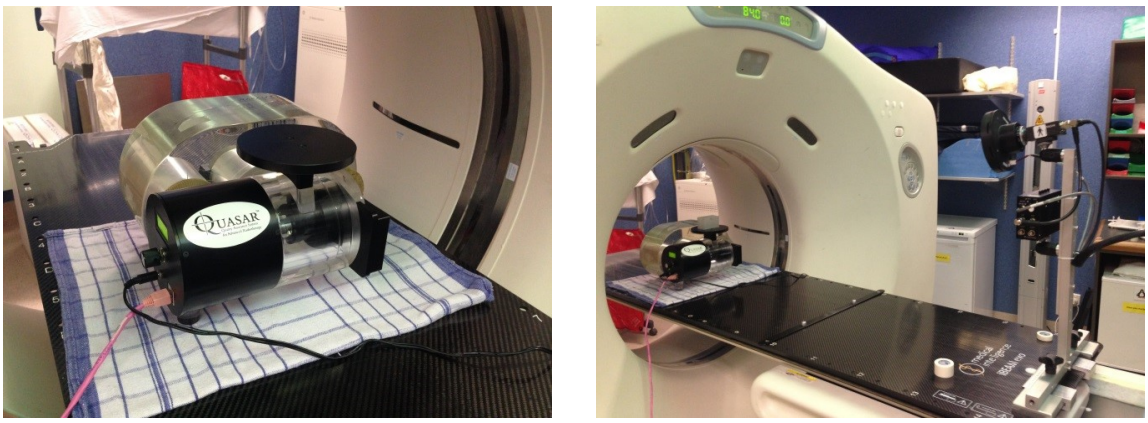

(a) (b)

Figure 2.4: The 4DCT acquisition set-up of the QUASAR Phantom for use with the Siemens CT scanner. (a) the positioning of the QUASAR phantom central in the bore of the CT scanner. (b) the position of the QUASAR phantom relative to the Varian RPM infrared camera.

camera to track the retro-reflective marker dots on a small Teflon box that is placed on the patient's chest or abdomen, which moves in the anterior/posterior direction. As the patient breathes the motion of the marker is tracked shown as a graphical representation of the marker position as a function of time. The Siemens 4D software then sorts the CT image data into phases and intensity projections using the imported RPM breathing trace.

2.2.3 Phantom Set-up

For the acquisition of the 4DCT of the QUASAR Phantom with each of the computer-generated breathing patterns, the lung insert was inserted into the left cavity and the right cavity was filled with a lung-equivalent insert. The motor cylinder was inserted into the central cavity and the magnet on the adjustable amplitude scale was aligned and connected to the magnet embedded in the lung insert. The DC motor was connected to the computer so that the breathing patterns could be loaded and delivered. Once the correct breathing patterned was loaded and the amplitude scale set, the RPM box was placed on top of the QUASAR motor platform and the external markers of the phantom were aligned to the external CT lasers.

2.2.4 Image Acquisition

For each of the different cork inserts, topograms were taken on the CT scanner to assess the straightness and rotation of the phantom, allowing for repositioning if needed. The scanning area was then adjusted to allow for scanning over the phantom only. The 4DCT and relevant respiratory motion file were both acquired and the respiratory motion file was imported to the CT console. The reconstruction process generated the AIP and a data set containing each of the 10 respiratory phases. Phase splitting was required to single out the mid-breath data set and to convert all 10 phases to the MIP. The three required image data sets (FB, AIP, and MIP) were then exported to the TPS.

2.3 Treatment Planning

2.3.1 ITV and PTV Contouring

The contouring of the two target volumes, the ITV and the PTV, was completed using the Monaco 5.1 TPS (Elekta, Inc) and utilised the MIP of each of the the gated CT scans for the difference cork inserts. Monaco was used as it is the clinical contouring tool used by Radiation Oncologists in our department for defining target volumes and critical structures. Contouring the ITV from the 4DCT MIP in Monaco was performed with the Lung preset selected, corresponding to a Window/Level setting of 1700/-300. Window and Level refers to the contrast of the image, where the window is the pixel range and level is the middle pixel value. As the tumour lesion was approximately circular in each of the axial slices, the Circle Shape tool was used to contour the position of the tumour for every slice where it was visible.

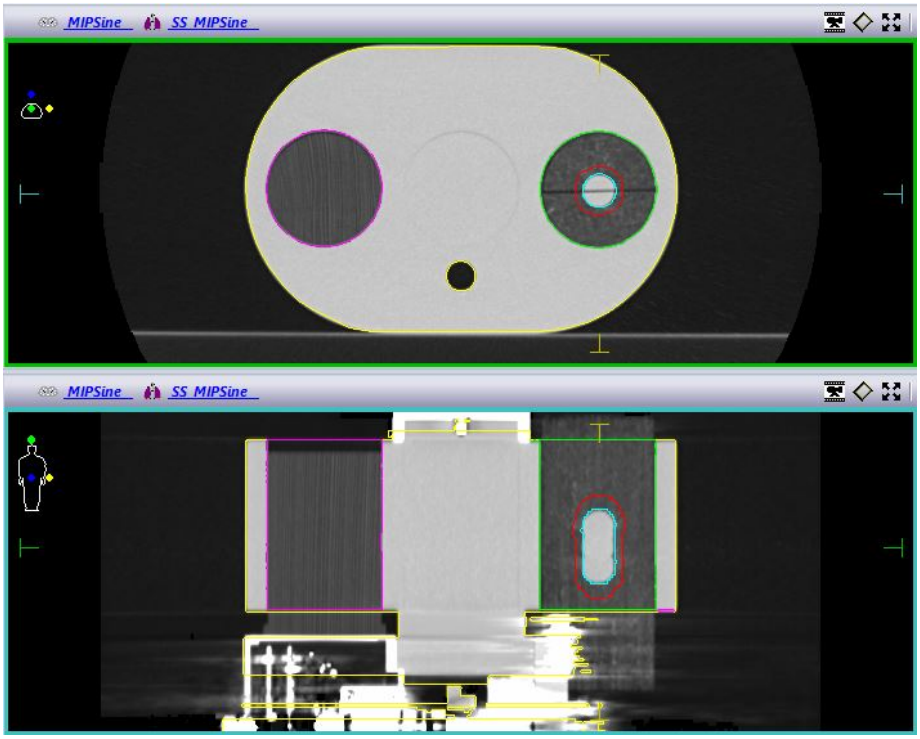

Figure 2.5: A representative Monaco 5.1 contour based on the MIP for the 22mm film cork insert. Cyan contour: ITV. Red contour: PTV. Green contour: Left Lung. Pink contour: Right Lung. Yellow contour: QUASAR Phantom body

An example of the contouring achieved in this study can be seen in Figure 2.5. For the cork inserts with the ion chamber holder, the ITV was contoured to exclude the plastic ion chamber insert. The inferior end of the ITV was determined as the axial slice when only the ion chamber insert was visible.

To contour the PTV, the Auto Structure Margin tool was used, where a new structure was created by adding a margin to an existing one. The clinical PTV margin guideline in our department for Lung SBRT planning is 1cm superior/inferior and 0.5cm in the axial plane, a requirement set in the TROG 09.02 trial. The superior/inferior direction refers to the line from head to feet, whereas the axial direction is the plane perpendicular to this.

To contour the left and right lungs, and the body of the QUASAR Phantom, the Auto Threshold tool was used. For the QUASAR phantom contour, the AutoThreshold was applied to all slices with a Window/Level of 1300/-850, corresponding to the AutoLung preset. For the left and right lungs, the Auto Threshold tool was used with the slice range limited to the length of the body of the QUASAR Phantom, with a Window/Level of 1200/400.

2.3.2 Lung SBRT Planning Protocol

The SBRT Lung treatment planning guidelines were established to follow the requirements of TROG trial 09.02. Initially the structure sets created on the cork insert MIP were copied to the corresponding average 4DCT scan and the mid breath CT scan, as seen in Figure 2.6. A Monaco treatment plan was then generated on the mid breath data set, utilising the 3D treatment delivery mode with the CCC dose calculation algorithm, the Monaco version of the convolution/superposition algorithm. Initially dose was prescribed to the isocentre, selected as the centre of the ITV. The MLCs were auto-conformed to the PTV volume, with MLC margins of 2mm used on all treatment fields.

Following standard Lung SBRT planning protocols, seven non-opposing beams were created and arranged, with all beams entering through the ipsilateral side of the QUASAR Phantom. Five coplanar beams were used to minimise the amount of overlap between beams, resulting in a gantry angle difference of 40°, between each coplanar beam. Two additional beams were added with a couch angle of 270°, oriented anterior to the QUASAR Phantom. To minimise the overlap with the

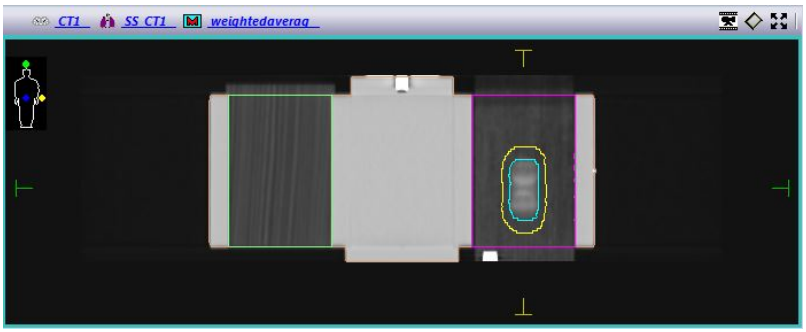

(a)

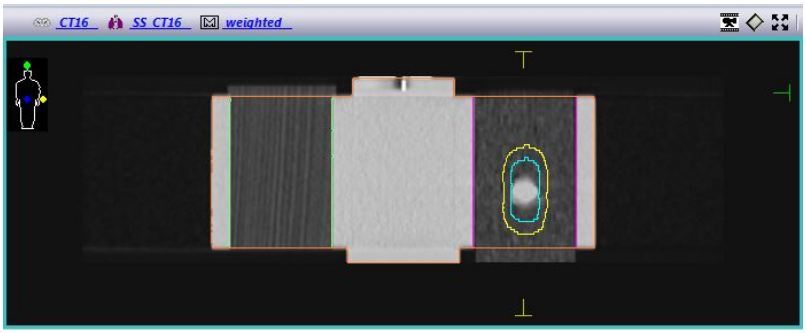

(b)

Figure 2.6: The representative Monaco 5.1 contours applied from the MIP to the AIP (a) and FB (b) 4DCT data sets.

coplanar beams, the 50% and 30% prescribed dose lines (isodoses) were examined and the incident angles of the two additional beams were adjusted to decrease the volume of these two isodoses.

The prescription dose was 48Gy in 4 treatment fractions, resulting in a dose per fraction of 12Gy. The plan was rescaled from delivering this dose to the centre of the ITV to delivering the prescription dose to the relative isoline of 80% to the PTV volume. This resulted in a maximum dose to the ITV of 120-130% of the prescribed dose. Due to the high dose gradients, this dose does not negatively affect the NTCP. As the aim of the treatment is to force an ablative dose to the ITV, this was considered acceptable. From this point, it was necessary to adjust the weighting of each of the beams to conform the ablative dose as tightly as possible to the PTV.

The mid breath plan was optimised by adjusting the weightings of the beams until the minimum dose to the PTV was the 95% isodose value and the conformity of the plan was at the highest achievable level. To assess the conformity of a plan, Monaco 5.1 uses the Conformity Index (CI) metric. This described the degree to which the prescribed isodose volume conforms to the shape

and size of the target volume [53]. While there are several different definitions for CI, Monaco 5.1 uses the van't Riet formula, which defines three volumes [54]:

1. TV1, the volume of the target that recieves the prescribed dose,
2. TV, the target volume,
3. and VR1, the total volume of the prescription isodose.

These three volumes are used in the following equation to calculate the CI for a specific prescribed dose (Gy).

$$CI = \frac{TV1^2}{TV \times VR1} \tag{2.1}$$

At this stage, the Monaco plan was saved as a template so that it could be applied to all CT scans for all of the different cork inserts. The Monaco plan was then applied to the average CT data set and the dose calculated. No changes were made to the beam weightings and the dose was rescaled to deliver the prescription dose to the relative isoline of 80% to the PTV volume. As a result, two treatment plans were generated for both the film and ion chamber cork inserts for each of the three possible tumour sizes, one for FB and one for AIP.

2.3.3 Overriding the Density of the Image Set

For the mid breath treatment plan, the EDs for both the ITV and the PTV were overridden to a variety of different values. Three different ED values were investigated corresponding to different proportions of lung and water. This included overrides corresponding to 75% lung material and 25% water, 50% lung material and 50% water, and 25% lung material and 75% water. Inherently, ED refers to the number of electrons per unit volume, with the units $10^{26} n/m^3$. However, ED values in radiotherapy are reported relative to water, resulting in a value of 1.000 for water. As a result, no units are reported for this value. For an average lung ED of 0.300 and a water ED of 1.000, this resulted in ED override values of 0.475, 0.650, and 0.825. A water density was selected as most lung tumours have an average ED close to this value.

To investigate the effect of these density override values on the dose calculated to the ITV and the PTV, three different ED override options were created. This included:

1. Overriding the ITV to the ED of water (1.000)
2. Overriding the PTV to the ED of:
   (a) 75% lung material and 25% water (0.475),
   (b) 50% lung material and 50% water (0.650),
   (c) 25% lung material and 75% water (0.825).
   (d) 100% water (1.000)
3. Overriding the ITV to the ED of water (1.000) and the PTV to the ED of:
   (a) 75% lung material and 25% water (0.475),
   (b) 50% lung material and 50% water (0.650),
   (c) 25% lung material and 75% water (0.825).

For each of these density overridden plans, the required MU was then recalculated with no additional changes made to the beam weightings. As the TPS algorithm calculates the MU based on the densities of the target volumes, a different MU was calculated for each plan so that the same prescribed dose could be achieved. A comparison was made on Monaco to the original mid breath and average CT data set plans in terms of plan conformity. To verify the effect of each of the density overrides on the dose delivered to the PTV and the ITV, the dose needed to be directly measured.

2.4 Dose Verification Methods

2.4.1 Ion Chamber Point Dose Measurements

Ion Chamber Equipment and Factors

The point dose measurements were made with a 0.13cc IBA Dosimetry compact air ionisation chamber, referred to as the CC13 ionisation chamber. Christchurch Hospital uses two ion chambers for QA purposes, the CC13 chamber and a Farmer chamber. The Farmer chamber has a sensitive volume of $0.6cm^3$, which is large compared to the field for the 15mm cork insert, so the graphite walls of the chamber influence the radiation field. For this study, the CC13 chamber was selected as it is small relative to the size of the fields being used. The physical dimensions and specifications of the CC13 chamber can be found in Table 2.6 [8].

The CC13 was cross-calibrated against the local reference ionisation chamber in accordance with with the International Atomic Energy Agency (IAEA) Technical Report Series (TRS) 398 code of practice for the 6MV photon beam [55]. The correction factors for the CC13, in conjunction with a PTW UNIDOS electrometer, were measured in August 2016 for the purpose of IMRT plan quality assurance. These corrections factors were used for the duration of the project and are displayed in Appendix B.

Measurement Process

Prior to each set of measurements being collected, the output of the linac was determined to correct for the day-to-day variations in the dose delivered per MU by the linac, and the temperature pressure correction ($k_{T,P}$) of the chamber was determined. The PTW Unidos Electrometer was used to create a potential difference of -300V across the ionisation chamber and to measure the charge collected by the central electrode of the ionisation chamber over the duration of the beam.

Ionisation Chamber	Cavity Volume (cm^3)	Cavity Length (mm)	Cavity Radius (mm)	Wall Thickness (g/cm^3)
IBA CC13	0.13	5.8	3	0.070

Table 2.6: Technical Specifications of the IBA CC13 Ionisation Chamber, taken from IBA Dosimetry [8]

The chamber was placed in each of the CC13 cork inserts and cork insert connected to the driving motor of the QUASAR Phantom using the magnet on the cork insert. The centre of the cork insert was then positioned at the isocentre of the linac using the patient setup lasers. Allowing for 5 minutes of warm up time, the ion chamber was pre-irradiated and the chamber electrometer combination nulled to minimise the effects of leakage on the measurements.

One at a time, each of the treatment plans were exported from Monaco 5.1 to the Oncology Information System, MOSAIQ, for delivery. Each treatment plan was exported, delivered and then measured in its entirety, with the ion chamber being irradiated with each treatment beam for each plan, with the average of 5 measurements taken to ensure reproducibility before the linac was moved to the next delivery position. Following the complete delivery of one plan, the next plan was exported from Monaco. Multiple linac output values were also measured over the course of the measurement process to ensure the linac was consistent. Following the delivery of all treatment plans for a single-sized insert, the initial plan was repeated to ensure there was no drift in the results as the linac warmed up.

The average charge collected (M_{Ave}) for each of the beams was recorded and corrected to a dose measurement based on the following equation. An extended explanation of the ionisation chamber charge-to-dose correction can be found in Appendix B.

$$\text{Dose} = \frac{M_{Ave} \times 100 \times (k_s \times k_{pol} \times k_{TP}) \times N_{D,w,Q_0}^{CC13} \times k_{Q,Q_0}}{\text{Linac Output}} \tag{2.2}$$

TPS Mean Dose Correction

To compare the average charge collected by the ion chamber to the expected mean dose calculated by the TPS, a correction needed to be applied to the statistics reported by the TPS. This is due to the fact that the chamber remains fixed inside the tumour insert, but it moves relative to the PTV. This results in an average dose being measured across the volume that the active part of the ion chamber covers. As the amplitude of motion is known to be 15mm, and the dimensions of the ion chamber cavity are specified in Table 2.6, the active volume of the chamber was contoured as a structure in Monaco, as seen in Figure 2.7.

The mean dose (Gy) to this chamber structure was reported by Monaco 5.1, and this value was

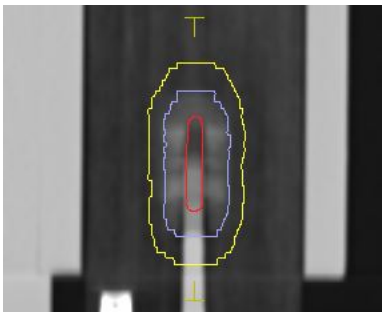

Figure 2.7: The Monaco 5.1 contours for the motion of the ion chamber active volume (red), the ITV (blue), and PTV (yellow), for the 22mm chamber insert.

compared to the mean dose determined by the ion chamber for all point dose measurements. The percentage difference between these two values was determined for each insert and treatment plan to compare the effect of density overrides on the agreement between the TPS and measured point doses.

2.4.2 EBT3 Gafchromic Film Dosimetry

To access the accuracy of the dose delivery in the QUASAR Phantom, a dosimeter that was capable of measuring dose distributions in two dimensions was required. The small field sizes and steep dose gradients present in SBRT plans require high spatial resolution. Radiochromatic film has become a routine tool for quality assurance in complex treatment plans and is an important part in testing the validity of dose calculation algorithms.

EBT3 films are the third generation of EBT type Radiochromatic film [56]. Compared to EBT2 film, EBT3 has a symmetrical structure of layers, with one active substrate layer that was 30 microns thick between polystyrene coated layers, both 125 microns thick, as can be seen in Figure 2.8. This

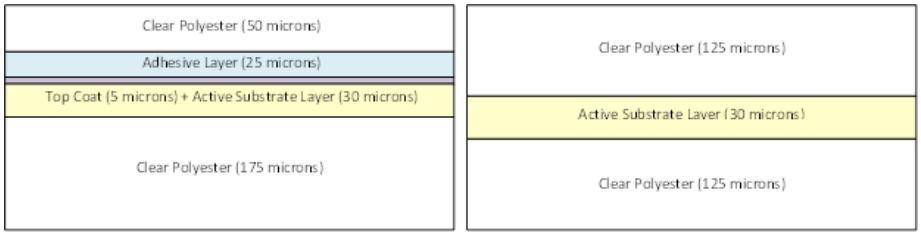

Figure 2.8: An illustration of the layering of Gafchromic EBT2 (left) and EBT3 (right) film

Scanning Feature:	
Mode:	Professional
Document Type:	Transparency
Film Type:	Positive
Image Type:	48 bit colour
Resolution:	75 dpi
Configuration:	No Colour Correction
Image Features:	Off

Table 2.7: The Epson Expression 11000XL scanner settings used in conjunction with the SNC Patient Film QA Software.

symmetry removes the face-up/down directional dependence, although the orientation dependence (portrait/landscape) still remains. A matte polyester substrate is included in the coating layers and consists of silica particles that induce a 5m gap between the film and the scanner surface, avoiding the creating of Newton Ring scanning interference patterns.

The Christchurch Oncology Physics department currently uses an Epson Expression 11000XL scanner for film dosimetry in conjunction with the Epson Scan software. For analysis purposes, EBT3 film was used in conjunction with the SNC Patient Film Analysis software (V6.6, Sun Nuclear Corporation), which was utilised in the evaluation and calibration of the EBT3 film. SNC Patient requires specific scanner settings in order to convert the film images to dose files. The key settings used for this project are defined in Table 2.7.

Dose Reduction Validation

From Figure 2.9, the red channel response for the EBT3 film is greatest in the dose region less than 10Gy, where the gradient of the line is the greatest. This is consistent with EBT3 being suitable for standard dose range measurements. A high level of response relates to more sensitive measurements, and as a result better resolution. The film response in the red channel decreases above 10Gy, introducing more uncertainty and poorer resolution. For this reason the dose was reduced from 12Gy per fraction to 3Gy for all film measurements. All other features of the treatment plan were kept the same.

Scaling the dose ultimately introduces additional errors to the film measurement due to the fact that a dose delivery variation of 1MU contributes to a larger overall percentage for a 3Gy

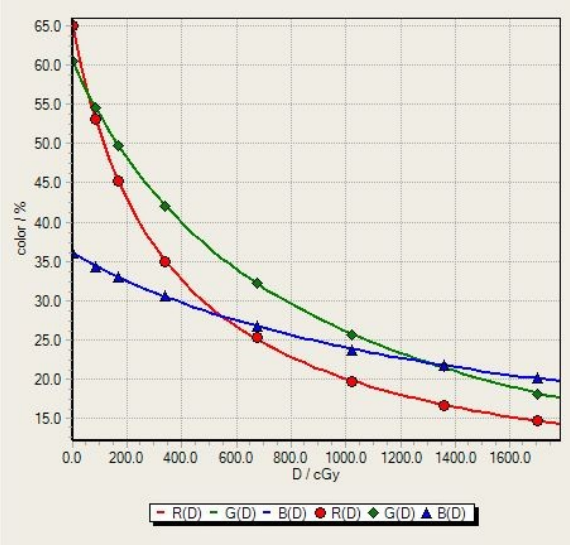

Figure 2.9: The green, red, and blue colour channel calibration curves for the EBT3 film for a dose range up to 20Gy, previously measured in the department.

plan compared to a 12Gy plan. To ensure the dose delivery uncertainties were kept to a minimum, the 22mm CC13 cork insert was used with a variety of delivery variations and the dose difference between the chamber and the expected dose from the treatment plan was measured. As the dose was reduced to a quarter of the original dose, the number of breathing cycles covered during a treatment was also reduced by 75%.

The introduced delivery variations were chosen to increase the number of breathing cycle completed during irradiation. This was achieved by decreasing the dose rate of the linac and increasing the speed of the QUASAR Phantom. This was also compared to keeping the dose rate and QUASAR Phantom breathing period the same and only reducing the dose.

Plan Delivery Protocol (Dose, Dose Rate, Seconds per Breath)	22mm Insert Dose Difference (%)
12Gy, Maximum Dose Rate, 4spb	0.1
3Gy, Maximum Dose Rate, 4spb	-0.3
3Gy, Half Dose Rate, 4spb	-0.6
3Gy, Quarter Dose Rate, 4spb	-0.5
3Gy, Maximum Dose Rate, 1spb	-0.3
3Gy, Half Dose Rate, 2spb	-0.5

Table 2.8: The Percentage Dose Difference (%) between the Ion Chamber measurement in the 22mm lung insert and the TPS dose for a variety of delivery protocols.

Table 2.8 shows the variations between the dose measured by the ion chamber and the TPS expected dose. Compared to the original 12Gy dose, the plan delivery protocols that gave the smallest differences were the standard delivery protocol with 3Gy, the maximum dose rate, and the standard QUASAR speed, and the protocol where the QUASAR phantom was sped up to cover one breathing cycle per second. Based on this, the decision was made to keep the delivery protocol the same between the 12Gy plan and the 3Gy plan, and only have the reduced dose as the difference.

Film Preparation

As the response of the Gafchromic EBT3 film varies with the batch, the time between the initial exposure and processing, and the scanner processing conditions, the accuracy of the film dosimetry can vary. To minimise the possible dosimetric changes, the films used in this project all came from the same batch, the time between irradiation and processing the film was kept to at least 24 hours, and calibration and test measurements were made at the start of each session to confirm the accuracy of the film dosimetry was within tolerance levels. The response of the EBT3 film is dependent on the film orientation, therefore after each film was irradiated, an orientation mark was made in one corner for the duration of the project.

The EBT3 film came in sheets with dimensions of 20.3cm × 25.4cm. The film used for the study had to fit the cross-sectional area of the lung insert which was 8cm × 17.5cm. The film was then cut into 6 smaller pieces that were approximately 6.8cm × 12.7cm. The dosimetric accuracy of the set-up was preserved by making the pieces of film slightly smaller than the area of the lung insert so that the film did not overlap the edge and cause the film to not sit flush.

Film Calibration

The film calibration for the EBT3 film involved creating a sensitometric curve specific to the batch of film. The optical density (OD) of the film (OD_{film}) was calculated for a range of dose values from ˜17cGy to ˜420cGy, based on the pixel values of the scanned irradiated film (PV_{film}) and the unirradiated film ($PV_{background}$).

$$OD_{film}^{colour} = log_{10}\frac{PV_{background}}{PV_{film}} \tag{2.3}$$

For dose calculation, the SNC Patient Film QA software uses the Net OD for the red colour channel, where the OD for the unirradiated film is subtracted from the OD of the irradiated film for the same colour channel.

$$OD_{net} = OD^{red}_{irradiated} - OD^{red}_{unirradiated} \tag{2.4}$$

The departmental protocol for film calibration was carried out on the batch of EBT3 film on a departmental linac. A 6MV linac output measurement was taken to correct the number of MU delivered to the film back to a correct dose value. Half a sheet of film was used, and cut into 8 equally sized pieces. Each piece of film, aside from one background piece, was placed on top of a 10cm stack of solid water, aligned to the central axis of a 3cm x 3cm field, covered with an additional 10cm stack of solid water, and a source to surface distance of 90cm set using the optical distance indicator on the head of the linac. Each individual piece of film was irradiated with either 20, 50, 100, 150, 250, 350, and 500cGy. The exact number of MU for each beam was also recorded. The output and the field size conversion factor for a 3cm x 3cm were used to convert the recorded number of MU to a dose value in cGy.

The film response curve was generated using SNC Patient. Each film was scanned and a central region of interest selected in the centre of each film to determine the mean pixel value. The curve was then generated from the table of mean pixel values to dose for the red channel. SNC Patient

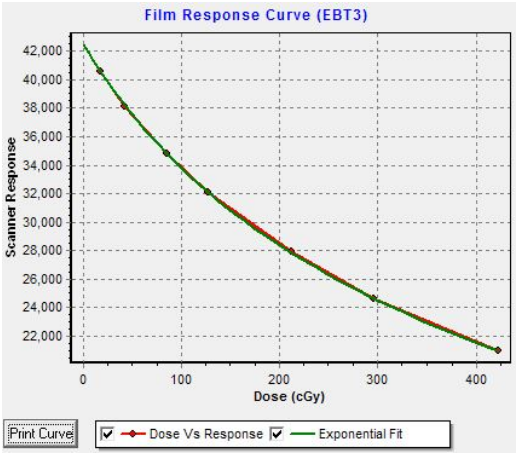

Figure 2.10: The Film Calibration Curve for the EBT3 Film batch, measured using SNC Patient for the red channel. Scanner response is equivalent to optical density.

then fitted an exponential curve to the data points, as seen in Figure 2.10. The fitting parameters for the exponential curve were then saved as a calibration file and referenced for each of the film measurements to convert them to a dose file.

Reference Frame Correction for the TPS Dose Planes

Following the acquisition of the film measurements, an issue arose with the direct comparison of the TPS dose plane and the film dose file. As the 4DCT was acquired, the dose distribution was generated relative to the frame of reference of the PTV, with the tumour lesion moving inside the PTV. However, for the film measurement the film was fixed relative to the motion of the cork insert, and so the frame of reference follows the position of the GTV. A representation of this concept can be seen in Figure 2.11.

To correct for this, a simple time-weighted average correction was applied to each dose value in the TPS dose plane. As the motion of the GTV was a well known sinusoid, with a fixed amplitude and period, the dose values only needed to be corrected in the direction of motion. As the TPS dose plane reported dose as a series of 1mm by 1mm voxels, a Visual Basic Macro was created that

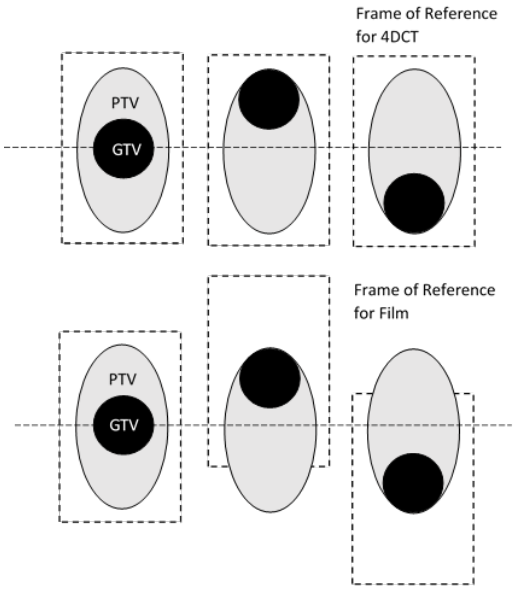

Figure 2.11: The location of the frames of reference, for the 4DCT scan and the film measurement, relative to the motion of the GTV and the fixed location of the PTV.

took the 15 dose values in the positive and negative Y directions, and scaled them by the sinusoidal waveform.

As the central voxel was covered twice as often as the voxel at the extreme of the tumour motion, this corresponded to a weighting of 1.0, while the extremities received a weighting of 0.5.

As this resulted in 30 data points being used for the weighted average, the following sinusoid was used for each data point, where n = 15 is the central point being corrected and n = 0, n = 30 are the extremity points.

$$Weight(n) = 0.5sin(\pi \times (n/30)) + 0.5 \tag{2.5}$$

This equation was then applied to the following time-weighted average equation, to calculate the dose received at a point n. This equation was applied to every data point in the TPS dose plane to generate the new frame of reference dose plane.

$$D(n) = \frac{\sum_{0}^{n=30} n \times weight(n)}{30} \tag{2.6}$$

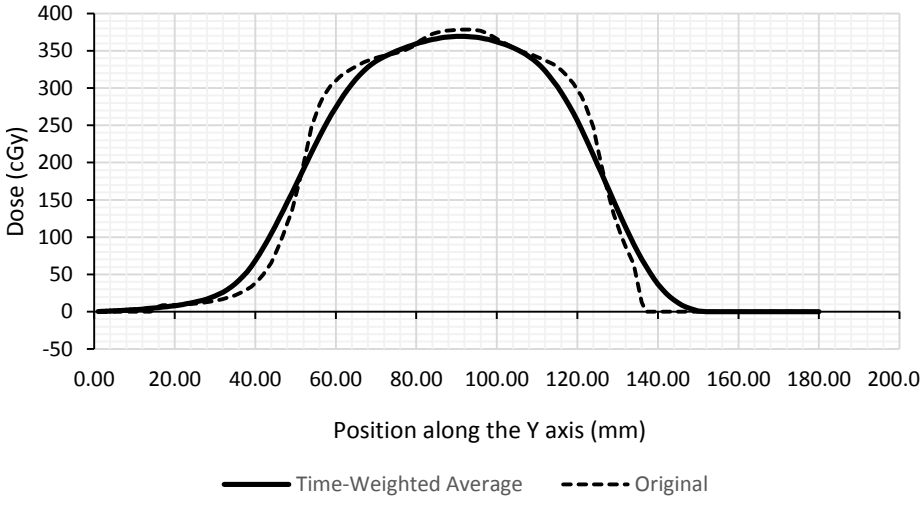

Figure 2.12: The effect of the time-weighted average correction on the original Monaco dose plane, specific to the 22mm cork insert.

3

Results

The Results chapter is separated into sections covering the plan quality in the treatment planning system and the measured aspects of the plan, both with point dose measurements and film. In each section, the impact of the various density overrides are analysed and compared to the two baseline plans, FB and AIP. Each density override plan was assessed and compared for a given tumour size. For the treatment planning section, the cork inserts for use with EBT3 film were used as these showed the most ideal representation of the tumour positions. The treatment plans were assessed in terms of overall plan quality, including target coverage and dose statistics, and the conformity and homogeneity of the dose distribution to the target volume. For the plan verification, each plan was delivered to both the ion chamber for a point dose measurement, and the EBT3 film for analysis of the 2D dose distribution.

3.1 Plan Quality

3.1.1 Target Coverage

The quality of each density override plan was indicated by DVH metrics. These metrics are used clinically to quantify certain aspects of the dose distribution over the target volumes. Clinical guidelines suggest that each Lung SBRT plan should be assessed in terms of coverage to the PTV, and doses received by the surrounding OARs, including the heart, skin, and spinal cord doses. As the QUASAR phantom is a simplified thorax phantom, it lacked the complexity to adequately model the OARs, so only the PTV coverage metrics were compared. However, as no plan details were altered aside from the densities of the target volumes, a change to the total number of MU delivered acts as a surrogate for OAR dose. Five PTV coverage metrics were assessed, including the Mean Dose (Gy), Maximum Dose (Gy), Minimum Dose (Gy), D_{90} and D_{95}. These metrics represent the mean, maximum, and minimum dose delivered to the entire volume of interest. The D_x type metrics indicate the minimum dose delivered to a percentage (x) of the volume of interest.

	Mean Dose (Gy)	Max Dose (Gy)	Min Dose (Gy)	D90 (Gy)	D95 (Gy)
FB	12.7	15.0	9.4	11.6	11.2
AIP	13.5	15.4	10.0	12.3	11.9
ITV	13.1	15.0	9.4	11.6	11.3
PTV = 0.475	14.1	15.2	10.8	13.1	12.7
PTV= 0.650	13.9	15.1	10.4	12.7	12.4
PTV = 0.825	13.9	15.1	10.4	12.8	12.4
PTV = 1.00	14.1	15.1	10.6	13.0	12.6
HPTV = 0.475	13.6	15.0	10.1	12.4	12.0
HPTV = 0.650	13.9	15.1	10.4	12.8	12.4
HPTV = 0.825	14.1	15.1	10.6	13.0	12.6

Table 3.1: The target coverage DVH metrics for each of the baseline plans and density override plans for the 15mm cork insert, reported by Monaco 5.1.

	Mean Dose (Gy)	Max Dose (Gy)	Min Dose (Gy)	D90 (Gy)	D95 (Gy)
FB	13.2	15.1	9.6	12.0	11.5
AIP	13.5	15.2	9.7	12.2	11.7
ITV	13.5	15.3	9.6	12.0	11.6
PTV = 0.475	14.0	15.1	10.2	12.9	12.4
PTV= 0.650	14.1	15.2	10.3	13.0	12.6
PTV = 0.825	14.3	15.4	10.5	13.2	12.8
PTV = 1.00	14.4	15.5	10.7	13.3	12.9
HPTV = 0.475	14.0	15.3	10.2	12.7	12.3
HPTV = 0.650	14.2	15.4	10.4	13.0	12.6
HPTV = 0.825	14.3	15.4	10.6	13.2	12.8

Table 3.2: The target coverage DVH metrics for each of the baseline plans and density override plans for the 22mm cork insert, reported by Monaco 5.1.

	Mean Dose (Gy)	Max Dose (Gy)	Min Dose (Gy)	D90 (Gy)	D95 (Gy)
FB	13.8	15.3	9.6	12.6	12.3
AIP	13.8	15.4	9.5	12.6	12.2
ITV	13.9	15.5	9.6	12.6	12.2
PTV = 0.475	14.5	15.7	10.2	13.6	13.3
PTV= 0.650	14.2	15.3	9.9	13.2	12.9
PTV = 0.825	14.3	15.4	9.9	13.4	13.0
PTV = 1.00	14.4	15.6	10.1	13.5	13.2
HPTV = 0.475	14.2	15.5	9.9	13.1	12.8
HPTV = 0.650	14.4	15.6	10.0	13.4	13.1
HPTV = 0.825	14.5	15.7	10.2	13.6	13.2

Table 3.3: The target coverage DVH metrics for each of the baseline plans and density override plans for the 30mm cork insert, reported by Monaco 5.1.

15mm Insert

The target coverage DVH metrics for the 15mm insert are displayed in Table 3.1. For the two baseline plan, FB and AIP, the AIP plan showed improved PTV doses compared to the FB plan. In an ideal Lung SBRT plan, 95% of the PTV should receive at least the prescribed dose. From the D95 values, the AIP plan is able to almost achieve the desired dose of 12Gy.

Comparing the baseline plans to the density overridden plans, in every case the target coverage was improved or at least remained the same. The ITV plan however did not show any significant difference to the FB plan, aside from a higher mean dose to the PTV. For the remaining 7 density overridden plans, the D95 value increased by 1.2 ± 0.4Gy compared to the FB plan, and 0.5 ± 0.4Gy compared to the AIP plan. Overall, the PTV = 0.475 treatment plan appears to provide the best target coverage across all target coverage metrics, although all density overridden plans show an improvement compared to the baselines. Following this, the high density overridden plans, PTV = 1.00 and HPTV = 0.825, showed comparable results.

22mm Insert

The target coverage DVH metrics for the 22mm insert are displayed in Table 3.2. Consistent with the 15mm insert results, the AIP plan showed improved PTV doses compared to the FB plan, however not by as great a margin. The ITV plan again did not show significant differences to the FB plan, aside from a higher mean dose to the PTV. For the PTV and HPTV plans, the D95 value increased by 1.1 ± 0.4Gy compared to the FB plan, and 0.9 ± 0.4Gy compared to the AIP plan.

Overall, the higher density overridden plans showed comparable results and appeared to provide the best target coverage across all target coverage metrics. The spread of the target coverage metrics were consistent with the 15mm results, suggesting that there was little change in the dose calculation process between the two different sized inserts.

30mm Insert

The target coverage DVH metrics for the 30mm insert are displayed in Table 3.3. Again, consistent with the 15mm and 22mm insert results, the AIP plan showed improved PTV doses compared to the FB plan. The ITV plan again did not show significant differences to the FB plan. For the PTV and

HPTV plans, the D95 value increased by 0.8 ± 0.3Gy compared to the FB plan, and 0.9 ± 0.3Gy compared to the AIP plan. Aside from the D90 and D95 results, which were largely consistent across all inserts, the mean, minimum, and maximum doses showed less of an improvement as the insert size increased from 15mm to 30mm.

3.1.2 Plan Conformity and Heterogeneity

In addition to the standard DVH metrics, the conformity and heterogeneity of each plan was determined and compared to the baseline plans. Four different metrics were used to assess how well the dose distribution was able to cover the treatment volume, three referring to different conformity indices and one heterogeneity index. As mentioned in Section 3.3.2, the base plan was generated by optimising the CI calculated by the Monaco TPS to the highest achievable value. For analysis purposes, this value along with $CI_{100\%}$ and $CI_{50\%}$ values were reported for each plan. The $CI_{x\%}$ type metrics indicate the ratio of the percentage (x) isodose volume to the volume of interest. Although a CI close to 1.00 indicates a perfect plan, the clinical guidelines suggest a $CI_{100\%}$ value in the region of 1.20 and a $CI_{50\%}$ as far away from 5.00 as reasonably achievable. The Heterogeneity Index (HI) indicates the dose uniformity inside the target volume, and is directly calculated from the DVH statistics. To calculate HI, the High Dose Reference (HDR) value (%) and the Minimum Dose Reference (MDR) value (%) are used to calculate $D_{x\%}$, the dose that covers x% of the tissue, in the following equation:

$$HI = \frac{D_{HDR\%}}{D_{MDR\%}} \tag{3.1}$$

The standard Monaco values for HDR and MDR were used, corresponding to 95% and 5%. The total number of MU was also reported as it represented a scaling factor for the dose calculated by Monaco, as this was the only plan feature than varied with the different density overrides.

	Total MU	$CI_{50\%}$	$CI_{100\%}$	CI	HI
FB	1469.9	4.87	0.87	0.76	1.27
AIP	1548.5	5.36	1.16	0.78	1.26
ITV	1460.2	4.82	0.89	0.79	1.31
PTV = 0.475	1449.6	4.79	1.18	0.86	1.18
PTV= 0.650	1494.5	5.08	1.18	0.83	1.20
PTV = 0.825	1457.8	4.87	1.15	0.85	1.20
PTV = 1.00	1447.7	4.80	1.15	0.86	1.19
HPTV = 0.475	1453.4	4.82	1.07	0.86	1.24
HPTV = 0.650	1450.7	4.82	1.13	0.86	1.21
HPTV = 0.825	1450.0	4.80	1.16	0.86	1.19

Table 3.4: The PTV conformity and heterogeneity metrics for each of the baseline plans and density override plans for the 15mm cork insert, reported by Monaco 5.1.

	Total MU	CI 50%	CI 100%	CI	HI
FB	1435.3	4.37	1.00	0.80	1.28
AIP	1454.2	4.47	1.07	0.80	1.28
ITV	1436.1	4.37	1.02	0.81	1.30
PTV = 0.475	1450.4	4.47	1.18	0.82	1.21
PTV= 0.650	1429.2	4.36	1.17	0.84	1.20
PTV = 0.825	1430.8	4.35	1.18	0.84	1.19
PTV = 1.00	1440.8	4.38	1.21	0.83	1.18
HPTV = 0.475	1436.4	4.38	1.14	0.84	1.23
HPTV = 0.650	1437.4	4.38	1.18	0.84	1.21
HPTV = 0.825	1439.1	4.38	1.20	0.83	1.19

Table 3.5: The PTV conformity and heterogeneity metrics for each of the baseline plans and density override plans for the 22mm cork insert, reported by Monaco 5.1.

	Total MU	CI 50%	CI 100%	CI	HI
FB	1414.1	4.64	1.22	0.80	1.22
AIP	1399.9	4.53	1.19	0.81	1.24
ITV	1403.6	4.57	1.20	0.81	1.24
PTV = 0.475	1410.3	4.56	1.31	0.78	1.16
PTV= 0.650	1406.1	4.62	1.28	0.78	1.17
PTV = 0.825	1392.2	4.53	1.27	0.79	1.17
PTV = 1.00	1398.0	4.53	1.28	0.79	1.16
HPTV = 0.475	1405.0	4.57	1.26	0.79	1.20
HPTV = 0.650	1406.5	4.57	1.29	0.78	1.17
HPTV = 0.825	1408.4	4.56	1.30	0.78	1.16

Table 3.6: The PTV conformity and heterogeneity metrics for each of the baseline plans and density override plans for the 30mm cork insert, reported by Monaco 5.1.

15mm Insert

The PTV conformity and heterogeneity metrics for the 15mm insert are displayed in Table 3.4. Large variations were present between the FB and AIP plan in terms of total number of MU calculated, $CI_{50\%}$, and $CI_{100\%}$, however there was little variation in terms of CI and HI. For the two baseline plans, the AIP plan showed improved $CI_{100\%}$, CI, and HI compared to the FB plan, however the $CI_{50\%}$ value was unacceptably high. The total MU delivered for each plan also varied by 5% between the FB and AIP plans.

Consistent with the target coverage metrics, the ITV plan showed the least amount of difference between it and the FB and AIP plans in terms of the conformity and heterogeneity of the dose distribution. For the PTV and HPTV plans, the CI value increased by 0.09 ± 0.02 compared to the FB plan, and 0.07 ± 0.2Gy compared to the AIP plan. Again, the PTV = 0.475 plan displayed the best CI and HI results, along with the PTV = 1.00 plan.

22mm Insert

The PTV conformity and heterogeneity metrics for the 22mm insert are displayed in Table 3.5. Consistent with the 15mm insert results, the AIP plan showed an improved $CI_{50\%}$ compared to the FB plan, and an improved $CI_{100\%}$ on the FB plan compared to the AIP plan. The ITV plan again did not show significant differences to the FB plan. For the PTV and HPTV plans, the CI value increased by 0.03 ± 0.01 for both the FB and AIP plan.

Overall, less variation can be seen between the different density overrides for the 22mm insert compared to the 15mm insert. The higher density overrides, specifically the HPTV = 0.475 plan, displayed the best conformity and heterogeneity indice results.

30mm Insert

The PTV conformity and heterogeneity metrics for the 22mm insert are displayed in Table 3.6. Contrary to the 15mm and 22mm insert results, the AIP plan showed minimal differences compared to the FB plan, as did the ITV plan. For the PTV and HPTV plans, the CI value decreased by 0.02 ± 0.01 for the FB plan, and 0.03 ± 0.01 for the AIP plan.

Although the CI values worsened, due to the small range of these results, this is a statistically insignificant effect. In combination with the target coverage metrics for the 30mm insert, the impact of density overrides is limited for large tumour volumes.

3.2 Plan Verification

3.2.1 Point Dose Verification

The majority of the point dose measurements were within the clinically accepted tolerance of ±3% compared to the dose calculated by the TPS. An uncertainty budget was carried out to assess the variation in measured dose with changes to the QUASAR phantom set-up, environmental conditions, and the linac output. As this was independent of the density override, but dependent on the insert size, an uncertainty in dose was generated for each cork insert. This corresponded to 0.7% for the 15mm insert, 0.5% for the 22mm insert, and 0.4% for the 30mm insert.

For each of the results, a Student's t-test was performed to compare the statistical significance of the density override results compared to the baseline FB plan. The overview and results of these can be found in Appendices C and D.

15mm Insert

The percentage difference point dose measurements for the 15mm insert are displayed in Figure 3.1. The largest percentage dose differences were present for the FB and AIP plans, with every density

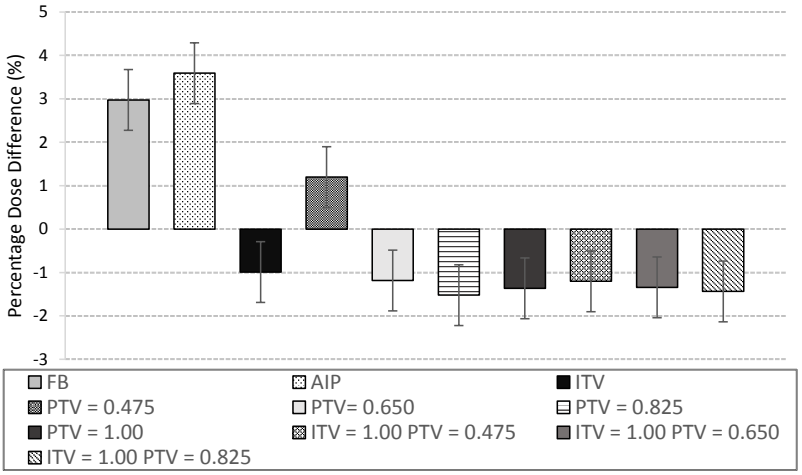

Figure 3.1: The percentage difference between the average dose to the ion chamber structure reported by Monaco and the measured dose to the ion chamber, for each of the baseline and density overridden plans for the 15mm cork insert.

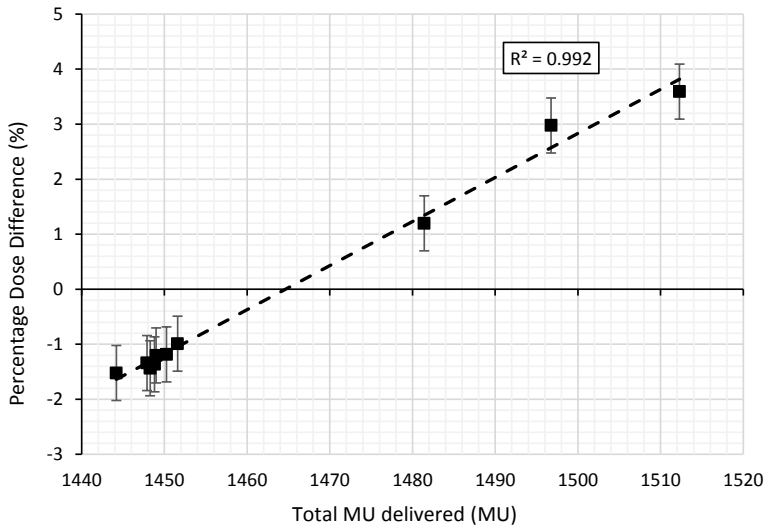

Figure 3.2: The relationship between percentage dose difference and the total MU delivered to the ion chamber for the 15mm cork insert.

overridden plan showing an improvement on the dose delivered to the ion chamber. Although the TPS metrics had suggested that the ITV plan showed the least amount of variation to the baseline plans, it was the best performing density override with a percentage difference of -0.99%. For each of the PTV and HPTV overrides, excluding the PTV = 0.475 plan, the percentage difference was approximately the same, taking into account the uncertainty in the results, with an average result of $-1.3 \pm 0.2\%$. All density overridden plans showed a statistically significance ($p<0.05$) difference to the FB plan, whereas the AIP plan showed no significant difference ($p = 0.342$). This supports the use of AIP as an equivalent method to FB in terms of dosimetric accuracy.

The percentage difference for each treatment plan and the total MU delivered were correlated, as seen in Figure 3.2. As the only value that changed from a plan delivery viewpoint was the MU, it acts as a quantifiable measure of the density override impact. A positive trend was displayed between percentage difference and total MU ($R^2 = 0.992$), indicating that to achieve perfect agreement between the treatment plan and the ion chamber measurement, a density override that generated the corresponding total MU could be used.

Achieving this in practice is a more complicated issue, as the density override does not change the total MU in a linear fashion, although there is a linear trend with percentage dose differences.

22mm Insert

The percentage difference point dose measurements for the 22mm insert are displayed in Figure 3.3. Again, the largest percentage dose differences were for the FB and AIP plans. The best performing density override was the PTV = 1.00 plan, with a percentage difference of -0.18%. For the density overridden plans, the PTV = 0.475 plan showed the largest percentage difference with 0.88%. For each of the PTV and HPTV overrides, excluding the PTV = 0.475 plan, the percentage differences were more comparable, taking into account the uncertainty in the results, with an average result of $-0.4 \pm 0.3\%$. Overall, each of the plans were within the clinically accepted tolerance of $\pm 3\%$, although there was a smaller range of results compared to the 15mm insert plans.

The percentage difference for each treatment plan and the total MU delivered were once again compared, as seen in Figure 3.4. The positive trend that was previously seen in the 15mm result remained between the percentage difference and total MU ($R^2 = 0.9532$), however the correlation was weaker. From Figure 3.4, the linear trend suggests that to achieve perfect agreement between the treatment plan and the ion chamber measurement, the plan needs to deliver 1436MU, which is approximately achieved with the PTV = 1.00 plan. As was consistent with the 15mm insert, all density overridden plans showed a statistically significance ($p<0.05$) difference to the FB plan, however the AIP plan showed no significant difference ($p = 0.087$).

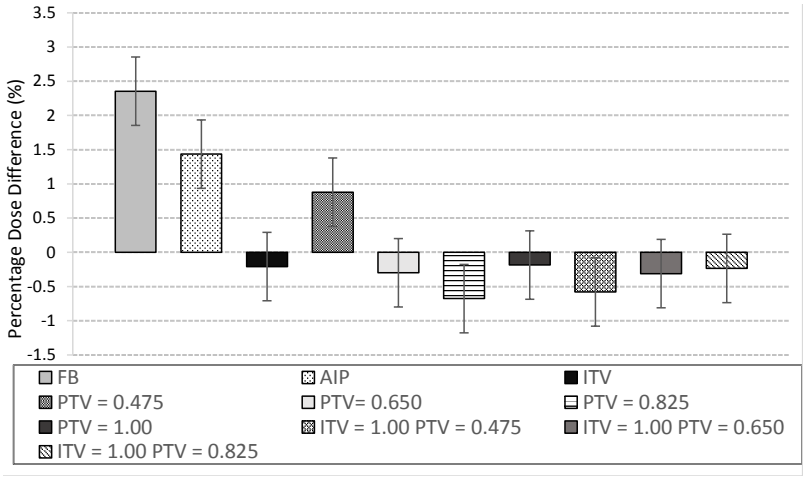

Figure 3.3: The percentage difference between the average dose to the ion chamber structure reported by Monaco and the measured dose to the ion chamber, for each of the baseline and density overridden plans for the 22mm cork insert.

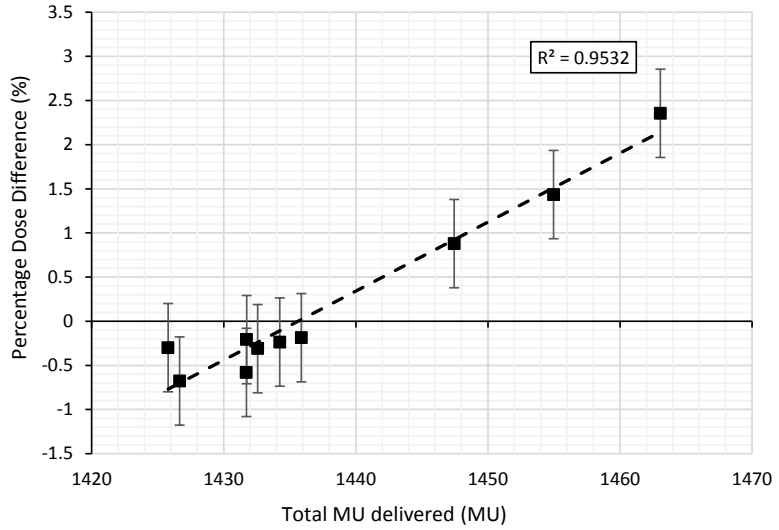

Figure 3.4: The relationship between percentage dose difference and the total MU delivered to the ion chamber for the 22mm cork insert.

30mm Insert

The percentage difference point dose measurements for the 30mm insert are displayed in Figure 3.5. Again, the largest percentage dose differences were for the FB plan, however the AIP plan achieved the best agreement with a percentage difference of 0.15%. For the density overridden plans, a large

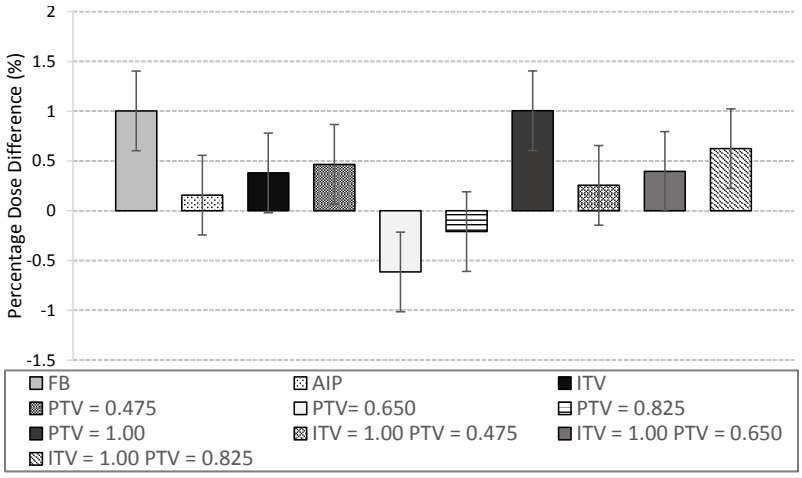

Figure 3.5: The percentage difference between the average dose to the ion chamber structure reported by Monaco and the measured dose to the ion chamber, for each of the baseline and density overridden plans for the 30mm cork insert.

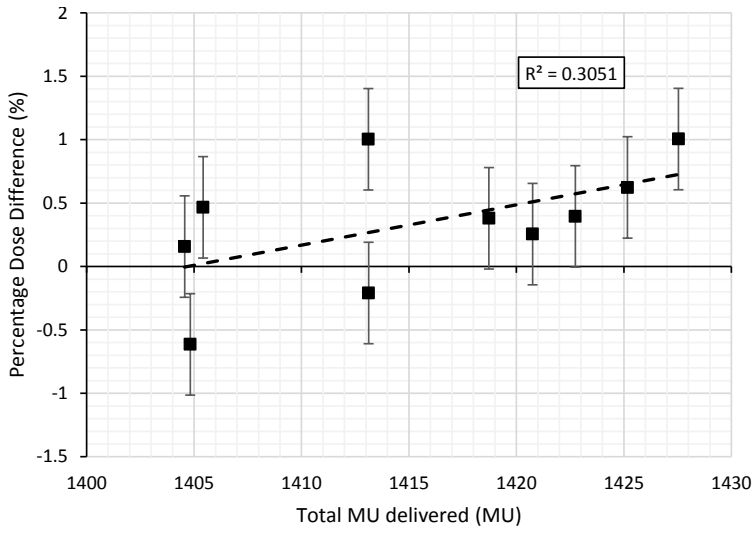

Figure 3.6: The relationship between percentage dose difference and the total MU delivered to the ion chamber for the 30mm cork insert.

range of possible percentage differences were seen, with an average result of $0.2 \pm 0.9\%$. Overall, each of the plans were well within the clinically accepted tolerance of $\pm 3\%$, with every plan at least achieving the same percentage difference that the best plan for the 15mm insert was able to achieve.

The percentage difference and the total MU were once again compared, as seen in Figure 3.6. The positive trend that was previously seen in the 15mm and 22mm results was much weaker ($R^2 = 0.3051$), however the total range of MU had also decreased to 27MU. This increased the impact of delivery variations on the calculated percentage differences. This result is consistent with the treatment planning metrics for the 30mm insert, suggesting that the density overrides have a limited impact for large tumour volumes. Across all plans, no statistical significance ($p<0.05$) was seen compared to the FB plan.

3.2.2 Film Dose Distribution Verification

The differences in gamma pass rates for the dose distribution of the various plans, measured using EBT3 film, can be seen in Figure 3.7. As there was no statistically significant change to the point dose accuracy with the density overridden plans compared to the baseline FB plan, film measurements were not conducted for the 30mm tumour insert as the process required at least 24

hours to obtains the results, as well as the resource cost of the film. Three absolute dose gamma analysis results were obtained (Criteria of 1%/1mm, 2%/2mm, and 3%/3mm) across two dose threshold levels (10% and 40%). Further explanation of the gamma analysis criteria can be found in Appendix A. The % threshold represents the dose range that is being compared, so that doses below the threshold, where there is more random noise, are not included in the comparison. A 10% threshold is used clinically for dose distribution verification, and an additional 40% threshold was chosen to minimise the effect of the sudden dose difference at the edge of the film.

15mm Insert

The average gamma pass rates for the 15mm insert are summarised in Figure 3.7a for the 10% threshold and Figure 3.7b for the 40% threshold. The clinically acceptable limits at Christchurch Hospital for absolute dose gamma criteria 2%/2mm is $> 80\%$ and 3%/3mm is $> 95\%$, however this is for a non-moving phantom where the tumour insert is water-equivalent, not lung-equivalent. Therefore results lower than this would still be accepted clinically at the discretion of the physicist. Often, failed points occur in the same region of the dose distribution, resulting in clusters of high or low doses. Avoiding these clusters, rather than randomly distributed failed points, is of more importance clinically as this is more indicative of issues in the treatment plan. From Figure 3.2, there was minimal differences shown between percentage-dose difference and total MU for the HPTV plans for the 15mm inserts, as well as between the PTV = 650, 825, and 1.00 plans. As a result, a representative selection was analysed for the dose distribution verification, with the FB, AIP, ITV, PTV = 475, PTV = 1.00, and HPTV = 0.475 plans being compared.

For the 10% and 40% thresholds, the FB plan was shown to have the lowest mean gamma pass rates across all criteria. The AIP and PTV = 1.00 plans were shown to have comparable pass rates within the range of the results. The best performing plan was the ITV override, which showed a 3%, 3mm pass rate of 92.7% for the 10% threshold, and 99.7% for the 40% threshold. This is comparable to the clinically accepted guidelines, and is consistent with the smallest percentage point dose difference seen in Figure 3.2. The PTV = 475 and HPTV = 0.475 plans also showed higher gamma pass rates than the FB and AIP plans, and were also consistent with corresponding percentage point dose difference results. Only the PTV = 1.00 plan showed a deviation for the

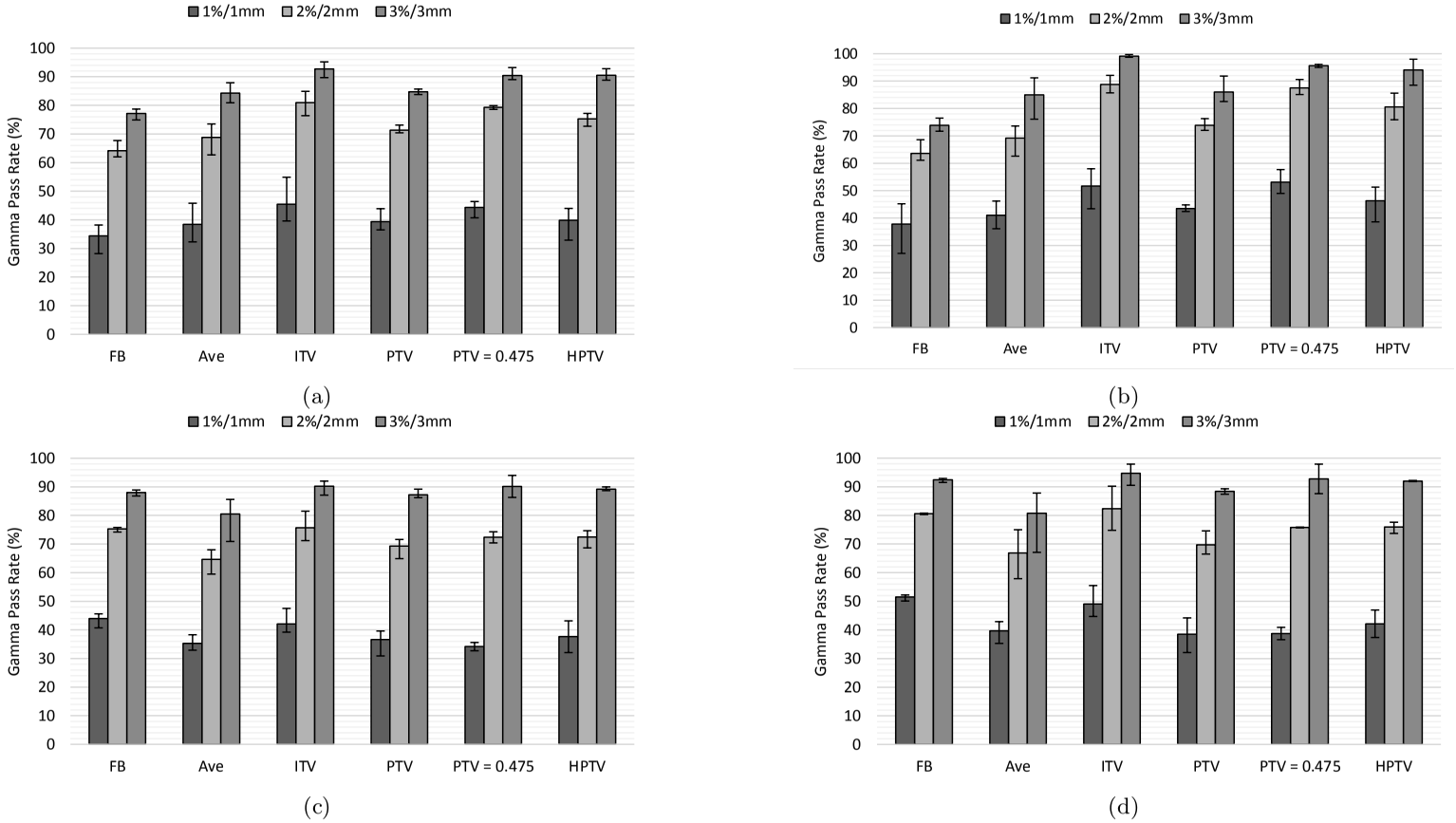

Figure 3.7: The mean gamma pass rates (%) and range (±%) between the film and TPS dose distributions. (a) 10% Threshold, 15mm insert, (b) 40% Threshold, 15mm insert, (c) 10% Threshold, 22mm insert, (d) 40% Threshold, 22mm insert

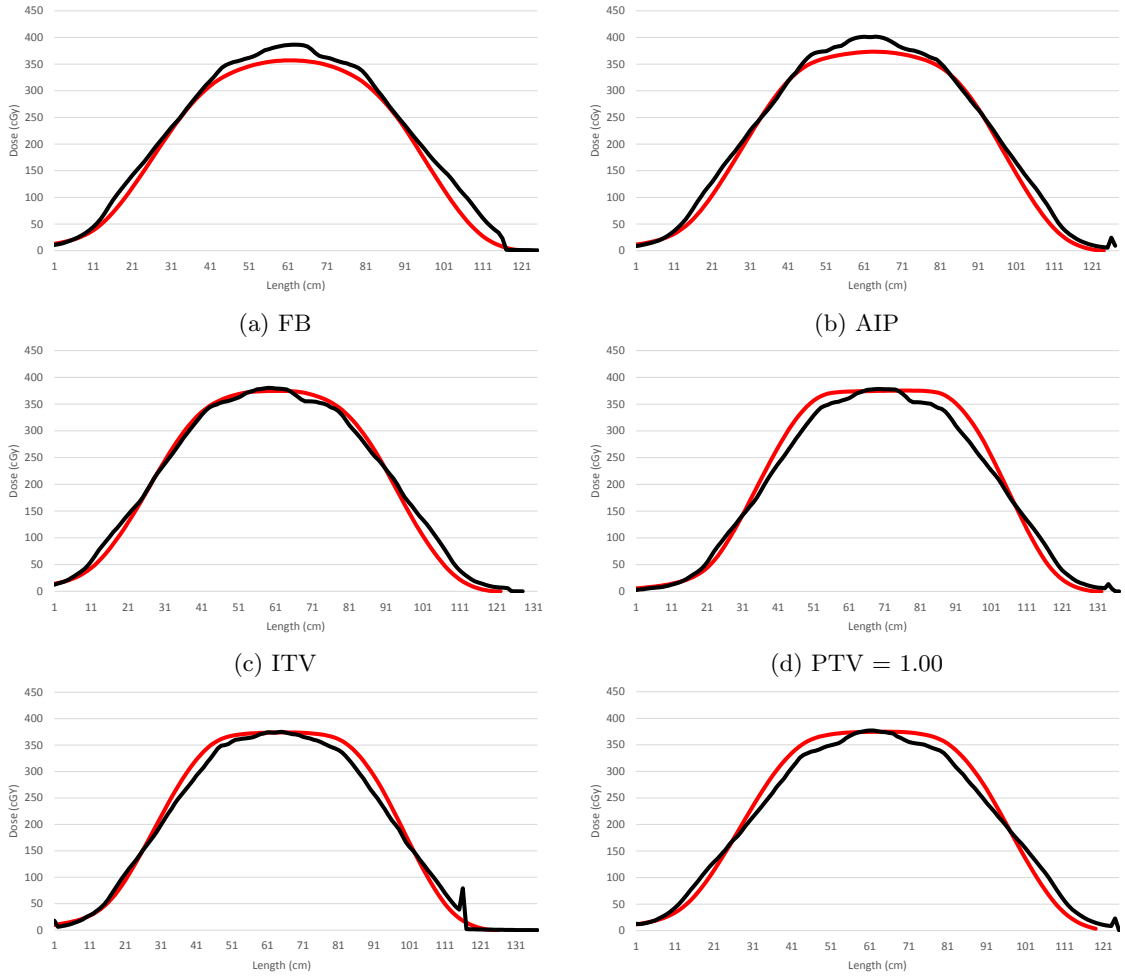

(a) FB

(b) AIP

(c) ITV

(d) PTV = 1.00

(e) PTV = 0.475

(f) HPTV = 0.475

Figure 3.8: The 15mm insert absolute dose profiles, along the central axis, for the film dose planes (black) and TPS dose planes (red).

point dose results.

The variations between the TPS profiles and film profiles in the direction of travel for each plan can be seen in Figure 3.8. In the FB and AIP film profiles, the central axis (CAX) dose is shown to be higher than the expected TPS dose, consistent with the point dose measurements. In the region equivalent to the position of the ion chamber for the point dose results, the percentage-dose difference between plan and film was found to be within 2% for the ITV plans. This is comparable to the point dose measurements, indicating both methods were able to determine the same dosimetric difference.

The ITV profiles show the closest agreement, across the high dose and low dose regions. The PTV = 1.00 profiles show that the central dose values are comparable, again consistent with the point dose measurements, but larger dose differences were seen in the low dose regions, contributing to the lower overall agreement between the dose distributions.

In terms of statistical significance, no plans showed a significant difference to the FB plan for the 10% and 40% TH with gamma criteria 1%/1mm. This is due to the high sensitivity of the measurement, creating more room for random error. For the gamma criterion 2%/2mm and 3%/3mm, the ITV, PTV = 0.475 and HPTV plans all showed the statistically significant differences to the FB plan ($p<0.011$). The PTV plan showed no consistent difference to the FB plan, with only 1 p-value less than 0.05 ($p = 0.12$).

Between the PTV = 0.475 and HPTV plan, no consistent statistically significant result was seen, outside the 10% TH 2%/2mm p-value of 0.045, indicating the difference between these two options is minimal.

22mm Insert

The average gamma pass rates for the 22mm insert are summarised in Figure 3.7c for the 10% threshold and Figure 3.7d for the 40% threshold. Consistent with the 15mm insert results, a representative selection was analysed for the dose distribution verification, with the FB, AIP, ITV, PTV = 475, PTV = 1.00, and HPTV = 0.475 plans compared.

For the 10% and 40% thresholds, the AIP and PTV = 1.00 plans had the lowest mean gamma pass rates across all criteria. The best performing plan was the ITV override, which showed a 3%,

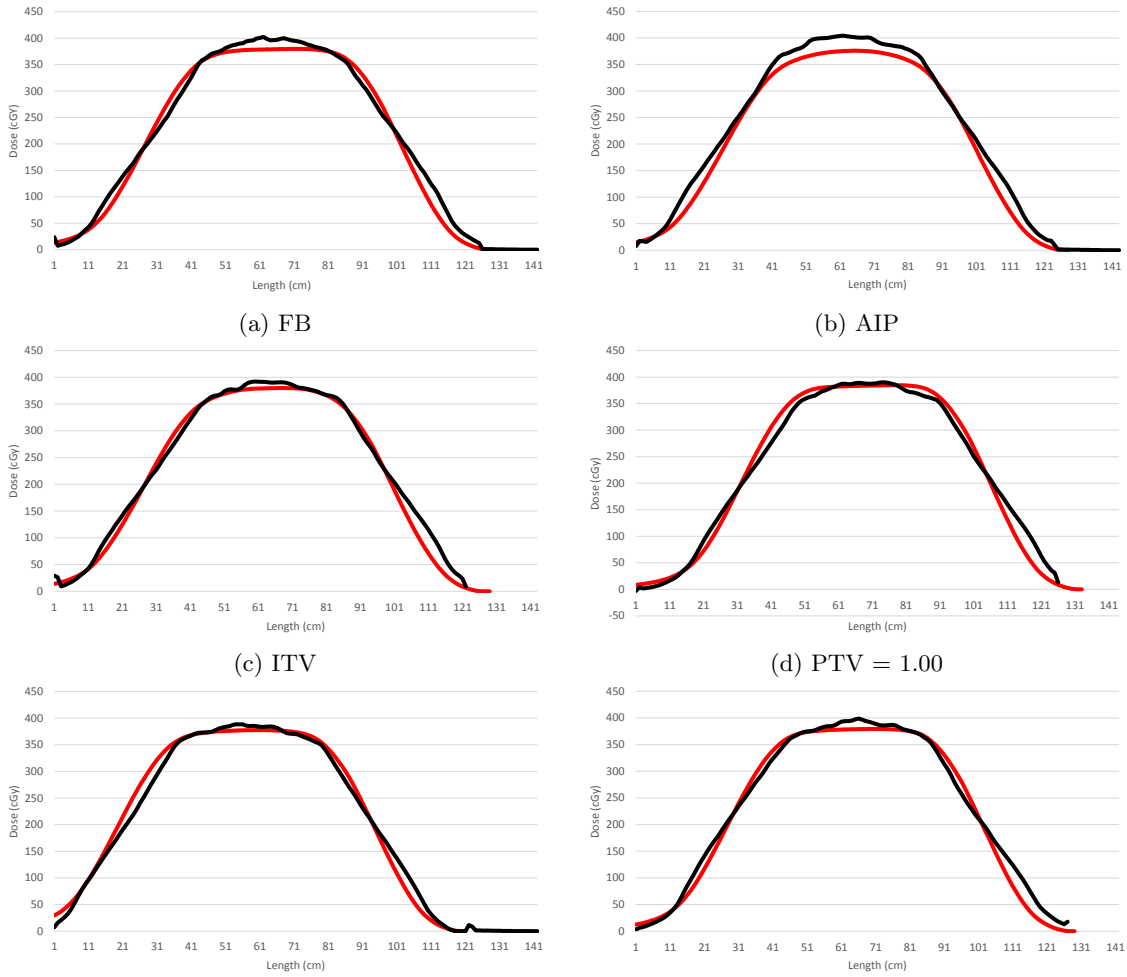

(a) FB

(b) AIP

(c) ITV

(d) PTV = 1.00

(e) PTV = 0.475

(f) HPTV = 0.475

Figure 3.9: The 22mm insert absolute dose profiles, along the central axis, for the film dose planes (black) and TPS dose planes (red).

3mm pass rate of 90.2% for the 10% threshold, and 94.7% for the 40% threshold, again comparable to the clinically accepted guidelines, and consistent with the percentage point dose difference seen in Figure 3.4. Overall, less variation in gamma pass rates was seen with the 22mm plans compared to the 15mm plans, consistent with the low variation seen in the point dose measurements.

The low variations between the TPS profiles and film profiles can also be seen in Figure 3.9. In the AIP film profile, the central film dose is higher than the expected TPS dose. The ITV profiles show the closest agreement, across both the high dose and low dose regions.

In terms of statistical significance, no plans showed a strong significant difference to the FB plan for the 10% TH with gamma criteria. This is due to the spread of high dose to the limits of the film, forming a large dose drop off and in turn a worse comparison to the TPS dose distribution. Only the PTV=0.0475 plan showed an improved, statistically significant result compared to the FB plan. Between the PTV = 0.475 and HPTV plan, no statistically significant result was seen.

3.3 Patient Case Study

While the results from the Phantom study show the viability of density overrides in Lung SBRT planning, these results are from a simplified system that does not correspond directly to a patient scenario. The breathing trace in the Phantom study is a basic sinusoidal pattern, which is easier for the CT scanner to reconstruct than the breathing trace of a patient with lung disease, where there may be a large number of irregular rhythms.

The amplitude chosen for the Phantom study also corresponded to a typical large breathing amplitude, so as to create a sufficiently large uncertainty in the 4DCT scan while remaining clinically relevant to a large number of situations. A range of different sized inserts were examined, corresponding to typical small, medium, and large tumours. The aim of this was to ensure the results of the density overrides were able to be applied to clinical situations.

The simplistic design of the QUASAR phantom resulted in a symmetric treatment plan that did not need to avoid any organs at risk, which is unrealistic in terms of clinical plans where doses to organs such as the spinal cord, skin, and heart always need to be considered.

Whilst collecting the results for the Phantom study, a patient presented to Christchurch Hospital Radiation Oncology Department for Lung SBRT treatment of a NSCLC far smaller than any seen in the clinic previously. The NSCLC had an ITV volume of $0.438cm^3$ and a PTV volume of $7.124cm^3$, far smaller than the Phantom study, where the volume of the 15mm diameter tumour ITV was $7.746cm^3$ and the PTV volume was $30.17cm^3$. Due to the small size of the tumour, there was concern expressed by the oncologist regarding the accuracy of the dose calculation algorithms, which are known to be less certain for small volumes. In addition to the small tumour volume, the patient presented with a large air pocket that overlapped the PTV. The presence of the air pocket further inhibited the accuracy of the TPS due to the additional need to calculate dose at the boundary of the air pocket and lung tissue. The coronal and sagittal slices of the contoured patient CT scan can be seen in Figure 3.10.

As an extension of the phantom study results presented in sections 4.1.1 and 4.1.2, the Monaco analysis was repeated for this complex clinical case. As this was a clinical case used for treatment, the delineation of the target volumes and the organs at risk was performed by the assigned radiation

Figure 3.10: Case Study Patient CT scan, taken from Monaco 5.1: (a) The coronal view of the NSCLC, showing the contoured ITV and PTV, and the overlap of the air bubble and PTV. (b) The sagittal view of the NSCLC. (c) The coronal view of the dose distribution of the original DCAT plan. (d) The sagittal view of the dose distribution of the original DCAT plan.

oncologist based on the ICRU clinical contouring guidelines.

The ITV was defined using the 4DCT MIP image, with the PTV generated from a 1cm superior-inferior and 5mm axial expansion of the ITV. As the tumour was less than 2.0cm from the chest-wall, 48Gy was prescribed in 4 fractions to the PTV, labelled PTV48. The region of the PTV that the air pocket overlapped was also contoured and labelled as 'bullae in PTV' so that the dose to the region could be taken in to account.

The treatment plan was generated by a radiation therapist with physics assistance due to the complexities of the plan. Although the plans for this research were 3D conformal radiotherapy plan, the case study patient was planned using Dynamic Conformal Arc Therapy (DCAT). DCAT is a rotational delivery technique in which the MLC shape is adjusted during a specified arc to conform to the target and avoid the nominated OARs. DCAT also has the advantage of avoiding the couch rotation required in 3D conformal lung SBRT planning, as well as decreasing the delivery time from approximately 45 minutes to 10 minutes. DCAT planning is a simplified form of IMRT, where a set of dose constraints are identified and the TPS iterates over possible delivery parameters until an acceptable plan is generated.

A 210° 6MV arc plan was generated on the AIP with IMRT constraints of delivering 48Gy to the PTV48. Although a different planning technique was used, the same conformity indices applied to the DCAT plan. The planning aim was for a CI50% of approximately 7, and a CI100% of approximately 1.2-1.3, with a maximum dose to the PTV of around 150% of the prescribed plan. However, due to the small size of the tumour achieving these planning aims was not achievable, so the higher dose and conformity indices were accepted at the oncologists discretion.

The target coverage statistics for the clinical plan can be seen in Table 3.7, and the conformity and heterogeneity indices can be seen in Table 3.8. For a prescribed dose of 12Gy per fraction, the maximum dose of 150% corresponds to 18Gy, lower than the reported maximum dose of 18.5Gy. The D95 dose in this case is clinically acceptable however, with a dose of 12.3Gy covering 95% of the PTV, a greater value than the prescribed dose. The conformity and heterogeneity indices for the clinical plan were significantly worse than the clinical guidelines recommended, with a CI50% of 8.29, a CI100% of 1.52, and a Monaco reported CI of 0.46.

	Mean Dose (Gy)	Max Dose (Gy)	Min Dose (Gy)	D90 (Gy)	D95 (Gy)
Clinical Plan	14.8	18.5	10.1	12.9	12.3
ITV	15.0	19.4	10.0	12.9	12.3
PTV = 0.475	15.1	17.1	9.4	13.5	12.8
PTV= 0.650	15.3	17.5	9.4	13.7	13.1
PTV = 0.825	15.9	18.2	9.8	14.3	13.5
PTV = 1.00	15.9	18.2	9.9	14.3	13.6
HPTV = 0.475	15.2	17.9	9.3	13.5	12.8
HPTV = 0.650	15.8	18.4	9.4	14.1	13.3
HPTV = 0.825	15.9	18.1	9.7	14.3	13.5

Table 3.7: The target coverage DVH metrics for each of the baseline plans and density override plans for the Case Study Patient DCAT plan, reported by Monaco 5.1.

	Total MU	CI 50%	CI 100%	CI	HI
Clinical Plan	2146.24	8.29	1.52	0.46	1.70
ITV	2138.94	8.23	1.52	0.47	1.74
PTV = 0.475	1910.76	6.07	1.05	0.67	1.75
PTV= 0.650	1853.16	5.81	0.99	0.70	1.79
PTV = 0.825	1846.26	6.26	1.19	0.61	1.82
PTV = 1.00	1819.66	6.03	1.15	0.64	1.81
HPTV = 0.475	1901.97	6.09	1.05	0.66	1.80
HPTV = 0.650	1864.64	6.49	1.22	0.60	1.82
HPTV = 0.825	1846.30	6.26	1.19	0.61	1.81

Table 3.8: The PTV conformity and heterogeneity metrics for each of the baseline plans and density override plans for the Case Study Patient DCAT plan, reported by Monaco 5.1.

The treatment team was interested in what improvements could be made to the plan by applying a density override to either the ITV or PTV and re-generating the plan. Although the patient was treated without any density overrides, a retrospective study was performed using the same density overrides as described in Section 3.3.3. Altering only the densities of the ITV and PTV, the DCAT plan was re-calculated and the target coverage and conformity indices compared to the original plan.

Comparing the clinical plan to the density overridden plans, the target coverage was improved or at least remained the same, a result consistent with the results from the 15mm tumour insert. The ITV plan showed the smallest difference compared to the clinical plan, aside from a higher maximum dose. For the remaining 7 density overridden plans, the D95 value increased by 0.9±0.4Gy compared to the clinical plan. The PTV = 0.475, PTV = 0.650, and HPTV = 0.475 were the only treatment plans able to keep the maximum dose to the PTV less than 150% to provide the acceptable target coverage across all metrics.

Consistent with the target coverage metrics, the ITV plan showed the least amount of difference to the clinical plans in terms of the conformity and heterogeneity of the dose distribution. For the PTV and HPTV plans, the Monaco CI value increased by 0.18 ± 0.06Gy compared to the clinical plan. The PTV = 0.825, and PTV = 0.825 plans displayed the closest conformity and heterogeneity indices to the clinical guideline recommendations, however all PTV and HPTV plans showed an improvement compared to the original plan, and would be clinically desirable.

4

Discussion

The following chapter discusses the key findings that were presented in the Results chapter. The key motivation for exploring the effect of density overrides is to improve the treatment of lung cancer with SBRT. This can be achieved in two different ways, improving the quality of the treatment plan, in terms of target coverage and conformity as discussed in sections 3.1.1 and 3.1.2, and improving the accuracy of the treatment delivery as discussed in section 3.2. This thesis investigated these two areas, comparing the plan quality and determining the dosimetric accuracy of the measured treatment compared to the planned treatment.

The relationship between these two areas is discussed, as both have an influence on patient outcomes so cannot be viewed independently. The magnitude of the differences seen in the Results section between the tumour sizes is reviewed, and as a result the total net effect on patient outcomes can be compared. As a change in ED for the ITV and PTV only resulted in a change in MU for this study, with no further optimisation performed, the relationship between calculated dose and tumour size can be compared, based on the known principles of dose calculation algorithms.

The significance of these results, clinically and statistically, and relationship to previously published work is then reviewed. The limitations of the phantom study are also outlined, with the differences between a phantom and a patient compared. Ultimately, the end goal of a phantom study is to relate the outcomes to clinical environments. The results of the patient case study and the phantom study are also discussed, so that clinical recommendations can be developed.

4.1 Plan Quality Analysis

This section covers the variations in target coverage, conformity, and homogeneity for each of the tumour sizes and investigated treatment plans. The differences and potential impact to the patient will be discussed.

4.1.1 Target Coverage

The clinical guidelines for Lung SBRT planning aim for the prescribed dose to cover 95% of the volume of the PTV, with the maximum dose limited to 150% of the prescribed dose. For the 15mm and 22mm inserts, the FB plans exhibited the lowest mean dose to the PTV, the lowest D95 values, and also the lowest maximum dose to the PTV. Across all inserts, the AIP plans performed better in terms of target coverage compared to the FB plans. This is consistent with previously published studies comparing FB to AIP plans[57].

In terms of the density overridden plans, the ITV plans showed the least amount of target coverage difference compared to either the FB or AIP plans, a result which was found to be consistent for all tumour sizes. This is expected, as the volume of the ITV is small compared to the volume of the PTV. For the 30mm tumour, a motion amplitude of 15mm corresponds to an ITV to GTV ratio of 2.5, so the volume of the ITV is not much large than the volume of the tumour at any one phase, whereas for the 15mm insert, the ITV to GTV ratio is 4. When the ITV is set to a density consistent with the known density of the GTV, this results in minimal differences for the 30mm insert and slightly improved target coverage for the 15mm insert.

Overriding the density of a target volume to a water-equivalent density is associated with better target coverage due to the fact that the CCC algorithm accounts for inhomogeneities by scaling dose kernels by the relative electron densities [58, 59]. Previous studies have shown that for the CCC algorithm, a lower lung density is associated with a decreased medium target dose [60].

This is consistent with the results seen for the PTV and HPTV overrides. Across all inserts, the planning aim of 95% of the PTV volume receiving the prescribed dose of 12Gy per fraction was achieved. In addition, none of these plans achieved unacceptably high max dose values, with the highest maximum point dose recorded as 15.7Gy for the 30mm insert PTV = 0.475 plan, corresponding to 130% of the prescribed dose. For the 15mm insert, the D95 value increased by $1.2 \pm 0.4Gy$ in the PTV and HPTV plans compared to FB, compared to $1.1 \pm 0.4Gy$ for the 22mm insert and $0.9 \pm 0.3Gy$ for the 30mm insert. The larger coverage differences between densities seen in the 15mm insert results are consistent with the LED principles stated previously, with the lowest differences seen in the 30mm insert. It would therefore be expected that the PTV=1.00

override should have the best target coverage, however this was only true for the 22mm insert. For the 15mm and 30mm inserts, the PTV=0.475 plans showed comparable target coverage to the PTV=1.00 plans, indicating that there are limitations to the heterogeneity accounting algorithm in Monaco 5.1.

High coverage of the prescribed dose to the target, while minimising hot spots, is critical to achieving a high therapeutic ratio. Not covering a sufficient volume of the tumour with a large enough dose can result in an unsuccessful treatment, as tumour control is not achieved. In addition, the presence of hot spots can lead to additional complications, such as necrosis. If the increased target coverage can be achieved with the higher density overrides, this would correspond to improved patient outcomes.

4.1.2 Conformity and Homogeneity

The clinical guideline used in this study recommend achieving a CI50% less than 5 and a CI100% in the region of 1.2-1.3. No guidelines existed for HI and CI reported by Monaco, so a comparison could only be made between plans for this study. As the objective of radiotherapy is achieving a high, homogeneous dose that is conformal to the target volume, the closer the CI and HI values to the ideal level, the more beneficial the treatment would be predicted to be. The ideal CI value is 1.0, whereas an acceptable HI is anything <2.0 based on the Radiation Therapy Oncology Group (RTOG) guidelines for SBRT [61, 62].

For all plans, the HI was found to be less than 2. This is expected as there were no irregular shapes in this study or OARs to avoid. Therefore, delivering a homogeneous dose to the PTV was less of an issue than it would be practically. For the 30mm insert, every plan showed a CI50% less than 5, and a CI100% in the region of 1.2-1.3. As a result, any of these plans would be deemed clinically acceptable. In terms of CI, there was a small change of 0.01 between the FB and PTV = 1.00 plans, which was clinically insignificant. For a large water-density PTV, the conformity would be expected to increase compared to the FB plan due to the complications associated with LED and forcing dose into lung volumes. This result again highlights the limitations of the heterogeneity accounting algorithms in Monaco 5.1, as seen in the target coverage results.

Conversely, the 15mm and 22mm insert results showed a large variety of conformity results,

with CI increasing in both cases for the higher density overrides. However, large variations were seen with the CI100% results. CI100% is highly sensitive to changes to the 100% isodose line. With the greater uncertainty seen in small fields and low densities, larger changes were seen in the 100% isodose line for the 15mm inserts compared to the 30mm insert. As these uncertainties were based on dose calculation in the lung-tumour interface, for the small tumours where the rind of the interface contributes to an overall larger percentage of the PTV, the consistency of the results is worsened. Although the conformity improves for the PTV and HPTV overrides in the 15mm and 22mm insert plans, there is lower confidence in these results. The stricter criteria of the CI metric compared to CI50% and CI100% makes it the metric from which clinical decisions should be based for small tumours.

Although improved target coverage and plan conformity are essential to improving patient outcomes, as the density overrides are an artificial plan optimising strategy, the improvements also need to be achieved in practice. If an improvement to the plan quality is associated with an unacceptably high uncertainty, then the plan has limited clinical benefit to the patient.

4.2 Plan Quality Verification

This section covers the variations in point dose and dose distribution measurements for each of the tumour sizes and treatment plans. The differences between the expected and measured results, in addition to the agreement between the two methods, and potential impact to the patient will be discussed.

4.2.1 Point Dose Verification

Varying levels of agreement were seen in the 10 plans investigated for the 15mm, 22mm, and 30mm inserts. While the 15mm and 22mm results showed positive correlation between the prescribed MU and the dose measured by the ion chamber, the same cannot be said for the 30mm insert. While there was an improvement in dosimetric accuracy seen using plans other than the FB plan, all results were within 1% of the expected dose, well below the acceptable clinical limit of 2%. As a result, there is a limited application for applying density overrides to large tumours. This suggests

the planning system performs adequately for calculating dose to large tumours, where the effect of the uncertainty of heterogeneity accounting algorithms is limited.

Moving to the 15mm and 22mm results, there was minimal difference between the ITV, PTV, and HPTV overrides aside from the PTV = 0.475 plan. This is consistent with there being little difference in MU between the plans, found to be 8MU for the 15mm insert and 10MU for the 22mm insert for a total delivered MU of approximately 1500MU. From the principles of LED, less fluence would be required in higher density overrides to result in the same desired dose coverage, resulting in less MU being delivered. This is consistent with the small range of 2MU between the PTV=1.00, HPTV=0.650, and HPTV=0.825 plans.

Larger percentage dose differences were seen in the 15mm insert compared to the 22mm insert, with the FB and AIP plans both outside the clinically accepted limited of 2%. Although the 15mm plans were still not within 1% of the expected dose, the improvement was significant enough that the density overrides would be more beneficial to the patient compared to the 22mm plans.

The ion chamber measurements are more accurate and consistent than the film measurements in terms of absolute dose. This is due to the fact the the dose being measured was along a relatively homogeneous section of the dose distribution, outside of any steep dose gradients that are more susceptible to variation. In addition, the characteristic of the CC13 ion chamber are well understood as it is used regularly and has a shorter calibration chain to the Primary Standard of Radiation in Australia (measured by Australian Radiation Protection and Nuclear Safety Agency, ARPANSA).

However, there is limited value to the ion chamber results as the dose being measured is only a small portion of the ITV. As several density overrides were found to be acceptable in terms of dose to the central region of the ITV, more weight is placed on the PTV - ITV doses than the central region in terms of what density override to recommend.

Based on the point dose results, there is limited application in overriding the ITV and PTV density for large tumours, with the most amount of benefit seen for smaller tumours where the risk of uncertainty is greater.

4.2.2 Dose Distribution Verification

For the six plans investigated in the dose distribution verification study, large variations were seen in terms of the range of gamma pass rates between the different plans. For the 15mm insert, three plans showed a statistically significant improvement to the baseline FB plan, however a larger number of samples is required to investigate the 1%/1mm gamma criteria. For the 20mm insert, only one plan (PTV = 0.475) showed a significant improvement compared to the baseline FB plan.

For both the 15mm and 22mm results, the ITV plan showed the high gamma pass rates for both the 2%, 2mm and 3%, 3mm criteria. Profiles through the centre of the tumour confirm the improved agreement between the ITV TPS dose plane and measured film dose plane.

This result can be explained conceptually by looking at the relationship between fluence and the respective densities of the GTV, ITV, and PTV. When the density of the ITV or PTV is overridden closer to the density of the GTV, less fluence is required to deliver the prescribed dose as conformal dose deposition is more achievable in higher density volumes. The lower fluence results in a reduction in the total MU prescribed when all other beam parameters are kept constant.

When this plan is delivered however, regardless of the position of the GTV inside the ITV, a higher proportion of the fluence will be deposited inside the higher density tumour compared to the surrounding lung material. As the tumour moves inside the ITV, the result is a higher dose overall to the ITV. As the FB plan is unable to predict this smearing out effect, the measured dose in the centre of the ITV will be higher than expected, a result that was consistently seen in both the ion chamber and film measurements.

The impact of the dose smearing effect is not only seen in the ITV plan, but the lower density PTV and HPTV plans as well. The gamma pass rates for these plans were only marginally worse than the ITV plans for both the 15mm and 22mm inserts. In these cases, larger variations were seen in the region away from the tumour's range of motion. This is consistent with the TPS overestimating the amount of dose that is deposited in lung density PTV due to the density override, causing the TPS profile to flatten out in the region of the PTV and then sharply drop off. In reality, this underestimates the fluence in the PTV-ITV region, with a higher percentage of dose scattering out of field of the PTV. This effect is also seen in the FB and AIP plans, so would not have a

significantly negative clinical effect over the ITV plan.

4.2.3 Relationship between Plan Quality and Plan Verification

A clinical recommendation from the phantom study results need to be based on two points; the improvement to the TPS dose statistics achieved with the density override, and the improvement to the dose delivery uncertainty achieved with the density override.

If the clinician is only concerned with improving the accuracy of the dose delivery, both point dose and dose distribution measurements compared to the TPS, and is not concerned with improving the target coverage or conformity of the plan, then an override of the ITV to an ED of 1.00 is recommended, based on the point dose and dose distribution measurements for the 15mm tumour insert.

However, the accuracy of the point dose and dose distribution measurements has a limited effect on patient outcomes if the plan quality is not at an acceptable level. The lower density PTV overridden plans consistently showed improved target coverage and conformity compared to the original plan for the smaller tumours, while still achieving improved dosimetric accuracy.

4.3 Limitations of the Study

As Lung SBRT is a highly complex area of radiotherapy, it was not possible to investigate every aspect of uncertainty that contributes to dosimetric accuracy. In this section, the limitation of the two examined areas of uncertainty, imaging and dose calculation, are discussed, as well as the limitations of the data collection process.

4.3.1 4DCT limitations

In the 4DCT section of the phantom study, only one breath cycle length of 4 seconds was examined as this represented the average patient seen in our department. However, a review of our clinical patients shows a range of different periods, from a minimum period of 2.36 seconds to a maximum period of 33.12 seconds, as seen in Table 2.5. The 33 second breathing period is not realistic however, as it was determined by the RPM system and found under inspection to be a software fault. The

patient in question had a highly irregular breathing pattern and coughed for a large portion of the scan. As a result, the software was unable to determine the true breathing period minima, and the period was artificially elongated. This highlights the large amounts of variation seen between regular sinusoidal breathing patterns and the irregular but clinically relevant breathing patterns of real patients. As it is possible to run acquired patient traces through the QUASAR phantom, this could be a useful extension as many patients do not breath the same during treatment as they do during 4DCT acquisition.

On a simpler level, investigating one breathing period limits the results as it does not fully expose the issues 4DCT has with the reconstruction of very fast or very slow breathing cycles, and the influence of these artifacts on dose calculation. In addition, only one breathing amplitude was examined in this study. The 15mm amplitude was chosen as it created a sufficient amount of positional uncertainty during treatment, while remaining clinically relevant. A useful extension would be to look at the influence of various breathing amplitudes and to see if the relationship between optimal density override and PTV/ITV ratio was maintained, however this was not possible given time constraints and difficulties accessing equipment outside clinical hours.

A further 4DCT limitation was the fact that the motion of the QUASAR phantom was constrained to the superior-inferior axis. Previous studies have looked at the effect of density overrides on three dimensional tumour motion, as well as two dimensional motion and found good agreement between the two[41]. However, the QUASAR phantom in our department was not capable of three dimensional rotation, so this extension was not feasible. Although this rotation results in a more patient-realistic 4DCT scan, the superior-inferior direction was considered the most important for the introduction of uncertainties as it encapsulates the CT acquisition and QUASAR tumour directions of motion.

4.3.2 TPS limitations

One TPS algorithm was used for dose calculation throughout this study, the CCC algorithm for Monaco 5.1. As it was not possible to compare the same 4DCT and treatment planning process to a different TPS, these results are only applicable to Monaco 5.1 and the CCC algorithm.

Clinically at Christchurch Hospital, two dose calculation algorithms are used for Lung SBRT

planning, CCC and MC. Although MC is the more accurate algorithm compared to CC, several studies have shown that superposition/convolution algorithms are an acceptable substitute for MC [58, 63, 60]. The results are also inherently limited by the dose calculation uncertainties specific to Monaco 5.1 in our centre, beyond the uncertainties generated in the heterogeneous regions. Comparing the same 4DCT procedure and planning protocol across different TPS and algorithms is a useful extension that removes the specificity of the results.

During the planning process, the beam weightings were optimised for the FB plan and kept constant across the AIP plan and density overridden plans. This was to minimise the influence of the users ability in making beam weighting adjustments and to compare only the effect of density override on the calculated MU. However, this has the limitation of the plan being applied to the density overridden data sets not being the most ideal. There is potential that the dose statistics could have been improved for the non-optimised plans, and so the results are conservatively low.

In addition, this study only focused on dose coverage in the ITV and PTV, and did not consider the influences of OARs. As a result, achieving adequate dose coverage was easier than it would be for a patient case, where dose to the skin, lungs, heart, and spinal cord need to be considered and kept below dose limits. Also, this resulted in simple, symmetric MLC shapes across the entire PTV region. An extension of this study could look at doses to OARs and developing cork inserts with avoidance structures, and contouring and reporting the dose to the spinal cord, patient contour, ipsilateral and contralateral lungs of the QUASAR phantom.

4.3.3 Dose Verification limitations

While both the ion chamber and film results showed good absolute dose agreement, they come with their own sets of limitations.

The CC13 chamber has the benefit of familiarity as it is used extensively in our department for IMRT plan quality assurance and small field measurements, however it is sensitive to positioning uncertainties. The uncertainties depend on the precision of position, as well as the field size and steepness of the dose gradients, which resulted in the increased uncertainties in the 15mm insert ($\pm$0.7%) compared to the 30mm insert ($\pm$0.4%).

For the smaller fields seen with the 15mm insert, the additional issues of small field dosimetry and

chamber volume averaging effects were present. Volume averaging is an issue for point dosimetry along steep dose gradients. Instead of the dose to the effective point of measurement of the chamber being measured, the dose over the entire chamber volume is measured which results in the average dose across the gradient being measured [64, 65]. The effect of this was minimised in this study as the active volume of the CC13 was contoured as a structure, due to the CC13 moving relative to the PTV during measurement. The average dose from the voxels in this structure was reported and compared to the average chamber reading.

For the point dose measurements, no comparison was made between the chamber at a static position and moving. To investigate the differences in uncertainty generated by the 4DCT and dose calculation process, comparing static and moving point dose results would be a useful extension.

The key issue with the CC13 chamber was the potential for the chamber to perturb the radiation field and artificially influence the dose measured. This effect is independent of the volume averaging affect, and is related to the material the the chamber is constructed of and the fact that a large volume of the water-density tumour is replaced with air. To minimise this, several studies recommend using a smaller volume ion chamber, diamond detector, or diode in place of a chamber like a CC13 [65, 66]. For this research, and due to the fact that the film was acting as a second absolute dose check, the CC13 chamber was deemed sufficient due to the increased familiarity with it's operation. For the purpose of of a more realistic point dose measurement, a smaller chamber may help decrease the uncertainties associated with the CC13 chamber.

The use of radiochromatic film is well documented in radiotherapy, and several studies have quantified and recommended its use for IMRT and stereotactic fields [64, 65, 67, 68, 69]. However there were inherent limitations to the use of EBT3 film in this study. Due to the required dose reduction from 12Gy to 3Gy, additional error was applied to the film measurements. While high-dose radiochromatic film would be ideal for this type of research, it was not available for the majority of the study and had not been used clinically in our department, so scope of intended use was not well understood.

In addition, the EBT3 film that is used for quality assurance in our department is only used for static dose distribution measurements. As dynamic measurements inherently have more uncertainty associated with them than static measurements, the criteria used in our department could not be

directly applied to the film results.

Other studies have investigated the use of film for dynamic measurements, and have shown that convolving the dose plane results in better agreement between dose distributions[70]. This study showed that gamma pass rates $> 90\%$ (3%, 3mm) could be achieved with this method, however this was only for a single tumour size.

Only one colour response channel was used in this study, the red channel, as this has the best response up to 10Gy. To improve the reproducibility of the results, multiple colour channels could have been used to ensure the results are consistent and to minimise background influences. The film analysis software for this study was also based on a manual registration of the film and TPS dose planes. Automating this process would minimise the influence of user-variability and improve the reproducibility of the results. Although the use of radiochromatic film is well understood for SBRT dosimetry, its use is less familiar than the CC13 in our department so improvements to acquisition and analysis procedures could also improve the results of this study.

4.4 Comparison to Previously Published Work

The previously published work that is most comparable to this study is the study by Wiant *et. al.* (2014) [41]. This study compared 5 different plans, a FB, AIP, ITV, PTV, and Hybrid plan. For the ITV and PTV plans, both target volumes were overridden to an ED of 1.00. For the Hybrid plan, the PTV-ITV volume was overridden to -200HU, corresponding most closely to the ED of 0.825 used in this study.

This study investigated the effect of the density overrides on dose statistics and verification with EBT3 film for three different breathing motions: 2D sinusoidal, 2D irregular, and 3D sinusoidal. This study also used a single-sized tumour insert with a diameter of 30mm. The results from the 2D sinusoidal breathing pattern showed that the best agreement between planned and measured dose was seen in the hybrid and PTV plans. Although no film results were collected for the 30mm insert in this study, the general agreement between the film and ion chamber measurements means a comparison can still be made.

In the study by Wiant *et. al.* (2014), the density overrides were applied and the plan re-

optimised, which resulted in minimal differences in the dose statistics between plans. The CI and Mean dose values were all approximately the same, with the only significant difference occurring with the Max dose to the PTV. The ITV plan showed the greatest increase in maximum dose compared to the FB plan, whereas the PTV and hybrid plans showed minimal differences.

This is not consistent with the plan quality results seen in this study for the 30mm insert. A reduction in CI was seen in the PTV and HPTV plans compared to FB, although this had minimal significance. The mean dose was increased by 5% in the PTV and HPTV plans compared to the FB and AIP plans, with the maximum dose also increasing by 2.6%. Minimal differences were seen between the ITV plan and the FB and AIP plans.

As the motion amplitude, tumour size, and breathing motion were the same between the two studies, there are two likely causes of these discrepancies. Firstly, this study did not optimise the beam weightings between plans, and so the small decrease in plan conformity seen between the PTV and HPTV plans is most likely due to the small changes in MU seen between plans in Table 3.6. However, although there is a small change in MU with the changing density of the target volumes, this has a relatively large effect on the dose calculation. As it is easier for the TPS to deliver dose to dense objects, the dose to the PTV would be expected to increase.

A second reason for the variation between results may stem from the differences between the two planning systems. The extent to which heterogeneity accounting algorithms were commissioned in the planning systems will affect the degree of accuracy in calculating dose for various density overrides. This is specific to the TPS, in this case Monaco 5.1 compared to Eclipse, the algorithm used, CCC compared to AAA, and the variations in accuracy of these. This suggests that the confidence put on different density overrides should be considered based on the TPS and algorithm used, and that clinical decisions should be made based on departmental-specific and equipment-specific results.

For dose verification, the study by Wiant *et. al.* showed that the hybrid and PTV plans exhibited the best agreement between planned and measured dose. The ITV plan showed better agreement than the FB and AIP plans, although it tended to underestimate dose at the edge of the PTV. For the FB and AIP cases, the measured dose was higher across the PTV compared to the planned dose. This is consistent with the FB results seen in the 30mm ion chamber measurements,

however this study showed no statistically significant relationship between density override and dosimetric agreement for the 30mm insert. This may be due to variations in measured dose due to set-up uncertainties, as well as the variations between different planning systems and algorithms.

In both studies, density overrides were shown to improve dosimetric accuracy, however in this study density overrides were shown to be clinically beneficial for small tumours only. As a result of these differences, the recommendation would be to compare a departments current Lung SBRT planning protocol to a small selection of override options to determine the clinic-specific best fit.

4.5 Case Study

Applying the conclusions from the phantom study to a patient case is an important extension in understanding the clinical impact of density overrides. While the phantom study dealt with simple tumour motions and geometries, patient cases are rarely this simple. Although the target volumes in the patient case study were far smaller than the target volumes in the phantom study, the extension is still an important one to make as these are the cases where uncertainties are inherently greater.

Compared to the 15mm insert results, the ITV plan still showed the highest maximum dose, and the extent of the difference between the clinical and ITV plan was greater than for the phantom study. This is consistent with larger variation in target coverage in smaller tumours due to the impact of LED. In terms of target coverage, all PTV and HPTV overrides show improved DVH metrics compared to the clinically used plan. Consistent with the results that were expected for the 15mm insert, the PTV=1.00 plan exhibits the highest mean dose and D95 values.

Although the PTV and HPTV overrides showed increased CI values compared to the clinical and ITV plans, the trend seen in the 15mm results was not seen in the case study results. Although the PTV=0.650 had the highest CI value, it resulted in a CI100% value of 0.99, well outside the acceptable range of 1.2-1.3. Large variations were also seen between this result and the HPTV = 0.650 result, with a CI difference of 0.1 and a CI100% difference of 0.23. Although these plans are similar, the large variations most likely result from the limitations and uncertainties associated with dose calculation in small lung tumours. As this case study involved an extremely small tumour,

the effect was magnified. Therefore limited value can be placed on the CI values for the case study patient.

In this case, based on the validation results of the 15mm tumour insert phantom study, either the PTV = 0.475 or HPTV = 0.475 density overrides would be recommended for high dosimetric accuracy and improved target coverage and conformity. As there was no consistent statistically significant difference between these two results, overriding the PTV only to an ED of 0.475 would be recommended as this is a one step process and the simplest to implement in a clinical guideline.

5

Conclusion

SBRT is a modern method for treating of lung cancer, however there are limitations to its accuracy due to small fields and tumour motion. This study investigated whether overriding the density of the target volumes improved the tumour coverage, the conformity of the plan, and the accuracy with which the plan was delivered. This was then applied to a range of tumour sizes to compare the effect of small fields on uncertainty in radiotherapy.

In a clinical SBRT lung protocol, the FB and AIP planning methods are the most common, and little statistical difference was seen between these plans in this study. In terms of the tumour coverage and plan conformity, a trend was demonstrated where, for the smaller tumours, the dose coverage and conformity improved when a PTV override was applied. This is consistent with the known principles of LED, however there were variations in the improvement when different density PTV overrides were applied. This suggests that there are limitations to the heterogeneity accounting algorithm, which introduces additional uncertainty to the results.

For the large 30mm tumour, minimal differences were seen in terms of plan quality and accuracy for the density overridden plans. This is in opposition to the results of previous studies, suggesting the results are department and equipment-specific. A trend was established between different sized tumours, with improvements to dosimetric accuracy seen as the tumour size decreased. Consistency was seen between the two dosimetric verification methods.

The results established in this study suggest a valid method for improving outcomes to patients with NSCLC treated with SBRT at Christchurch Hospital, particularly for small tumours.

Future Work

The case study results support the trend of improved plan quality and accuracy with a density override of PTV = 0.475, however this result would need to be verified clinically before implementation. Although the reduction in MU seen with the density overridden plans would result in a lower dose being received by OARs, this effect would need to be investigated and quantified before a reliable conclusion could be made.

Further work may be undertaken to investigate the full influence of density overrides for small tumour sizes with varying size of ITV and PTV. This would involve comparing different motion amplitudes set on the QUASAR phantom. In addition to this, patient breathing traces could be examine to form a more patient-specific conclusion. This study only investigated one TPS dose calculation algorithm, CCC. Further study could be undertaken, looking specifically at MC algorithms and the effect this improvement in accuracy has on the over uncertainty of SBRT Lung treatment planning.

Bibliography

[1] M. Joiner and A. V. D. Kogel, *Basic Clinical Radiobiology Fourth Edition*. 2009. iv, 5

[2] M. Beyzadeoglu, G. Ozyigit, and C. Ebruli, *Basic Radiation Oncology*. Springer-Verlag Berlin Heidelberg, 2010. iv, 6, 7

[3] ICRU, "International Commission on Radiation Units and Measurements. Prescribing, Recording, and Reporting Photon-Beam Intensity-Modulated Radiation Therapy (IMRT) ICRU Report 83," 2010. iv, 8

[4] S. R. Cherry, J. Sorenson, and M. E. Phelps, *Physics in Nuclear Medicine (4th Edition)*, vol. 31. 2012. iv, 10

[5] P. Mayles, a. Nahum, J. C. Rosenwald, and N. Papanikolaou, *Handbook of Radiotherapy Physics: Theory and Practice*, vol. 35. 2008. iv, 4, 10, 13, 15, 17, 21, 22, 23

[6] E. Podgorsak, "Radiation Oncology Physics: A Handbook for Teachers and Students," *British journal of cancer*, vol. 98, p. 1020, 2008. iv, 2, 11, 14, 15, 17, 18, 25, 101, 102, 103

[7] ICRU, "Tissue Substitutes in Radiation Dosimetry and Measurement. ICRU Report 44," 1989. vi, 31, 33

[8] IBA Dosimetry, "Brochure: Detectors for Relative and Absolute Dosimetry: Ionisation Chambers and Diode Detectors," *IBA Dosimetry GmbH*, 2011. vi, 44

[9] Ministry of Health, *Mortality 2012 Online Tables*. Ministry of Health, Wellington, 2015. 1

[10] Cancer Society of New Zealand, "Lung Cancer/Matepukupuku Pukahukahu: A guide for people with lung cancer," 2014. 1

[11] Ministry of Health, *Cancer: New Registrations and Deaths 2012*. Ministry of Health, Wellington, 2015. 1

[12] A. Barrett, J. Dobbs, and T. Roques, *Practical Radiotherapy Planning Fourth Edition*. CRC Press, 2009. 1, 7

[13] J. L. Meyer, *IMRT, IGRT, SBRT: Advances in the treatment planning and delivery of radiotherapy: Second edition*. Basel, Karger, 2011. 1, 2

[14] ICRU, "International Commission on Radiation Units and Measurements. Prescribing, Recording and Reporting Photon Beam Therapy. ICRU Report 50," 1993. 8, 21

[15] ICRU, "International Commission on Radiation Units and Measurements. Prescribing, Recording and Reporting Photon Beam Therapy (Supplement to ICRU Report 50)," 1999. 8

[16] N. Papanikolaou, J. J. Battista, A. L. Boyer, C. Kappas, E. Klein, and T. R. Mackie, *AAPM report 85:Tissue Inhomogeneity Corrections for Megavoltage Photon Beams. Report of the AAPM radiation therapy committee task group 65.* No. 85, 2004. 9, 10, 11, 13

[17] B. Disher, *The Impact of Lateral Electron Disequilibrium on Stereotactic Body Radiation Therapy of Lung Cancer*. PhD thesis, The University of Western Ontario, 2013. 10, 12

[18] W. Fu, J. Dai, and Y. Hu, "The influence of lateral electronic disequilibrium on the radiation treatment planning for lung cancer irradiation.," *Bio-medical materials and engineering*, vol. 14, no. 1, pp. 123–126, 2004. 12

[19] T. R. Mackie, E. El-Khatib, J. Battista, and J. Scrimger, "Lung Dose corrections for 6- and 15-MV x-rays," *Medical Physics*, vol. 12, no. 3, pp. 327–332, 1985. 13

[20] M. Dahele and D. B. Mclaren, "Stereotactic Body Radiotherapy," *Clinical Oncology*, vol. 27, pp. 249–250, 2015. 14

[21] L. Potters, M. Steinberg, C. Rose, R. Timmerman, S. Ryu, J. M. Hevezi, J. Welsh, M. Mehta, D. A. Larson, and N. A. Janjan, "American Society for Therapeutic Radiology and Oncology and American College of Radiology Practice Guideline for the performance of stereotactic body radiation therapy," 2004. 14

[22] K. Franks, P. Jain, and M. Snee, "Stereotactic Ablative Body Radiotherapy for Lung Cancer," *Clinical Oncology*, vol. 27, no. 5, pp. 280–289, 2015. 14, 15, 16

[23] K. H. Kang, C. C. Okoye, R. B. Patel, S. Siva, T. Biswas, R. J. Ellis, M. Yao, M. Machtay, and S. S. Lo, "Complications from Stereotactic Body Radiotherapy for Lung Cancer.," *Cancers*, vol. 7, no. 2, pp. 981–1004, 2015. 15

[24] A. Martin, S. Thomas, S. Harden, and N. Burnet, "Evaluating Competing and Emerging Technologies for Stereotactic Body Radiotherapy and Other Advanced Radiotherapy Techniques," *Clinical Oncology*, vol. 27, no. 5, pp. 251–259, 2015. 15

[25] A. E. Nahum, "The Radiobiology of Hypofractionation," *Clinical Oncology*, vol. 27, no. 5, pp. 260–269, 2015. 16

[26] M. B. Sharpe, T. Craig, and D. J. Moseley, "Image guidance: Treatment target localization systems," in *Frontiers of Radiation Therapy and Oncology*, vol. 40, pp. 72–93, 2007. 17

[27] G. T. Y. Chen, J. H. Kung, and E. Rietzel, "Four-dimensional imaging and treatment planning of moving targets.," *Frontiers of radiation therapy and oncology*, vol. 40, no. 1, pp. 59–71, 2007. 19, 20

[28] F. J. Lagerwaard and S. Senan, "Lung cancer: Intensity-modulated radiation therapy, four-dimensional imaging and mobility management," in *Frontiers of Radiation Therapy and Oncology*, vol. 40, pp. 239–252, 2007. 19, 20

[29] G. Bouilhol, M. Ayadi, R. Pinho, S. Rit, and D. Sarrut, "Motion artifact detection in four-dimensional computed tomography images," *Journal of Physics: Conference Series*, vol. 489, no. 1, p. 012024, 2014. 20

[30] S. J. Castillo, R. Castillo, E. Castillo, T. Pan, G. Ibbott, P. Balter, B. Hobbs, and T. Guerrero, "Evaluation of 4D CT acquisition methods designed to reduce artifacts," *Journal of Applied Clinical Medical Physics*, vol. 16, no. 2, pp. 23–32, 2015. 20

[31] A. Nisbet, I. Beange, H. S. Vollmar, C. Irvine, A. Morgan, and D. I. Thwaites, "Dosimetric verification of a commercial collapsed cone algorithm in simulated clinical situations," *Radiotherapy and Oncology*, 2004. 21, 24

[32] R. E. Bentley and J. Milan, "An interactive digital computer system for radiotherapy treatment planning," *The British Journal of Radiology*, vol. 44, no. 527, pp. 826–833, 1971. 21

[33] ICRU, "International Commission on Radiation Units and Measurements. Use of Computers in External Beam Radiotherapy Procedures with High-Energy Photons and Electrons. ICRU Report 42," 1987. 21

[34] P. Cherry and A. Duxbury, *Pratical Radiotherapy: Physics and Equipment.* No. 1, 2009. 21, 22

[35] L. Lu, "Dose calculation algorithms in external beam photon radiation therapy," *International Journal of Cancer Therapy and Oncology*, vol. 1, no. 2, pp. 01025–01028, 2013. 22, 23

[36] M. Pearson, P. Athertony, R. Mcmeneminy, F. Mcdonaldy, G. Mazdaiy, P. Mulvennay, and G. Lambert, "The Implementation of an Advanced Treatment Planning Algorithm in the Treatment of Lung Cancer with Conventional Radiotherapy," *Clinical Oncology*, vol. 21, pp. 168–174, 2009. 24

[37] U. Haedinger, T. Krieger, M. Flentje, and J. Wulf, "Influence of calculation model on dose distribution in stereotactic radiotherapy for pulmonary targets," *International Journal of Radiation Oncology Biology Physics*, 2005. 24

[38] B. Zhao, Y. Yang, T. Li, X. Li, D. E. Heron, and M. S. Huq, "Dosimetric effect of intrafraction tumor motion in phase gated lung stereotactic body radiotherapy," *Medical Physics*, vol. 39, no. 11, p. 6629, 2012. 24, 26

[39] L. Fu, H. Perera, S. Rudoler, and Y. Yu, "Can PTV Density Be Overridden for SBRT Lung Planning?," *Medical Physics*, vol. 40, 2013. 26, 28

[40] D. Wiant, C. Yount, J. Pursley, J. Terrell, J. Maurer, and B. Sintay, "On the Validity of Target Density Overrides for RapidArc Lung SBRT Treatment Planning," *Medical Physics*, vol. 40, 2013. 26, 27, 28

[41] D. Wiant, C. Vanderstraeten, J. Maurer, J. Terrell, and B. Sintay, "On the validity of density overrides for VMAT lung SBRT planning," *Medical Physics*, vol. 41, 2014. 26, 27, 28, 83, 86

[42] T. Zhuang, A. Magnelli, T. Djemil, G. Videtic, and P. Xia, "Dosimetric Impact of Temporal Variation of Electron Density within Planning Target Volume for Lung Cancer SBRT," *Medical Physics*, vol. 38, 2011. 26

[43] C. Shang and C. Vargas, "Structure Density Variations between Free Breathing CT and RespirationGated 4D CT in Lung SBRT," *Medical Physics*, vol. 38, 2011. 26

[44] L. Appenzoller, C. Robinson, and K. Moore, "Predictive Factors Influencing LowDose Conformality in Lung SBRT," *Medical Physics*, vol. 38, 2011. 26

[45] D. Wiant, J. Terrell, and B. Sintay, "Target Definition in TomoTherapy Lung SBRT Treatment Plans," *Medical Physics*, vol. 38, 2011. 26

[46] D. Pokhrel, R. Badkul, H. Jiang, H. Saleh, C. Estes, J. Park, P. Kumar, and F. Wang, "Dosimetric Evaluation of Centrally Located Lung Tumors: A Monte Carlo (MC) Study of Lung SBRT Planning," *Medical Physics*, vol. 41, 2014. 26

[47] Y. Tsuruta, M. Nakata, M. Nakamura, Y. Matsuo, K. Higashimura, H. Monzen, T. Mizowaki, and M. Hiraoka, "Dosimetric comparison of Acuros XB, AAA, and XVMC in stereotactic body radiotherapy for lung cancer," *Medical Physics*, vol. 41, 2014. 26

[48] H. Fakir, D. Hoover, and J. Chen, "Evaluation of SmartArc and RapidArc for lung SBRT treatment planning and delivery," *Medical Physics*, vol. 39, 2012. 26

[49] A. Chen, Q. Li, S. McNair, and K. Xu, "Target Dose Characterization by Monte Carlo versus Pencil Beam Algorithm for Lung Stereotactic Body Radiation Therapy (SBRT): A Preliminary Analysis in 20 Successfully Treated Patients," *Radiation Oncology Biology*, 2011. 26

[50] C. Ong, W. Verbakel, J. P. Cuijpers, B. J. Slotman, and S. Senan, "Dosimetric impact of interplay effect on rapidarc lung stereotactic treatment delivery," *International Journal of Radiation Oncology, Biology, Physics*, vol. 79, no. 1, pp. 305–311, 2011. 31

[51] K. Chang, S. Hung, Y. Chie, A. Shiau, and R. Huang, "A comparison of physical and dosimetric properties of lung substitute materials.," *Medical Physics*, vol. 39, no. 4, pp. 2013–20, 2012. 33

[52] R. Mayer, P. Liacouras, A. Thomas, M. Kang, L. Lin, and C. B. Simone, "3D printer generated thorax phantom with mobile tumor for radiation dosimetry," *Review of Scientific Instruments*, vol. 86, no. 7, 2015. 33

[53] L. Feuvret, G. Noël, J. J. Mazeron, and P. Bey, "Conformity index: A review," vol. 64, no. 2, pp. 333–342, 2006. 42

[54] A. Riet, A. Mak, M. Moerland, L. Elders, and W. Van Der Zee, "A conformation number to quantify the degree of conformality in brachytherapy and external beam irradiation: Application to the prostate," *International Journal of Radiation Oncology Biology Physics*, vol. 37, no. 3, pp. 731–736, 1997. 42

[55] International Atomic Energy Agency, "IAEA Technical Report Series No.398," *Atomic Energy*, pp. 1–229, 2000. 44

[56] V. Casanova Borca, M. Pasquino, G. Russo, P. Grosso, D. Cante, P. Sciacero, G. Girelli, M. La Porta, and S. Tofani, "Dosimetric characterization and use of GAFCHROMIC EBT3 film for IMRT dose verification.," *Journal of applied clinical medical physics / American College of Medical Physics*, no. 2, p. 4111. 46

[57] E. D. Ehler and W. A. Tomé, "Lung 4D-IMRT treatment planning: An evaluation of three methods applied to four-dimensional data sets," *Radiotherapy and Oncology*, vol. 88, no. 3, pp. 319–325, 2008. 77

[58] Y. Zhao, G. Qi, G. Yin, X. Wang, P. Wang, J. Li, M. Xiao, J. Li, S. Kang, and X. Liao, "A clinical study of lung cancer dose calculation accuracy with Monte Carlo simulation.," *Radiation oncology (London, England)*, vol. 9, no. 1, p. 287, 2014. 77, 84

[59] A. Ahnesjö, "Collapsed cone convolution of radiant energy for photon dose calculation in heterogeneous media.," *Medical physics*, vol. 16, no. 4, pp. 577–592, 2013. 77

[60] L. R. Aarup, A. E. Nahum, C. Zacharatou, T. Juhler-Nøttrup, T. Knöös, H. Nyström, L. Specht, E. Wieslander, and S. S. Korreman, "The effect of different lung densities on the accuracy of various radiotherapy dose calculation methods: Implications for tumour coverage," *Radiotherapy and Oncology*, vol. 91, no. 3, pp. 405–414, 2009. 77, 84

[61] E. Shaw, R. Kline, M. Gillin, L. Souhami, A. Hirschfeld, R. Dinapoli, and L. Martin, "Radiation therapy oncology group: Radiosurgery quality assurance guidelines," *International Journal of Radiation Oncology*Biology*Physics*, vol. 27, no. 5, pp. 1231–1239, 1993. 78

[62] T. Kataria, K. Sharma, V. Subramani, K. P. Karrthick, and S. S. Bisht, "Homogeneity Index: An objective tool for assessment of conformal radiation treatments.," *Journal of medical physics / Association of Medical Physicists of India*, vol. 37, no. 4, pp. 207–13, 2012. 78

[63] F. Hasenbalg, H. Neuenschwander, R. Mini, and E. J. Born, "Collapsed cone convolution and analytical anisotropic algorithm dose calculations compared to VMC++ Monte Carlo simulations in clinical cases," *Phys. Med. Biol. Phys. Med. Biol*, vol. 52, no. 52, pp. 3679–3691, 2007. 84

[64] D. a. Low, P. Parikh, J. F. Dempsey, S. Wahab, and S. Huq, "Ionization chamber volume averaging effects in dynamic intensity modulated radiation therapy beams," *Medical Physics*, vol. 30, no. 7, p. 1706, 2003. 85

[65] W. U. Laub and T. Wong, "The volume effect of detectors in the dosimetry of small fields used in IMRT.," *Medical physics*, vol. 30, no. 3, pp. 341–347, 2003. 85

[66] M. Bucciolini, F. B. Buonamici, S. Mazzocchi, C. De Angelis, S. Onori, and G. A. P. Cirrone, "Diamond detector versus silicon diode and ion chamber in photon beams of different energy and field size.," *Medical Physics*, vol. 30, no. 8, pp. 2149–2154, 2003. 85

[67] N. Farah, Z. Francis, and M. Abboud, "Analysis of the EBT3 Gafchromic film irradiated with 6MV photons and 6MeV electrons using reflective mode scanners," *Physica Medica: European Journal of Medical Physics*, vol. 30, pp. 708–712, sep 2014. 85

[68] O. A. García-Garduño, J. M. Lárraga-Gutiérrez, M. Rodríguez-Villafuerte, A. Martínez-Dávalos, and M. A. Celis, "Small photon beam measurements using radiochromic film and Monte Carlo simulations in a water phantom," *Radiotherapy and Oncology*, vol. 96, no. 2, pp. 250–253, 2010. 85

[69] M. Williams and P. Metcalfe, "Radiochromic Film Dosimetry and its Applications in Radiotherapy," *AIP Conference Proceedings*, vol. 1345, no. 1, pp. 75–99, 2011. 85

[70] J. Lehmann, M. Caloz, Q. Leturgie, S. Corde, S. Downes, and D. Thwaites, "4D lung SBRT: Dosimetric assessment using Gafchromic films," 2014 Combined Scientific Meeting, 2014. 86

[71] D. a. Low, W. B. Harms, S. Mutic, and J. a. Purdy, "A technique for the quantitative evaluation of dose distributions.," *Medical physics*, vol. 25, no. 5, pp. 656–61, 1998. 99

[72] A. Chaikh, J.-Y. Giraud, E. Perrin, J.-P. Bresciani, and J. Balosso, "The choice of statistical methods for comparisons of dosimetric data in radiotherapy.," *Radiation oncology (London, England)*, vol. 9, p. 205, 2014. 104

Appendices

A

Gamma Analysis

Comparing measured and calculated dose distributions for 3D TPS is necessary for ensuring the plan is dosimetrically and geometrically accurate. The Gamma Analysis criterion was developed by Low *et. al.* in 1998 to define a new parameter to act as a tolerance for distance-to-agreement (DTA) and dose-differences in low and high dose gradients [71].

DTA is the distance between a measured point dose and the nearest point in the calculated dose distribution that matches that dose. In a high dose gradient region, a small spatial offset can cause large dose differences. Dose difference may not be important in high gradient regions, and the DTA result can be used in its place. Using dose-difference and DTA together can act as a measure of the plan quality.

Low *et. al.* outlines the method for determining the acceptance criteria considering dose-difference and DTA simultaneously.

Symbol	Description
ΔD_M	Dose-difference criterion
Δd_M	DTA criterion
r_m	Measurement point
r_c	Calculated point
x and y	spatial location of r_c relative to r_m
$[D_m(r_m)]$	Dose at measurement point
$[D_c(r_c)]$	Dose at calculated point
δ	Difference between $[D_m(r_m)]$ and $[D_c(r_c)]$

Table A.1: A list of parameters used for gamma analysis calculations

A value Gamma (γ) is defined to describe a pass-fail criteria where:

$$\begin{aligned} \gamma(r_m) \leq 1, pass \\ \gamma(r_m) > 1, fail \end{aligned} \tag{A.1}$$

The γ value is based on the following equation:

$$\gamma(r_m) = min\{\Gamma(r_m, r_c)\}\forall\{r_c\}, | \tag{A.2}$$

Where

$$\Gamma(r_m, r_c) = \sqrt{(\frac{r^2(r_m, r_c)}{\Delta d_M} + \frac{\delta^2(r_m, r_c)}{\Delta d_M})} \tag{A.3}$$

$$r(r_m, r_c) = |r_c - r_m|, \tag{A.4}$$

$$\delta(r_m, r_c) = D_c(r_c) - D_m(r_m) \tag{A.5}$$

The γ values are calculated for every point in a dose distribution, and the γ pass rate is the percentage of total points that pass the defined γ criterion. A standard γ criterion is ΔD_M=1-3% and Δd_M=1-3%. It is also possible to look at the pass and fail points on the dose distribution to evaluate specific regions of failure.

B

Ion Chamber Calibration Factors

Equation B.1 corrects a charge reading from the dosemeter to a dose reading. This section will outline each of the terms, where they originate, and how the values were determined for use in this study.

$$\text{Dose to water at a point} = \frac{M_{Ave} \times 100 \times (k_s \times k_{pol} \times k_{TP}) \times N^{CC13}_{D,w,Q_0} \times k_{Q,Q_0}}{\text{linac output}} \tag{B.1}$$

Symbol	Description
Dose	Measured Dose (cGy)
M_{Ave}	Average charge collected (nC)
k_s	Ion recombination factor
k_{pol}	Polarity correction factor
$k_{T,P}$	Temperature Pressure correction factor
N^{CC13}_{D,w,Q_0}	CC13 Calibration Factor (Gy/nC)
k_{Q,Q_0}	Beam Quality correction factor
Output	Linac Output factor

Table B.1: The list of factors used in the charge-dose correction equation

Of the factors listed in Table B.1, some are determined at the time of measurement (M_{Ave}, $k_{T,P}$, linac output), some are determined in the department specific to the chamber (k_s, k_{pol}), and some are determined by the chain of calibration to a primary dosimetry standard.

The following measurements are made in the department, specific to the linac, conditions, and chamber:

- The $k_{T,P}$ correction factor: Accounts for the change in the number of atoms inside the chamber volume compared to standard calibration conditions (T = 21°C, P = 1013.25mBar), as this changes relative to the temperature (T, °C) and pressure (P, mBar) of the environment.
- Polarity correction factor, k_{pol}: Under identical conditions, polarising potentials of opposite polarity may yield different charge readings in an ionisation chamber[6]. Determined in the

department by comparing the difference in charge collected between (+) polarity and (-) polarity.

- Ion recombination correction factor, k_s: Dependent on the voltage applied between the measuring and collecting electrodes of the ionisation chamber. When the chamber is used below a desired voltage level, some of the charged particles recombine and are not detected, resulting in lower charge[6].

- Output: The amount of radiation delivered by the linac is determined by an MU ionisation chamber in the head of the machine. This MU chamber corrects the radiation delivery of the linac (MUs) to a dose value (cGy). The output of the machine, how much dose in cGy is measured when a set amount of MU is delivered, is determined to correct day-to-day variation in the state of the linac [6].

- Average charge collected, M_{Ave}: Determined by the average of several electrometer readings, measured in nC.

To maintain a traceable radiation dosimetry system, a calibrated local reference dosimeter that can be traced to a primary standard, and a number of field dosimeters which are calibrated against it are required. The concept of the Gray is based on a gold standard J/kg value, and Primary Standard Dosimetry Laboratories measure this with the highest achievable accuracy, using a primary standard for dose. All dosimeters are calibrated in a chain against these laboratories to determine a local reference dosimeter, which has a calibration value and associated uncertainty value. The local reference is then cross-calibrated with the field ion chambers, in this case a CC13 to determine another calibration factor and uncertainty[6]. This is the value N_{D,w,Q_0}^{CC13} for this study.

The Beam Quality correction factor, k_{Q,Q_0}, corrects for the differences between the reference

Description (Symbol)	Parameter
Calibration Factor (N_{D,w,Q_0}^{CC13})	0.271 Gy/nC
Ion Recombination Factor (k_s)	1.005
Polarity Correction Factor (k_{pol})	1.000
Beam Quality Correction Factor (k_{Q,Q_0})	0.995

Table B.2: Summary of the absolute dose correction factors of the IBA CC13 ionisation chamber.

beam, typically a Co-60 beam, and the local user beam. This difference occurs in the spectrum of the beams, so the radiation detected at the same physical point will be different[6]. The values are used in our department, specific to the CC13 ion chamber, can be seen in Table B.2.

C
Student's T test and Coefficients of Determination

A two-tailed, two-sampled Student's T test of equal variance was used to assess if there was a statistical difference between the various methods. Typically in radiation oncology, the significance level (α) is set to 0.05 (p-value) [72]. This corresponds to a 5% chance that there is a statistically significant result when there is actually no difference. P-values less than 0.05 are considered statistically significant, while values equal to or over 0.05 are not considered significant.

One-sided Two-sided	95% 90%	97.5% 95%
1	6.314	12.71
2	2.920	4.303
3	2.353	3.182
4	2.132	2.776
5	2.015	2.571
6	1.943	2.447
7	1.895	2.365
8	1.860	2.306
9	1.833	2.262
10	1.812	2.228

Table C.1: Student's t value, for one-side and two-sided critical region and various degrees of freedom (1-10)

The R^2 value is the coefficient of determination, and gives information about the goodness of fit of a trend line. A value of 1 indicates that the fitted model explains all variations, while a value of 0 shows there is no relationship, and a value in between represents the percentage of variability that can be accounted for.

D

Statistical Significance

The following tables show the p-values for the ion chamber and film results used in this study. The Students T-test parameters are discussed in Appendix C.

D.1 Ion chamber results

Treatment Plan	p-value		
	15mm	22mm	30mm
AIP	0.342	0.087	0.061
ITV	**0.002**	**0.003**	0.129
PTV = 0.475	**0.002**	**0.003**	0.176
PTV= 0.650	**0.036**	**0.022**	**0.008**
PTV = 0.825	**0.002**	**0.003**	**0.021**
PTV = 1.00	**0.001**	**0.002**	0.996
HPTV = 0.475	**0.002**	**0.002**	0.084
HPTV = 0.650	**0.002**	**0.003**	0.136
HPTV = 0.825	**0.002**	**0.003**	0.310

Table D.1: The statistical significance of the ion chamber measurements, where each result is compared to the FB plan for each tumour size. A p-value less than 0.05 is deemed significant.

D.2 15mm Film results

Dose Threshold	γ criteria	p-value				
		AIP	ITV	PTV	PTV 0.475	HPTV
10%	1%/1mm	0.468	0.124	0.400	0.051	0.306
	2%/2mm	0.274	**0.005**	0.091	**0.001**	**0.008**
	3%/3mm	**0.039**	**0.001**	**0.012**	**0.002**	**0.001**
40%	1%/1mm	0.630	0.118	0.946	0.064	0.274
	2%/2mm	0.252	**0.001**	0.902	**0.001**	**0.011**
	3%/3mm	0.080	**0.0001**	0.348	**0.0001**	**0.003**

Table D.2: The statistical significance of the film measurements for the 15mm insert, where each result is compared to the FB plan for each threshold and gamma criteria.

Dose threshold	γ criteria	p-value
10%	1%/1mm	0.319
	2%/2mm	**0.045**
	3%/3mm	0.973
40%	1%/1mm	0.220
	2%/2mm	0.099
	3%/3mm	0.614

Table D.3: The statistical significance between the 15mm insert film results for the PTV = 0.475 and HPTV plans, for each threshold and gamma criteria.

D.3 22mm Film results

Dose Threshold	γ criteria	p-value				
		AIP	ITV	PTV	PTV 0.475	HPTV
10%	1%/1mm	0.065	0.807	0.212	0.087	0.720
	2%/2mm	0.056	0.878	0.144	0.336	0.658
	3%/3mm	0.335	0.323	0.754	0.599	1.000
40%	1%/1mm	**0.033**	0.666	0.071	**0.035**	0.593
	2%/2mm	0.123	0.781	**0.043**	**0.003**	0.801
	3%/3mm	0.284	0.445	**0.024**	0.925	0.454

Table D.4: The statistical significance of the film measurements for the 22mm insert, where each result is compared to the FB plan for each threshold and gamma criteria.

Dose Threshold	γ criteria	p-value
10% TH	1%/1mm	0.190
	2%/2mm	0.653
	3%/3mm	0.463
40% TH	1%/1mm	0.080
	2%/2mm	0.063
	3%/3mm	0.984

Table D.5: The statistical significance between the 22mm insert film results for the PTV = 0.475 and HPTV plans, for each threshold and gamma criteria.